Fall 2008

The Synthesis and Physicochemical Characterization of New Monothiophosphate Materials

Nathan Takas

THE SYNTHESIS AND PHYSICOCHEMICAL CHARACTERIZATION OF NEW MONOTHIOPHOSPHATE MATERIALS

A Dissertation

Submitted to the Bayer School of Natural and Environmental Sciences

Duquesne University

In partial fulfillment of the requirements for

the degree of Doctor of Philosophy

By

Nathan J. Takas

December 2008

THE SYNTHESIS AND PHYSICOCHEMICAL CHARACTERIZATION OF NEW MONOTHIOPHOSPHATE MATERIALS

By

Nathan J. Takas

Approved October 08, 2008

Dr. Jennifer A. Aitken Assistant Professor of Chemistry and Biochemistry (Dissertation Director)	Dr. H. M. Kingston Professor of Chemistry and Biochemistry (Committee Member)	Dr. Jeffrey D. Evanseck Professor of Chemistry and Biochemistry (Committee Member)
Dr. David W. Seybert Dean, Bayer School of Natural and Environmental Sciences Professor of Chemistry and Biochemistry	Dr. P. Shiv Halasyamani Associate Professor of Chemistry University of Houston, Houston, TX (Outside Reader)	Dr. Jeffry D. Madura Chair, Department of Chemistry and Biochemistry Professor of Chemistry and Biochemistry
	Dr. Omar W. Steward Professor Emeritus of Chemistry and Biochemistry (Committee Member)	

ABSTRACT

THE SYNTHESIS AND PHYSICOCHEMICAL CHARACTERIZATION OF NEW MONOTHIOPHOSPHATE MATERIALS

By

Nathan J. Takas

December 2008

Dissertation Supervised by Dr. Jennifer A. Aitken

The following dissertation focuses on the chemistry of materials incorporating the monothiophosphate anion. The monothiophosphate anion is a member of the oxythiophosphates, a family of compounds in which phosphorus is bound to both oxygen and sulfur. This chemical characteristic places the metal oxythiophosphates between the well known families of the metal phosphates and thiophosphates. While both the metal phosphates and thiophosphates have been reported numerous times in the literature, the oxythiophosphates are rare, with only 29 compounds reported prior to this dissertation.

Three new monothiophosphate materials are presented in this work, as well a new polymorph of a previously known compound. $LaPO_3S$ and $NdPO_3S$ hydrates are found to mimic the structure of the orthophosphate mineral rhabdophane; $FeCl_3$ is found to undergo a metathesis reaction with α-Na_3PO_3S at room temperature to produce an iron

containing monothiophosphate material; and evidence of γ-Na_3PO_3S is presented. Water is found to play a key role in the chemistry of the monothiophosphate anion. Upon exposure to a humid atmosphere, reactions and phase transitions are found to occur, which require thermal or mechanochemical force to proceed under dry conditions. The hard/soft, acid/base chemistry of the monothiophosphate anion is also found to dominate both the products which are formed and the manner in which they oxidize or decompose.

The materials examined in this dissertation were characterized by powder X-ray diffraction, powder neutron diffraction, differential thermal analysis, thermogravimetric analysis, diffuse reflectance UV/Vis/NIR and IR, as well as photoluminescence spectroscopy. Additionally, second harmonic generation properties were measured.

DEDICATION

To my Parents for making it possible

To Mr. Bill Harmon for making it nascent

To Dr. Larry Curtin for making it challenging

To Dr. Daryl Mincey for making it funny

To Dr. Jennifer Aitken for making it matter

To Mrs. Tara Takas for making it tolerable

To my Children for making it worthwhile

ACKNOWLEDGEMENTS

First, I would like to thank my wife, for her unending support. Without her, this would not have been possible. I would also like to thank my advisor, Dr. Aitken, for pushing me to always do better. I intend to continue to try to improve the quality of my work because of the lessons that I have learned here. Thanks to my committee, who have always found time to address my questions, and talk me back from the ledge.

Special thanks to Jonathan Lekse , my labmate, friend and occasional partner in crime over the last four years. Thanks to Jin Lei Yao, Carl Brunetta, and Erin Divito for both intelligent and whimsical discussions that helped me to learn and laugh. Thank you to Lauren Slomka, Megan Hart, Dawneé Sloan, and Austin Savatt, the undergraduate and high school students who shared in the work presented here.

Thank you to Dr. P. Shiv Halasyamani and Dr. Kang-Min Ok (University of Houston) for the SHG measurements. Thank you to Dr. Peter Wildfong (Duquesne University) for fruitful discussions about phase transformations and solid-state kinetics. Thank you to Dr. Matthias Zeller (Youngstown State University) and Dr. Cora Lind (Toledo University) for translations of German references. Nancy Giles, and Xiaocheng Yang (West Virginia University) are thanked for photoluminescence measurements. I gratefully acknowledge the patient assistance of Mr. Evan Maxey and Dr. Jim Richardson (Intense Pulsed Neutron Source at Argonne National Laboratory) for the careful design of the *in-situ* controlled-humidity apparatus.

Thank you to the Bayer School of Natural and Environmental Sciences at Duquesne University for funding. Thank you to the Department of Chemistry and Biochemistry for the travel funds which made my trip to Argonne National Lab possible. Thank you to the Nobel Dick fund for supporting this work. Thank you also to Argonne National Lab and the Intense Pulsed Neutron Source for beam time (IPNS-4557). The PANalytical powder X-ray diffractometer was purchased with funds from the National Science Foundation (Grant No. DUE-0511444).

TABLE OF CONTENTS

Page

LIST OF TABLES

LIST OF FIGURES

Figure #: Page

LIST OF EQUATIONS

LIST OF ABBREVIATIONS

ATP.....Adenosine Triphosphate

DTA.....Differential Thermal Analysis

EDS.....Energy Dispersive Spectroscopy

EMF.....Electromotive Force

HTSS.....High-Temperature Solid-State

IPNS.....Intense Pulsed Neutron Source

IR.....Infrared

NHE.....Normal Hydrogen Electrode

NLO.....Non-Linear Optics

PL.....Photoluminescence

PXRD.....Powder X-ray Diffraction

RH.....Relative Humidity

RTSS.....Room-Temperature Solid-State Metathesis

SAX.....Small Angle X-ray Scattering

SEM.....Scanning Electron Microscopy

SHG.....Second Harmonic Generation

TEM.....Transmission Electron Microscopy

TGA.....Thermogravimetric Analysis

Chapter 1

An Introduction

1. Solid State Chemistry And Materials Science

The definition of solid state chemistry is worth considering before there are too many other ideas with which to contend. It is often assumed that the materials studied under the auspices of solid state chemistry were necessarily formed from solid reactants in a neat mixture at high temperatures (commonly in excess of 500° C). This assumption is not rigorously accurate. Many synthetic options are available to the solid state chemist, such as: precipitation from solution,[1,2] hydrothermal/solvothermal synthesis,[3,4] low/high temperature flux reaction,[5] solid state metathesis,[6,7] or neat reaction at high temperature.[8]

Solid state chemistry is, at its root, concerned with the chemistry and physicochemical properties of solids. No single synthetic method is capable of characterizing solid state chemistry. The one fact that is capable of typifying solid state chemistry is that the properties of the materials studied are directly dependant the materials existing in the solid phase under standard conditions. One may also note that there exist many solids which do not fall directly under the current regime of solid state chemistry. Examples of these include many molecular covalent solids. The reason that these materials might not be included as subjects of study in solid state chemistry is the fact that many of the properties of these materials often do not originate explicitly from the fact that they are solids, but rather from their molecular structure. The properties of

these materials are largely the same whether they are in a solid form or dissolved in some solvent medium. Solid state chemistry therefore targets the formation of new solids with properties which are directly tied to that state of matter.

Materials science is an emerging discipline which seeks to produce new materials which may fill a technological void. These materials are often solids, but have no other real restriction other than that they accomplish the desired goals. In this persuit, materials science incorporates elements of chemistry, physics, and engineering. Materials are sought in this discipline with specific and targeted properties, a philosophy largely taken from engineering. The desired material however, must be synthesized using whatever methods lend themselves to the production of a phase-pure product, this trend necessarily draws from chemistry. The final product must be accurately characterized. The origins of the properties discovered should be determined, modeled, or theoretically described. This step draws from the practices of both chemistry and physics. Finally, the material, when suitable, would be used in the production of new technologies, a practice which is again characteristic of engineering. Many of the most common characterization methods employed in materials science are nonstandard practices in many other chemical disciplines. Examples of these include powder X-ray diffraction, electron microscopy, differential thermal analysis, thermogravimetric analysis, diffuse reflectance spectroscopy, magnetometry, and electrical properties measurements. Many of these techniques will be encountered, time and again, throughout the body of this dissertation, as methods of characterization of the oxythiophosphate materials.

2. What is an Oxythiophosphate?

There are thousands of known metal orthophosphates (commonly referred to as simply phosphates) in the literature.[9-12] The sulfide analogues, tetrathiophosphates, containing oxidized phosphorus bound exclusively to sulfur are plentiful as well.[13-16] Oxythiophosphates, compounds in which oxidized phosphorus is bound to both sulfur and oxygen, are scarce. Of the 29 known compounds in this field, most contain the monothiophosphate $[PO_3S]^{-3}$ or dithiophosphate $[PO_2S_2]^{-3}$ anions.[17-20] Only two examples of the trithiophosphate $[POS_3]^{-3}$ anion are known,[17,21] but calculations have shown it to be stable toward disproportionation into $[PS_4]^{-3}$ and $[PO_2S_2]^{-3}$.[22] Subsequent experiments though have shown that the trithiophosphate anion is capable of disproportionation.[23]

One motivation to explore the family of the oxythiophosphates, is to probe the differences and similarities with the all oxygen $[PO_4]^{3-}$ and all sulfur $[PS_4]^{3-}$ containing analogues in a given system. Each of these end members to the series,$[PO_xS_{4-x}]^{3-}$, have been widely investigated in the inorganic and solid state literature, while the bridging family of the oxythiophosphates remains conspicuously absent from much of the inorganic and solid state literature (see Table 1-1).

Of course, the most desirable result of any project in materials chemistry would be to produce a new and technologically useful material. Therefore, one might ask, "Why might oxythiophosphates be useful as materials?" To answer that question, the number of useful phosphate and tetrathiophosphate materials should be considered.

Table 1-1: Known oxythiophosphates and dates of first report.

Compound	Year of Earliest Report	Reference
$Na_3PO_3S \cdot 12H_2O$	1847	49
$Na_3PO_2S_2 \cdot 11H_2O$	1885	17
$Na_3POS_3 \cdot 11H_2O$	1885	17
α-Na_3PO_3S [a]	1940	24
$Mn_3(OH)_2P_2O_6S_2 \cdot H_2O$	1949	25
KH_2PO_3S	1965	26
$Na_4P_4O_8S_4 \cdot 6H_2O$	1979	27
$Cs_4P_4O_8S_4$	1979	27
$(NH_4)H_2PO_3S$	1983	28
$(NH_4)_2HPO_3S$	1983	28
$Sr_2P_4O_8S_4 \cdot 10H_2O$	1989	29
$Ba_2P_4O_8S_4 \cdot 10H_2O$	1989	29
$Mg_2P_4O_8S_4 \cdot 10H_2O$	1989	29
$Ca_2P_4O_8S_4 \cdot 10H_2O$	1989	29
$LaPO_2S_2 \cdot 5.5H_2O$	1991	20
$NdPO_2S_2 \cdot 5.5H_2O$	1991	20
$K_3P_3O_6S_3$	1992	30
$Cs_3P_3O_6S_3$	1992	30
$Rb_3P_3O_6S_3 \cdot 2H_2O$	1992	30
$((CH_3)_3Sn)_3PO_3S$	1993	31
$BaH_2P_2S_3O_6 \cdot C_2H_5OH$	1994	33
$[Co(C_2H_8N_2)_2Cl_2]H_3P_2S_2O_6$	1994	32
$[Co(C_2H_8N_2)_2Cl(H_2O)]H_3P_2S_2O_6 \cdot H_2O$	1994	33
$Ca_3(PO_xS_{4-x})_2$	1997	34
$Zr(HPO_3S)_2 \cdot 1.5H_2O$	2000	19
$Hf(HPO_3S)_2 \cdot 1.5H_2O$	2000	19
$(C_5H_5NH)H_2PO_3S$	2000	35
$Na_3PO_2S_2$	2003	23
Na_3POS_3	2003	21

[a] The polymorphism of Na_3PO_3S had not yet been discovered at the date of this report; the α designation is now added to distinguish it from other phases.

Several phosphate based materials are used or are being developed as lithium ion battery cathodes,[36] cement additives,[37] bone replacements,[38] ion-exchange materials,[39] and non-linear optical (NLO) materials,[40] just to name a few; and tetrathiophosphate materials also show promising properties of non centrosymmetry,[41] lithium ion conductivity,[42] and photoluminescence.[43]

The chemical substitution of sulfur for oxygen, which distinguishes an oxythiophosphate from an orthophosphate, necessarily results in an alteration of the observed chemical properties. However, oxythiophosphates can, at least in some cases, mimic the structure of a related orthophosphate phase. (Examples of this will be presented later.) Therefore a structure with desirable properties may be targeted in the development of new oxythiophosphates, but its properties should be different from the "inspirational" orthophosphate. Whether such a change will improve the desired property or not will remain to be seen on a case-by case basis.

Such property modifications may be exploited for use in ion-exchange materials, which are in demand due to the proliferation of contaminated water sources, especially in developing nations.[44,45] Criteria defining the utility of ion-exchange materials are that they accept and selectively bind heavy metal ions with both a high weight efficiency and high cost efficiency. In general, metal phosphates are highly insoluble in water, supporting the hypothesis that their "daughter" compounds, the oxythiophosphates, will be similarly insoluble in water. This insolubility is necessary for the removal of contaminants by a filtration system. Furthermore, the soft base character of the substituted sulfur moiety should increase selectivity for heavy metals.

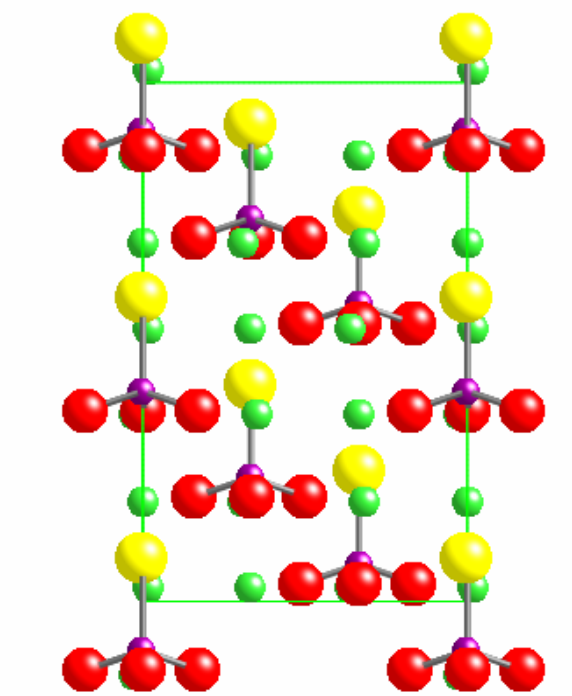

Fig. 1-1: The crystal structure of sodium monothiophosphate taken from the ICSD. (ICSD# 412368) [46] Oxygen is red; phosphorus is purple, sulfur is yellow; sodium is green.

Noncentrosymmetric NLO materials are also of technological interest due to their ability to double the frequency of a given light source, an effect known as second harmonic generation (SHG).[47,48] For instance, the light from a Nd:YAG laser producing light of wavelength 1064 nm (IR) may be frequency doubled to 532 nm (green). Applications for this process are in tunable lasers. The presence of a noncentrosymmetric building block, such as the monothiophosphate anion, may enhance the probability of creating materials which are also crystallographically noncentrosymmetric. One example of a noncentrosymmetric oxythiophosphate material is Na_3PO_3S [68] (see Fig. 1-1). Although the monothiophosphate anion itself is noncentrosymmetric, it is the packing of these anions in the crystal structure which creates a bulk noncentrosymmetric structure.

3. The Early History of Oxythiophosphates (1847-1940)

The history of the oxythiophosphates is interesting to note, since their discovery actually predates that of the first tetrathiophosphate material. The first report of the synthesis of an oxythiophosphate material dates to 1847 in an article by Wurtz.[49] Since this paper predates acceptance of Avogadro's theory of molecular and atomic mass, the formulae presented to the reader are subject to scrutiny. Nonetheless, Wurtz describes the synthesis of sodium monothiophosphate hydrate (originally presented as $P(O^3S^2) \cdot 3NaO$)[a] by reaction of "detergent of sodium" (perhaps sodium oxide or, more likely, sodium hydroxide, presented as NaO) with "chlorosulfure of Sérullas" (possibly thiophosphoryl chloride, presented as $P(Cl^3S^2)$).[a] Interestingly, Wurtz sent a sample of his isolated crystals to a colleague for inspection. By careful examination of crystal habit (faces, angles, etc.) [50] de la Provostaye determined that $Na_3PO_3S{\cdot}12H_2O$ crystallized in a primitive rhombohedral motif, a fact which would not be proven until 1982, some 67 years after the acceptance of X-ray crystallography and 135 years after the compound's first discovery.[51]

[a] For the sake of historical accuracy, this formula appears as it did in the original publication with superscripts used where subscripts are currently accepted. The modern form of these chemical formulae might be approximately: $P(O_3S_2) \cdot 3NaO$ and $P(Cl_3S_2)$.

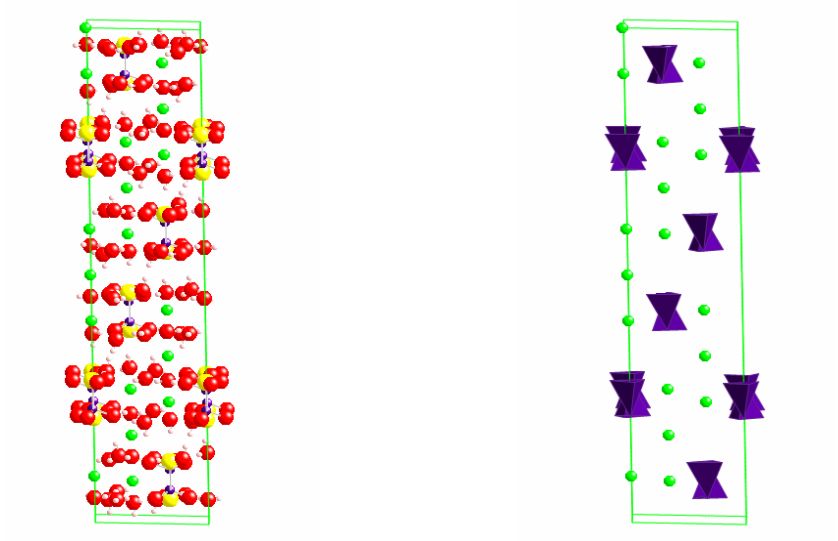

Fig. 1-2: Structure of $Na_3PO_3S \cdot 12H_2O$. Left: ball and stick model showing all atoms. Sodium is green; oxygen is red; phosphorus is purple, sulfur is yellow and hydrogen is pink. Right: polyhedral model showing only sodium atoms and disordered.$[PO_3S]^{3-}$ tetrahedra .

The structure of $Na_3PO_3S \cdot 12H_2O$ was eventually solved and found to be disordered with respect to the monothiophosphate anion (see Fig. 1-2). This disorder involves the orientation of the $[PO_3S]^{3-}$ tetrahedra. All of the $[PO_3S]^{3-}$ tetrahedra are aligned with the P-S bond along the c-axis, however half are oriented in one direction, while half are oriented in the opposite direction. The body centers of each of these were

orientations falls on the same position. This overlap of various orientations on a single position is what leads the structure being described as disordered. If only a single orientation set would be chosen to visualize the structure, and the waters of hydration removed, one would quickly and easily see the relationship between the structure of the hydrated phase and that of the anhydrous phase, α-Na_3PO_3S.

The next reported syntheses of oxythiophosphates occurred in a paper written by C. Kubierschky in 1885 on the synthesis of the hydrates of sodium monothiophosphate ($Na_3PO_3S \cdot 12H_2O$), sodium dithiophosphate ($Na_3PO_2S_2 \cdot 11H_2O$) and sodium trithiophosphate ($Na_3POS_3 \cdot 11H_2O$).[17] The method used in this preparation involves the hydrolysis of P_4S_{10} in solutions of sodium hydroxide with subsequent fractional crystallizations. Kubierschky describes how the isolated sodium trithiophosphate may be further hydrolyzed to produce the sodium dithiophosphate, which may be isolated or further hydrolyzed to form sodium monothiophosphate. The observation of iterative hydrolysis coupled with the fact that the solids obtained are hydrates may leave room for some speculation as to the purity of the materials isolated. Nonetheless, the materials isolated were examined by elemental analysis (the techniques common to this time period are not explicit), and found to be acceptably close to the calculated values.

The literature on oxythiophosphates again becomes silent, this time for 65 years, until Zintl and Bertram reported the high temperature synthesis of anhydrous sodium monothiophosphate.[24] The synthesis reported is quite simplistic; $NaPO_3$ is heated with Na_2S to between 450 and 750° C. As part of their work-up, however, an aqueous recrystallization is employed, causing the final isolated product to be the same hydrate as previously reported.

4. The Recent Literature (1965-2008)

Research into the field of oxythiophosphate materials has increased over the last several decades to an average rate of less than one new material per year. This extraordinarily slow growth rate has left this vein of materials chemistry only 29 isolated

and characterized materials. On the other hand, this very small body of work in the literature has allowed this current project plenty of synthetic real estate to explore.

4.1 KH_2PO_3S (1965)

The synthesis of KH_2PO_3S is worthy of a brief discussion, as it is synthesized by a rather counterintuitive process.[26] The authors of the first publication on this material were actually attempting to prepare potassium disulphanediphosphonate, $K_4O_3PSSPO_3$. Using an established method to oxidize monothiophosphate to disulphanediphosphonate, they attempted to precipitate this anion from aqueous solution in the presence of potassium ions. Rather than forming the expected material, they instead crystallized KH_2PO_3S. This paper goes on to note that KH_2PO_3S decomposes in the presence of water at 100° C to form KH_2PO_4 and H_2S, and that it disproportionates between 200 and 400° C forming H_2S and KPO_3. Here then is an example of an oxythiophosphate being formed spontaneously from another oxythiophosphate, but both seem chemically fragile and prone to decomposition.

4.2 Tetrathiocyclotetraphosphates (1979-1989)

The crystal structures of $A_4P_4O_6S_4{\cdot}nH_2O$ and $AE_2P_4O_6S_4{\cdot}nH_2O$ [29] (where A is an alkali metal, AE is an alkaline earth cation and n = 0, 6, 10) were determined between 1979 and 1989 by a group of Russian researchers.[27,29,52] This work established the structure of the tetrathiocyclotetraphosphate anion,$[P_4O_6S_4]^{4-}$, as being planar with respect to the phosphorus ring. This structure can be described as a ring of PO_3S tetrahedra, which are connected by corner-shared oxygen atoms. The sulfur atoms are exclusively located at terminal positions on the ring (see Fig. 1-3). Unfortunately,

Fig. 1-3: The structures of the tetrathiocyclotetraphosphate (left) and trithiocyclotriphosphate (right) anions. Phosphorus is purple; oxygen is red; sulfur is yellow. Note that sulfur is not bridging in either anion.

chemical characterization was limited to infrared and thermal decomposition, so generalities regarding the reactivity of these materials cannot be made.

4.3 Ionic conductivity of $Na_3PO_xS_{4-x}$ (1980-2003)

A commonly cited motive to study the chemistry of the monothiophosphate anion, in this work, is the potential that substitution of sulfur into the simplistic $[PO_4]^{3-}$ tetrahedron may allow modification of the observed properties. This ability to tune properties is widely coveted in solid state chemistry as a means to obtain materials with specific, desirable, technologically useful properties. Jansen et al. demonstrated, over the course of a decade, that sulfur substitution into the phosphate anion is an effective means of changing, at least some, of the properties observed.

Jansen and Pompetzki synthesized all integer members of the series $Na_3PO_xS_{4-x}$ (x = 0-4). They then determined the crystal structure of all but one of these materials from powder diffraction data.[21,23,53-57,68] The hypothesis put forth by Jansen et al. was that the ionic conductivity of the series $Na_3PO_xS_{4-x}$ would increase with each incremental substitution of sulfur, and that the activation energy would concomitantly

decrease. This idea was based upon the idea that higher anionic polarizability would lead to higher cationic conductivity.

In their final paper on the subject,[23] the authors were able to validate their hypothesis with the addition of a caveat. The five integer members of the series $Na_3PO_xS_{4-x}$ were found to exist in three different structure types. If the contribution of structure type is not considered, the activation energy of the ionic conductivity does indeed follow this trend with the singular exception of Na_3PO_3S. If one only compares materials of similar structure types, then the ionic conductivity can be ranked as: $Na_3PO_4 > Na_3PS_4$ and $Na_3PO_2S_2 > Na_3POS_3$. Na_3PO_3S cannot be compared to another member of the series, as it is not isotypic with any other member of the series. The individual structures of the materials were also found to play a critical role on the ionic conductivities, but the predicted trend was found to be generally supported.

A singular criticism of this work is that the synthetic method employed was based on the hydrolysis of P_4S_{10} reported by Kubierschky.[17] As discussed earlier, this method yields a crystalline hydrated phase, which may or may not continue to hydrolyze in the solid state (anecdotal evidence of the smell of H_2S emanating from the hydrated material is suggestive of decomposition). The method used by Jansen et al. to dehydrate these materials was reported as freeze drying, but no specific details were given. This series of reports cannot, therefore, be considered to be above reproach, but does, nonetheless, represent the highest quality of the oxythiophosphate literature.

4.4 $LnPO_2S_2 \cdot 5.5\ H_2O$ (Ln = La, Nd) (1991)

A group of Russian researchers were able to synthesize $Ln(PO_2S_2) \cdot 5.5H_2O$, (where Ln = La, and Nd) [20] (see Fig. 1-4). This structure is interesting for its one-

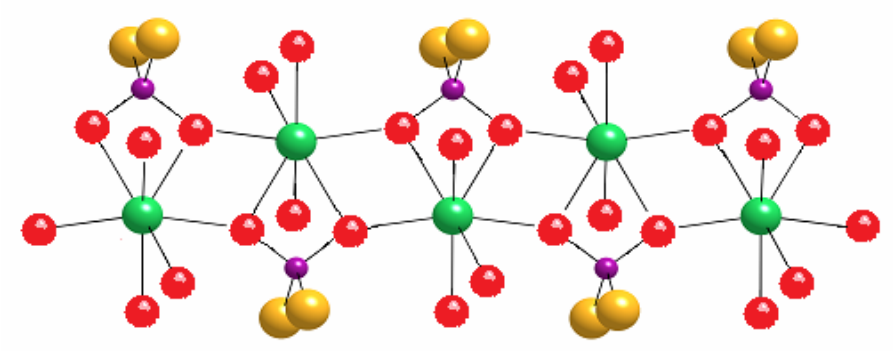

Fig. 1-4: The one-dimensional structure of $Ln(PO_2S_2) \cdot 5H_2O$. *Ln* = La, Nd or Pr. Phosphorus is purple; Sulfur is yellow; Ln is green; oxygen is red. Hydrogen atoms have been omitted for clarity.[20]

dimensional chains of $Ln(PO_2S_2)$, which run parallel to [111], and the pronounced hard/soft base preference of the lanthanide cation. Each of the lanthanide atoms in this structure exist in a 9-coordinate geometry and are exclusively contacted by oxygen atoms. These oxygens originate from 3 coordinated waters and three dithiophosphate anions. Each oxygen of any given dithiophosphate anion is coordinated to two lanthanide atoms. The two sulfur atoms of each dithiophosphate anion are uncoordinated. $Ln(PO_2S_2) \cdot 5.5H_2O$ is an example of a cation exhibiting oxophillic/chalcophillic discrimination. This structure clearly shows that the hard acid lanthanide ion would prefer to be coordinated by the hard base oxide ion, and particular attention should be paid to the fact that the oxygen and sulfur are not found to be disordered.

Both $LnPO_2S_2 \cdot 5.5H_2O$ structures were found to be monoclinic. While one of the two known phosphate structures of the early lanthanides is also found to be monoclinic,[58] the two structures are not related. In this case then, one may draw the conclusion that substitution of the dithiophosphate anion for the orthophosphate anion caused a change in structure. The question may then be posed: *How would substitution of*

the monothiophosphate anion affect the structure? Would a new structure be formed, or might it mimic the structure of the lanthanide dithiophosphate or one of the lanthanide orthophosphates? This very question shall be the focus of Chapter 4.

4.5 $[(CH_3)_3Sn]_3PO_3S$ (1993)

For comparison with other related compounds, Shihada successfully prepared $[(CH_3)_3Sn]_3PO_3S$, or tris (trimethyltin) monothiophosphate.[31] The material was prepared by precipitation from aqueous solution by reaction of trimethyltin chloride with an aqueous solution of sodium monothiophosphate. The analogous tris (trimethyltin) phosphate also was prepared. Shihada makes particular note that, "Rapid filtration of the product should be carried out to avoid the hydrolysis of the thiophosphate [sic] to the corresponding phosphate." This note represents a recurring theme in the chemistry of the oxythiophosphates: hydrolysis and decomposition. Further characterization revealed that the sulfur of the monothiophosphate anion was selectively coordinated to tin and was not observed to display IR or raman vibrations which would indicate a free P-S group. This indicates that the sulfur is selectively binding to tin whenever possible, giving another example of hard/soft acid/base discrimination in the oxythiophosphate system. During the synthesis, the phosphate material did not immediately precipitate from solution as the monothiophosphate did, however crystals of the phosphate could be grown. Unfortunately, neither the tris (trimethyltin) monothiophosphate powder, nor the tris (trimethyltin) phosphate crystals were structurally characterized by diffraction methods, so the crystallographic structures of these seemingly related materials remains unknown.

4.6 Nanoparticulate $Ca_3(PO_xS_{4-x})_2$ (1997)

Nanoparticles are a very popular topic in current research, and research into this field has even reached the rarely explored family of the oxythiophosphates. The formation of calcium oxythiophosphates was reported in 1997, in an uncontrolled stoichiometry of $Ca_3(PO_xS_{4-x})_2$.[34] The term uncontrolled is used since each of the anions: $[PO_4]^{3-}$ $[PO_3S]^{3-}$,$[PO_2S_2]^{3-}$,and $[POS_3]^{3-}$ were found in significant proportions in the final product. The colloidal product was formed by a reverse-micelle reaction between calcium hydroxide and a mixture of P_4S_{10} and P_4S_9 in organic media. The authors noted that the final product was a brown oily colloid. Transmission electron micrographs (TEM) and small angle X-ray scattering (SAX) revealed that the particles were spherical in shape and had an average particle size of 1.7 nm. The polydispersity of the nanoparticles was rather broad, with particles ranging in size between 1 and 8 nm. While the variable composition of the particles was prohibitive to making any determination of property alterations by quantum confinement effects, this paper did make an important, albeit implied contribution to the general knowledge of the chemistry of oxythiophosphates. A mixture of calcium oxythiophosphates is insoluble in the aqueous phase of the reverse micelle. This is important as it demonstrates that the exceedingly low aqueous solubility of calcium phosphate [59] is shared, at least to a significant extent, by other members of the series $[PO_xS_{4-x}]^{3-}$. Such observations allow one to make predictions regarding which synthetic conditions will be more likely to produce new oxythiophosphate materials in the future.

4.7 $H_2Zr(PO_3S)_2 \cdot 1.5H_2O$ and $H_2Hf(PO_3S)_2 \cdot 1.5H_2O$ (2000)

As we have seen oxythiophosphates remained in relative obscurity with respect to materials applications for many, many years, and have received only the smallest fraction of the attention that has been bestowed on related compounds such as the phosphates and tetrathiophosphates. To our knowledge, only Dorhout et al. have synthesized an oxythiophosphate material with a specific application and rational design in mind.[19,60]

It has been previously shown that a metal's hard/soft acid/base preferences might affect the manner in which an oxythiophosphate binds to a given metal. Dorhout et al. made use of this selectivity to design an oxythiophosphate material which would mimic the general structural motif of the related orthophosphate material.

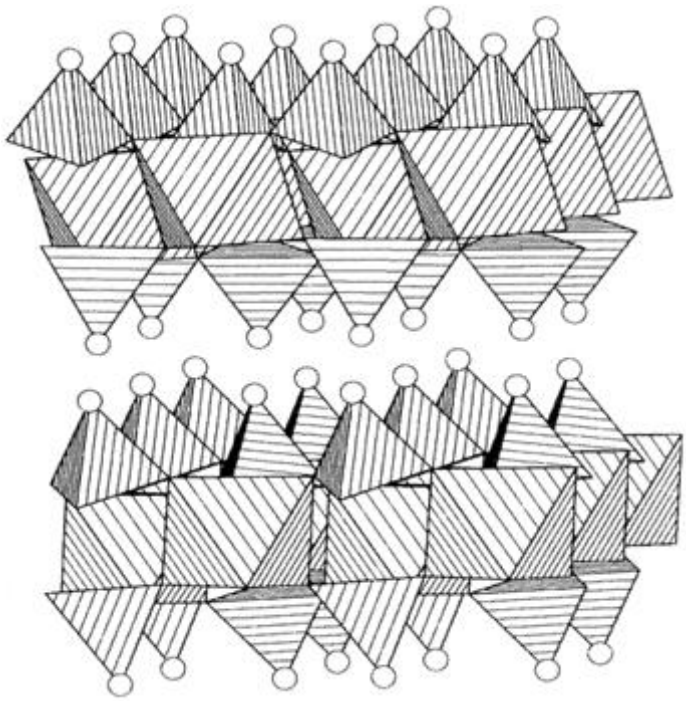

Fig. 1-5: The proposed structure of $H_2Zr(PO_3S)_2$ as adapted from Dorhout et al.[19] Open circles at tetrahedral apices represent the S^{2-} anion.

In 1964, Stynes reported that the structure of $H_2Zr(PO_4)_2$ was a layered structure,[39] in which zirconium was ligated by two phosphate groups in an octahedral fashion. The uncoordinated apices of the phosphate groups were found to be protonated as a means of maintaining charge neutrality. This material was also shown to be capable of ion exchange with hard cations, such as potassium and calcium. Later, Dourhout, et al. reported that the structure of $H_2Zr(PO_3S)_2$ was layered, as well [19] (see Fig. 1-5). They found that this material was also able to ion exchange, with typically softer, more toxic ions, such as zinc and cadmium. This example has encouraged the prospect that new ion-exchange materials may be intelligently designed and optimized based on the structures of known phosphate "parent compounds".

5. Dimerization

The aqueous chemistry of the monothiophosphate anion has also been moderately explored. In several studies, the monothiophosphate anion was found to form a new disulfide bond by formation of the $[O_3PSSPO_3]^{4-}$ dimer,[26,32,33,61] also known as the disulfanediphosphonate ion. Ferricyanide can be reduced by the monothiophosphate anion under sufficiently basic conditions, (pH 5-13).[61] Under sufficiently acidic conditions, (5 to 0.1M HCl) the same dimer could also be formed by allowing $[PO_3S]^{3-}$ to reduce iodine to iodide, which was detected as I_3^-. (In 0.1M HCl, the dimer was found to oxidize further yielding elemental sulfur.). These findings clearly demonstrate both the flexibility of the monothiophosphate reaction system as well as its intrinsic disadvantage of potential decomposition, a disadvantage shared by many, if not all, of the oxythiophosphate anions.

Papers on the structures of the disulfanediphosphonate and the related trisulfanediphosphonate ions were published by Janickis and Marøy.[32,33] These ions have the general connectivity of $[O_3PS_nPO_3]^{4-}$. When n=2, the disulphanediphosphonate ion is formed, which is the oxidation product formed by reaction of monothiophosphate with iodine or ferricyanide under sufficiently acidic conditions. While the synthetic methods employed were largely replications of the work of others, several of the materials reported were novel, but no further characterization was offered. The publications were limited in scope, reporting only the crystallographic structures of the materials. These studies also afforded the structure of KH_2PO_3S, to be discussed later.

6. Decomposition under acidic conditions

The sensitivity of the monothiophosphate anion under oxidizing conditions has already been noted [25] but, anecdotal evidence might well also be discussed. When sodium monothiophosphate is dissolved in neutral or acidic solutions, one cannot help but to instantly note the smell of rotten eggs emanating from the fresh solution. This smell is characteristic of dihydrogen sulfide, H_2S. The rate of decomposition need not be fast for detection by smell to take place, as the human nose is sensitive to H_2S down to the level of 0.02ppm.[62] At such low levels of sensitivity, it could be argued that acidic decomposition may actually be a quite slow process; however, one must recognize that it is occurring and take steps to either avoid or minimize it.

7. Electrochemistry

The electromotive force (EMF) of the oxidation of $[PO_3S]^{3-}$ to $[O_3PSSPO_3]^{4-}$ at a platinum electrode was found to be ~0.0V relative to a normal hydrogen electrode (NHE) at neutral pH.[63] The relationship between EMF and pH was generally linear from pH =

1 to 11, with the EMF ranging from 0.35 to -0.2V relative to NHE. This process was also found to be electrochemically reversible. This research also uncovered that the EMF of the oxidation was affected by the presence of oxygen above pH = 6. The authors did not investigate or speculate as to the role that oxygen played in this alteration of the EMF measurements. What one would expect to be innocuous spectator ions present in solution also had a large impact on the oxidation. A simple substitution of potassium counterions for sodium counterions in the buffer solution reduced the rate constants by 50%, but the rate constant was found to vary little with temperature between 25 and 40° C. The overriding conclusion to be found in this study is that the dimerization of monothiophosphate is very sensitive to the minutia of a reaction system.

8. Biochemical studies

Several biochemical studies have taken advantage of the monothiophosphate anion for various reasons. For instance, sodium monothiophosphate has been used as a reducing agent to destroy neutral disulfide bonds, or form new anionic disulfide bonds. In a study of the partial opening of disulfide bonds in ribonuclease and lysozyme,$[PO_3S]^{3-}$ was able to reduce neutral protein disulfide bonds by forming the $[RS\text{-}SPO]^{2-}$ species from the native RS-SR' bond.[63] This reactivity allowed researchers early insight into how the conformation of proteins may affect their biological activity.

Other biochemical investigations have made use of the monothiophosphate anion. For instance, the stereoselectivity of snake venom exonuclease by formation of Up(S)A and Up(R)A was determined in 1979 by Burgers and Eckstein.[64] Studies of the substitution of monothiophosphate into adenosine triphosphate (ATP) have also been made by Pecoraro et al.,[65] who were able to probe whether the prochiral nature of ATP

had any effect on metal binding by ATP. They concluded that indeed this prochiral nature did have an effect on metal binding.

9. General trends in the chemistry of oxythiophosphates

While the literature of the inorganic oxythiophosphates is sparse, one overwhelming theme is that in most of the structurally characterized materials, sulfur and oxygen have preferential binding characteristics and are not typically found to be randomly disordered. Examples of this effect include: KH_2PO_3S, $LnPO_2S_2 \cdot 5.5H_2O$,$[(CH_3)_3Sn]_3PO_3S$, $H_2Zr(PO_3S)$, and $H_2Hf(PO_3S)$. Furthermore, most of the successful reactions of oxythiophosphates occur in water. This conclusion may be a bit difficult to come to terms with as much of this introductory chapter has been dedicated to demonstrating the difficulty of working with the monothiophosphate anion in aqueous solutions. In fact, demonstrating that the monothiophosphate anion has not decomposed is a challenge that will characterize much of the remainder of this dissertation, as new materials are discovered and characterized. Furthermore, this paradoxical relationship with water will also recur several times as well, as the presence of small amounts of water makes possible two very unusual solid state reactions.

10. General acid/base properties

The acid/base properties of the monothiophosphate anion must be considered if any rudimentary comparison to the orthophosphate anion is to be debated. Previously, Na_3PO_3S was reported to have been titrated with 1M HCl.[61] These titration results showed that $pK_{b1} = 3.6$, $pK_{b2} = 8.25$ and $pK_{b3} > 12$. The values for the orthophosphate anion have been shown to be: $pK_{b1} = 1.62$, $pK_{b2} = 6.79$ and $pK_{b3} = 11.87$.[66] The comparison of these values demonstrate that at each base association, the

monothiophosphate anion is a weaker base than orthophosphate. This, of course must be linked to the sulfur substitution which gives rise to the distinct properties of the monothiophosphate anion; however, the reasons for this may be a little more convoluted.

An explanation of this aqueous acid base character may be derived from the crystal structures of α-Na_3PO_3S and KH_2PO_3S (see Fig 1-6). The structure of KH_2PO_3S has been solved by Janickis and Marøy.[32] The P-S bond length in this structure is 1.9681(7) Å; there is one P-O bond of 1.5244(16) Å and two other P-O bonds of 1.5754(11) Å. These two longer P-O bonds are found for the oxygen atoms which are also bonded to the two hydrogen atoms in the structure. In this structure, the two hydrogen atoms are selectively coordinated to oxygen. Thus it could be stated that interactions of hydrogen are preferentially directed toward oxygen.

The case could also easily be made that assignment of hydrogen atomic positions are often fallible and one should not therefore rush to hasty conclusions. The other bond lengths, however, can be used to make inferences about the bond order of the various bonds within the complex anion, by using the equation put forth by Altermatt and Brown.[67] This equation states that the bond order(s) is equal to the exponential of the unperturbed (singular) bond length minus the observed bond length divided by an empirical constant B, having a value of 0.37.

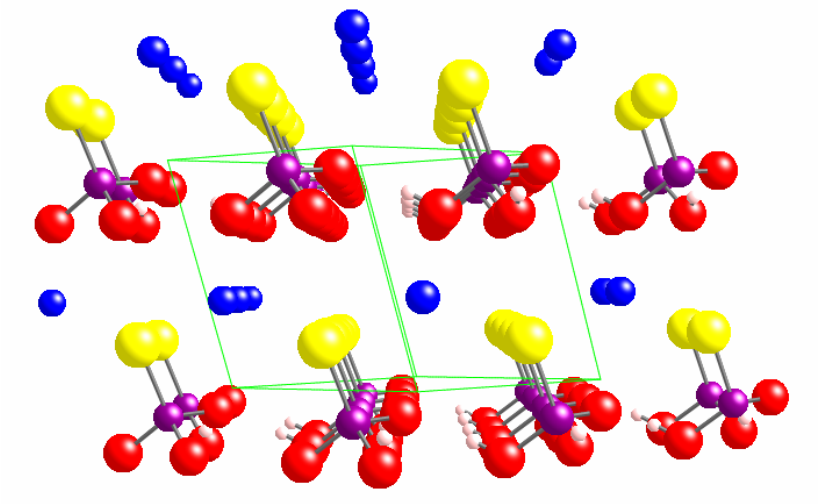

Fig. 1-6: The crystal structure of KH_2PO_3S.[32] K is blue; P is purple; O is red; S is yellow; H is pink.

$$s = \exp[(r_o - r)/B] \qquad \text{Eq. 1-1}$$

Substituting r_o and B with the experimentally observed bond distances, the P-S bond has a bond order of 1.61 and the P-O bonds have one bond order of 1.28 and two of 1.12. Summing these reveals a total of 5.13 bonds on phosphorus. Repeating the same calculation on the experimentally observed α-Na_3PO_3S bond distances (three P-O distances 1.513(1)Å and the P-S distance 2.112(1)Å), the P-S bond has a bond order of 1.09 and the three P-O bonds each have a bond order of 1.32. Summing these reveals a total of 5.05 bonds on phosphorus, which is close to the anticipated value of 5.

These calculations are based, however, on the critical assumption that P is in the 5+ oxidation state and that both sulfur and oxygen are in the 2- oxidation state. The nature of the calculation serves as a check that the oxidation state assignment is correct. If the oxidation assignment is correct, the sum of the bond valences should equal the assigned oxidation state of the central atom.[67] The close agreement in the case of Na_3PO_3S shows that indeed the assignment of P^{5+}, O^{2-} and S^{2-} are appropriate in this case.

The greater discrepancy in the case of KH_2PO_3S may be due to the bonding of two hydrogen atoms onto the $[PO_3S]^{3-}$ anion. This slightly covalent interaction effectively removes a small amount of electron density from the P-O bond. The case can therefore be made that the bond orders of O and S change in response to the immediate coordination sphere based on this data.

The original question at hand was why the monothiophosphate anion should be a weaker base than orthophosphate. First, let us consider that hydrogen interactions with the monothiophosphate anion seem to favor oxygen coordination. Second, let us consider the P-O bond order of the naked monothiophosphate anion as in α-Na_3PO_3S. The P-O bond order is 1.38, significantly higher than the ideal P-O bond order of 1.20 in orthophosphate. Thus, at the preferred site of coordination, orthophosphate has significantly more undedicated electron density to share with an encountered hydrogen ion than does monothiophosphate, making monothiophosphate a weaker base.

11. Conclusions

Oxythiophosphates offer a unique opportunity to materials science and to solid state chemistry. The structure/property and composition/property relationships can be explored in new ways using this system as a model. The substitution of sulfur into a phosphate material should produce changes in chemical properties, while the structure of the material may or may not remain effectively unaltered. An opportunity to resolve these competing factors is not often found.

Over the course of this dissertation, it will be demonstrated that the determination of the crystal structure of α-sodium monothiophosphate,[68] its effective use as a reagent in the formation of a new material,[19] as well as the short list of academic studies

previously mentioned have brought new life, interest and potential to this family of complex anions. This family of anions may allow the development of materials with tunable properties, or simply the opportunity to explore a chemical system which has remained largely overlooked for more than a century.

References

[1] E. Matejevic, Pure Appl. Chem. 60 (1988) 1479-1491.

[2] S. Schweizer, A. Taubert, Macromol. Biosci. 7 (2007) 1085-1099.

[3] G. Demazeau, J. Mater. Sci. 43 (2008) 2104-2114.

[4] K. Byrappa, T. Adschiri, Prog. Cryst. Growth Ch. 53 (2007) 117-166.

[5] M. J. Davis, M. D. Smith, K. E. Stitzer, H.-C. zur Loye, J. Alloy Compd. 351 (2003) 95-100.

[6] R. G. Blair, A. Anderson, R. B. Kaner, Chem. Mater. 17 (2005) 2155-2161.

[7] T. K. Mandal, J. Gopalakrishnan, J. Mater. Chem. 14 (2004) 1273-1280.

[8] Solid State Chemistry and Its Applications, A. West, J. Wiley (2004) New York.

[9] A. Clearfield, A. Bortun, S. Khainakov, L. Bortun, V. Strelko, V. Khryaschevskii, Waste Manag. 18 (1998) 203-210.

[10] A. A. Belik, B. I. Lazoryak, K. V. Pokholok, T. P. Terekhina, I. A. Leonidov, E. B. Mitberg, V. V. Karelina, D. G. Kellerman, J. Solid State Chem. 162 (2001) 113-121.

[11] I. Parreu, J. Gavaldà, J. Massons, F. Díaz, M. Aguiló, Chem. Mater. 15 (2003) 5059-5064.

[12] W. Tong, G.-G. Xia, Z.-R. Tian, J. Liu, J. Cai, S. Suib, J. Hanson, Chem. Mater. 14 (2002) 615-620.

[13] M. G. Kanatzidis, Curr. Opin. Solid. St. M. 2 (1997) 139-149.

[14] G. Ouvrard, R. Brec, J. Rouxel, Mater. Res. Bul. 20 (1985) 1181-1189.

[15] M. Evain, R. Brec, M.-H. Whangbo, J. Solid St. Chem. 71 (1987) 244-262.

[16] E. Prouzet, G. Ouvrard, R. Brec, Solid St. Ionics 31 (1988) 79-90.

[17] C. Kubierschky, J. Prakt. Chem. 31 (1885) 93-111.

[18] P. K. Dorhout, Abstr. Pap. Am. Chem. Soc. 223 (2002) 683-CHED Part 1.

[19] A. E. Gash, P. K. Dorhout, S. H. Strauss, Inorg. Chem. 39 (2000) 5538-5546.

[20] K. Palkina, S. Maksimova, N. Chibiskova, T. Tripol'skaya, G. Wolf, T. Kuvshinova, Neorg. Mater. 27 (1991) 1028-1031.

[21] M. Pompetzki, M. Jansen, Z. Anorg. Allg. Chem. 629 (2003) 1929-1933.

[22] W. Brockner, B. Jendrzok, F. Menzel, V. Jensen, M. Ystenes, J. Molec. Struc. 319 (1994) 85-100.

[23] M. Pompetzki, R. E. Dinnebier, M. Jansen, Solid State Sci. 5 (2003) 1439-1444.

[24] E. Zintl, A. Bertram, Z. Anorg Allg. Chem. 245 (1940) 12-15.

[25] E. Thilo, E. Schone, Z. Anorg. Chem. 259 (1949) 225-232.

[26] F. Fehér, F. Vial, Z. Anorg. Allg. Chem. 335 (1965) 113-125.

[27] G.-U. Vol'f, M. Meisel, Neorg. Mater. 15 (1979) 953-956.

[28] H. Grunze, Z. Chem. 23 (1983) 138.

[29] T. B. Kuvshinova, G.-U. Vol'f, T. N. Kuz'mina, M. S. Pautina, Neorg. Mater. 25 (1989) 1349-1355.

[30] K. K. Palkina, S. I. Maksimova, N. T. Chibiskova, M. S. Pautina, G.-U. Vol'f, T. B. Kuvshinova, Neorg. Mater. 28 (1992) 1486-1490.

[31] A.-F. Shihada, Z. Naturforsch. 48b, (1993) 1781-1783.

[32] V. Janickis, K. Maróy, Acta Chem. Scan. 48 (1994) 461-464.

[33] V. Janickis, K. Maróy, Acta Chem. Scan. 48 (1994) 465-470.

[34] B. Delfort, A. Chivé, L. Barré, J. Colloid Interf. Sci. 186 (1997) 300-306.

[35] B. Ziemer, A. Rabis, Acta Cryst. C56 (2000) e94.

[36] R. Ruffo, R. A. Huggins, C. M. Mari, M. Piana, W. Weppner, Ionics 11 (2005) 213-219.

[37] D. M. Wellman, K. E. Parker, S. v. Mattigod, G. E. Fryxell, Res. Lett. Mater. Sci. (2008) Article ID 238736

[38] B. I. Beletskii, V. I. Shumskii, A. A. Nikitin, E. B. Vlasova, Glass Ceram+ 57 (2000) 322-325.

[39] A. Clearfield, J. A. Stynes, J. Inorg. Nucl. Chem. 26 (1964) 117-129.

[40] J. Wang, J. Wei, Y. Liu, X. Yin, X. Hu, Z. Shao, M. Jiang, Prog. Cryst. Growth Ch. 40 (2000) 3-15.

[41] J. A. Aitken, M. G. Kanatzidis, Inorg. Chem. 40 (2001) 2938-2939.

[42] H.-J. Deiseroth, S.-T. Kong, H. Eckert, J. Vannahme, C. Reiner, T. Zaiss, M. Schlosser, Angew. Chem. Int. Edit. 47 (2008) 755-758.

[43] Z. Huang, V. B. Cajipe, B. Le Rolland, P. Colombet, W. J. Schipper, G. Blasse, Eur. J. Sol. State Inor. 29 (1992) 1133-1144.

[44] T. Clarke, Nature Sci. Update. (June 25, 2003) http://www.nature.com/nsu/030623/030623-7.html

[45] F. R. Seigel, J. Geochem. Explor. 55 (1995) 265-273.

[46] M. Pompetzki, M. Jansen, Z. Anorg. Allg. Chem. 628 (2002) 641-646.

[47] S. Yamada, I.-Y. S. Lee, Anal. Sci. 14 (1998) 1045-1051.

[48] G. D. Boyd, A. Ashkin, J. M. Dziedzic, D. A. Kleinman, 137 (1965) 1305-1320.

[49] M. A. Wurtz, Ann. Chim. Phys. 3 (1847) 472-482.

[50] M. F. de la Provostaye, Ann. Chim. Phys. 3 (1847) 481.

[51] B. M. Goldstein, Acta Cryst. B38 (1982) 1116-1120.

[52] V. V. Ilyukhin, V. R. Kalinin, T. B. Kuvshinova, Neorg. Mater. 24 (1988) 828-835.

[53] M. Jansen, U. Henseler, J. Solid State Chem. 99 (1992) 110-119.

[54] M. Witschas, H. Eckert, H. Freiheit, A. Putnis, G. Korus, M. Jansen, J. Phys. Chem. A 105 (2001) 6808-6816.

[55] D. M. Von Weich, M. Jansen, Z. Anorg. Allg. Chem. 461 (1980) 101-108.

[56] E. Lissel, M. Jansen, E. Jansen, G. Will, Z. Kristallogr. 192 (1990) 233-243.

[57] M. Pompetzki, L. van Wüllen, M. Jansen, Z. Anorg. Allg. Chem. 630 (2004) 384-388.

[58] H. Assaaoudi, A. Ennaciri, A. Rulmont, Vib. Spectrosc. 25 (2001) 81-90.

[59] The CRC Handbook of Chemistry and Physics 84th Ed., D. R. Lide Editor-in-Chief, CRC Press, Washington D.C., 2004.

[60] I. A. Stenina, A. D. Aliev, P. K. Dorhout, A. B. Yaroslavtsev, Inorg. Chem. 43 (2004) 7141-7145.

[61] H. Neumann, I. Z. Steinberg, E. Katchalski, J. Am. Chem. Soc. 87 (1965) 3841-3848.

[62] A. Khanna, R. Kumar, S. S. Bhatti, Appl. Phys. Lett. 82 (2003) 4388-4390.

[63] H. Neumann, I. Z. Steinberg, J. R. Brown, R. F. Goldberger, M. Sela, European J. Biochem. 3 (1967) 171-182.

[64] F. Eckstein, P. Burgers, Biochemistry 18 (1979) 592-596.

[65] V. L. Pecoraro, J. D. Hermes, W. W. Cleland, Biochem. 23 (1984) 5262-5271.

[66] T. L. Brown, H. E. Lemay, B. E. Bursten, Chemistry: The Central Science 8th Ed., Prentice Hall, Upper Saddle River, NJ, 2000.

[67] I. D. Brown, D. Altermatt, Acta Cryst. B 41 (1985) 244-247

[68] M. Pompetzki, M. Jansen, Z. Anorg. Allg. Chem. 628 (2002) 641-646.

Chapter 2

Sodium Monothiophosphate: More Than a Beginning [a]

Abstract:

Oxythiophosphate compounds, which contain anions comprised of oxidized phosphorus bound to oxygen and sulfur, are scarce and, in general, poorly characterized. Although α-Na_3PO_3S has been known for over a century, little has been revealed about this compound. Here we present thermal analysis and second harmonic generation efficiency of α-Na_3PO_3S. Details about its transformation to the high-temperature β-phase are discussed. Under vacuum, α-Na_3PO_3S undergoes one endothermic event at 553° C upon heating and two exothermic events at 504° C and 467° C upon cooling. β-Na_3PO_3S can be trapped upon quenching Na_3PO_3S from high temperature. We have observed that the β-phase converts back to the α-phase at room temperature. Interestingly, relative humidity has been determined to catalyze this phase transformation. α-Na_3PO_3S oxidizes at 315° C in air to produce $Na_4P_2O_7$ and Na_2SO_4. Upon exposure to 1064nm incident radiation, noncentrosymmetric α-Na_3PO_3S produces a second harmonic generation efficiency 200x that of α-quartz and is nonphase matchable (Type 1).

---

[a] Reproduced in part, with permission, from N. J. Takas, J. A. Aitken, Inorg. Chem. 45 (2006) 2779-2781.

1. Introduction

Metal oxythiophosphates are compounds that contain metals bound to anions comprised of oxidized phosphorus bonded to oxygen and sulfur. There are few oxythiophosphates reported in the literature, with less than thirty compounds published, to date [1-6]. Considering the outstanding structural diversity and myriad of useful applications that exist for the related metal phosphates and thiophosphates, such as ion-exchange [7-9], catalysis [10-12], batteries [13-15] and nonlinear optics [16-18], it is imperative to develop the almost nonexistent class of oxythiophosphates. Although the crystal structure of α-Na_3PO_3S has been solved using neutron powder methods [19], recent solid-state NMR experiments have introduced the possibility of disorder in this structure [20]. Although no direct structural information is offered in this

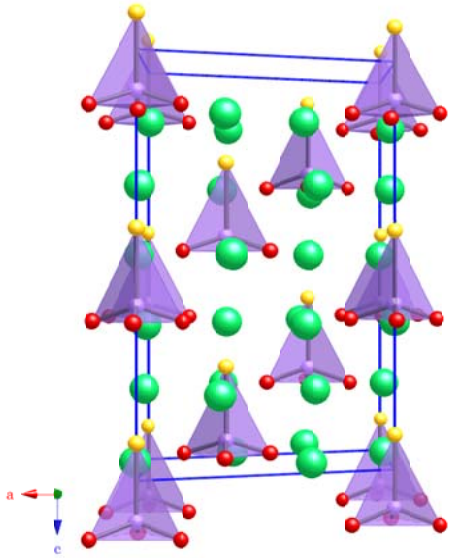

Fig. 2-1: The structure of α–Na_3PO_3S viewed down the crystallographic *b*-axis.[21] It is easy to see that the structure is noncentrosymmetric, since all of the tetrahedra point in the same direction along the *c*-axis. Sodium atoms are green; phosphorus atoms are purple; oxygen atoms are red and sulfur atoms are yellow.

report, indirect evidence confirming the noncentrosymmetry of the structure (see Fig. 2-1) is offered by the determination of the second harmonic generation (SHG) properties for the material. The thermal stability of the material in air as well as *in vacuo* is also presented.

β-Na_3PO_3S, previously reported by Jansen et al., can be trapped by quenching samples of Na_3PO_3S from high temperature [20]. We present the first report of a phase transition from the β-phase back to the α-phase at room temperature. Interestingly, this transition is catalyzed by atmospheric water, even though neither form of the material is hydrated.

Phase transitions catalyzed by atmospheric water are well known in the pharmaceutical literature [22-24]. These transitions most often involve conversions between anhydrous and hydrated states. A few transitions among anhydrous glasses and anhydrous crystalline states have also been reported. In these processes, adsorbed water acts as a plasticizing agent, which lowers the glass transition temperature, enhancing the molecular mobility to an extent that rapid recrystallization occurs [22,23]. Phase transitions between two anhydrous inorganic solid, crystalline phases catalyzed by relative humidity are exceedingly rare [25,26].

2. Experimental:

2.1 Synthesis

2.1.1 Synthesis of α-Na_3PO_3S

Initially, we planned to use α-Na_3PO_3S as a starting material to form new metal oxythiophosphates. We attempted to prepare α-Na_3PO_3S using solid-state reactions in

which the reactants were combined in stoichiometric proportions and heated (≤ 800° C) [27]. Although α-Na_3PO_3S formed, there were also impurities present as determined by powder X-ray diffraction (PXRD). Later, following the preparation method outlined by Yasuda and Lambert [28], a pure white microcrystalline material was obtained by a solution reaction to form the hydrate, which was subsequently dehydrated.

2.1.2 Synthesis of β-Na_3PO_3S

An experiment was performed to trap the high-temperature, β-phase of sodium monothiophosphate. Roughly 0.1g of α-Na_3PO_3S was sealed in a fused-silica tube and heated to either 600 or 650° C at a rate of 10° C/min in a Lindberg/Blue Minimite furnace, held at that temperature for one minute and cooled to 490º C at a rate of 10º C/min. The sample was allowed to equilibrate for ten minutes at 490º C. The fused-silica tube was removed from the furnace at 490º C and quenched in an ice water bath. PXRD was obtained.

2.2 Physical Measurements

2.2.1 Powder X-ray Diffraction (PXRD)

X-ray powder diffraction patterns were obtained on a Rigaku D/max-B, powder X-ray diffractometer in a Bragg-Brentano geometry, using graphite monochromated copper Kα radiation (1.5406 Å) and operating at 35kV and 22.5mA. Intensities were recorded with a scintillation detector. Samples were prepared by adhering the sample to double-stick tape over a glass specimen slide. All diffraction patterns were collected from 10 to 70° in 2θ using a step size of 0.024° at a scan rate of 1 to 2°/min.

2.2.2 Thermogravimetric Analysis (TGA)

Thermogravimetric analysis (TGA) was obtained on a Shimadzu TGA-50. The instrument was consistently operated in the 20mg sensitivity setting. TGA data were recorded using the Shimadzu TA60-WS collection program. Samples were ground and placed in Pt crucibles. All samples were heated at a rate of 10° C/min in air. TGA residues were routinely examined using PXRD.

2.2.3 Differential Thermal Analysis (DTA)

Differential thermal analysis (DTA) was obtained on a Shimadzu DTA-50. The differential signal was balanced prior to the beginning of each experiment. Data were recorded using the Shimadzu TA60-WS collection program. Experiments were performed at a rate of 10° C/min for the sample in air and 2° C/min for the sample under vacuum. Samples were contained in one of two ways: alumina pans or carbon coated fused-silica ampoules sealed under vacuum (~10^{-3}mbarr). All DTA samples were referenced against an alumina sample contained similarly and of comparable mass. Multiple heating and cooling cycles were performed in the DTA experiments to differentiate between reversible and irreversible thermal events. DTA residues were examined using PXRD.

2.2.4 Second Harmonic Generation (SHG)

Second harmonic generation of α-Na_3PO_3S was measured using a modified Kurtz NLO system using a Nd:YAG laser as a 1064 nm monochromatic light source. A Continuum Minilite II laser, operating at 15 Hz, was used for all measurements. The resulting SHG, i.e. green light of 532 nm, was collected by reflection and measured using

a photomultiplier tube in combination with a narrow band-pass filter. A phase matching experiment was also performed. The material was sieved into distinct particle size ranges: <20μm, 20-45μm, 45- 63μm, 63- 75μm, 75-90μm, 90- 106μm, 106- 125μm, 125- 150μm, and >150μm using WS Tyler stainless steel sieves. The SHG response was measured for each distinct particle size range in the same manner as the previously described bulk experiment.

3. Results and Discussion

Differential thermal analysis (DTA) under vacuum revealed that Na_3PO_3S undergoes no irreversible structural changes from room temperature to 650° C (Fig. 2-2). Three reversible thermal events were observed during the experiment: an endothermic event at 553° C upon heating, and two exothermic events at 504° C and 467° C upon cooling.

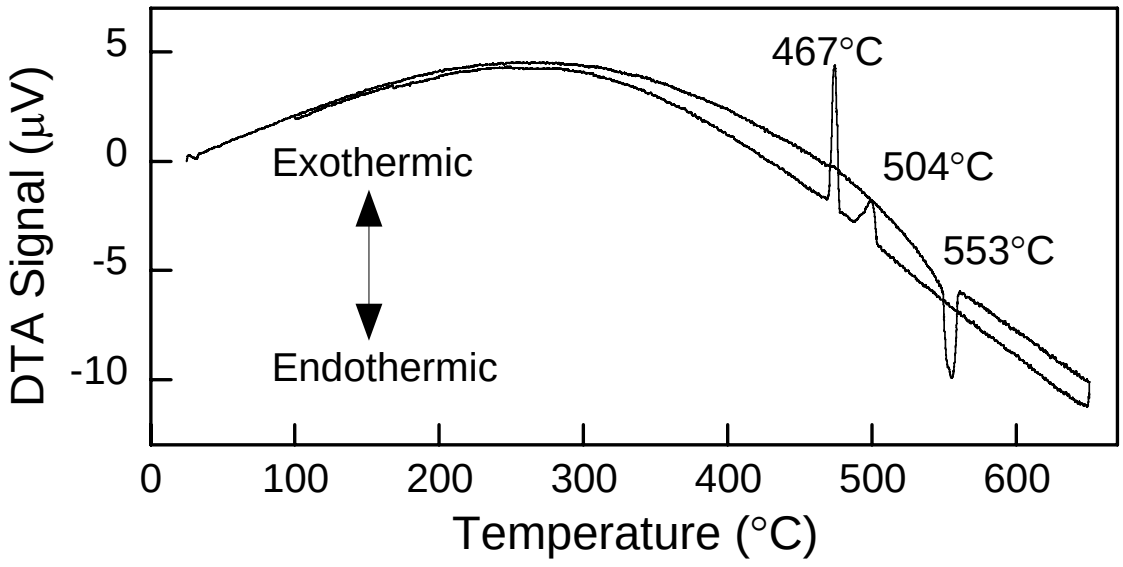

Fig. 2-2: Differential thermal analysis (DTA) diagram obtained for Na_3PO_3S under vacuum.

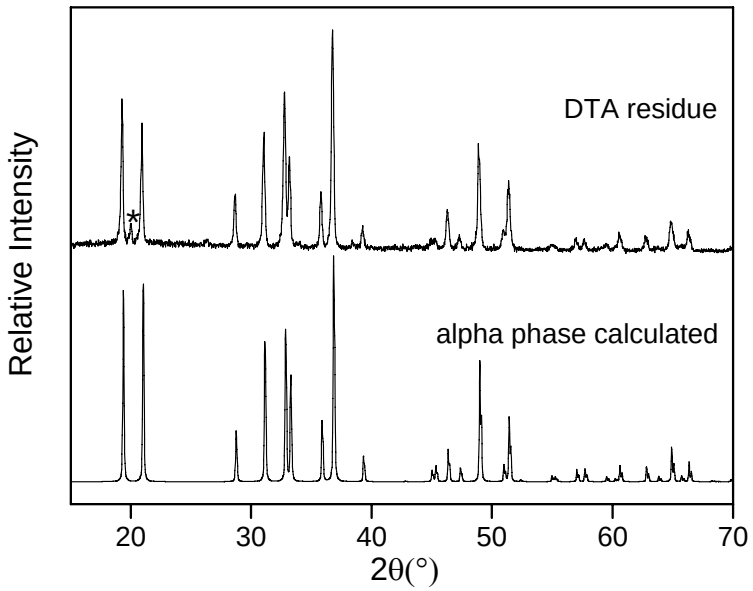

Fig. 2-3: Powder X-ray diffraction pattern of Na_3PO_3S after DTA in vacuum. The asterisk denotes a peak belonging to the β-phase.

PXRD of the DTA residue indicated the presence of α-Na_3PO_3S, as well as a minor amount of the β-phase.

Jansen et al. have reported the endothermic event to be a melting point based upon observation of the heating cycle in a differential scanning calorimetry experiment [21]. However, our observations of the material at high temperature and observation of the morphology of the material after quenching would tend to disagree with this assessment. At temperatures greater than 553° C, the sample appears as a sintered solid and has never been observed to take the shape of its container. The possibility that this endotherm may correspond to a transition to a γ-phase therefore cannot be excluded. It is clear to us, that the two exotherms correspond to the crystallization of the β- and α-phases respectively, based on the following data. Quenching Na_3PO_3S in an ice-water bath from 490° C demonstrated that the β-phase exists between 504 and 467° C. Slow

cooling of the sample (<10° C/min) yeilds only the α-phase. Quenches from temperatures between 600 and 650° C did not reveal the presence of a γ-phase by PXRD; only the β-phase could be observed. This suggests that *if* there is a γ-phase, it is highly unstable.

The first observation of a room-temperature phase transition from β- to α-Na_3PO_3S occurred serendipitously. Na_3PO_3S was quenched from 600° C into ice water, ground, and a PXRD of the trapped β-phase was obtained (see Fig. 2-4). After the PXRD was

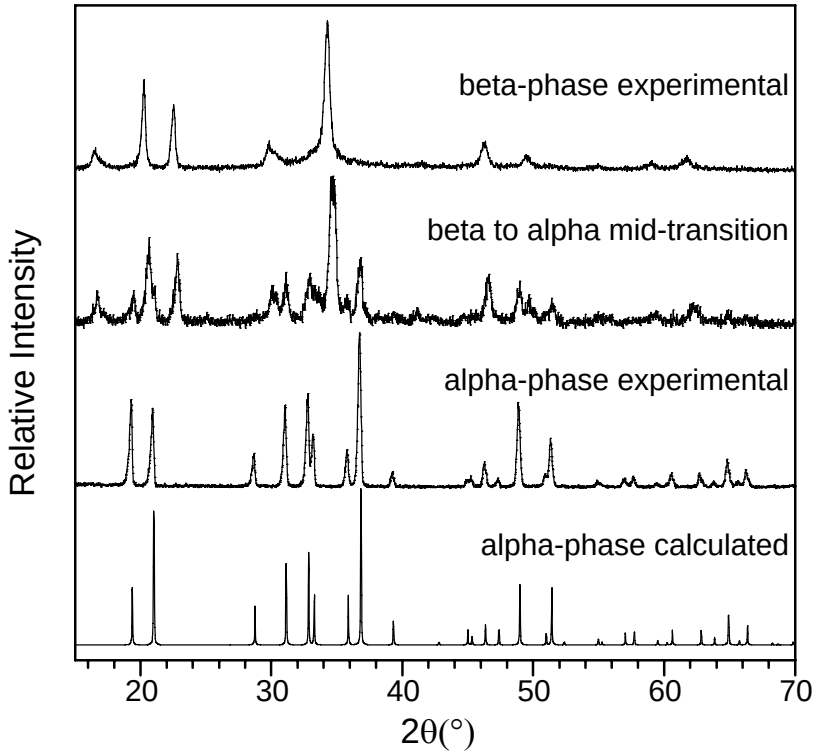

Fig. 2-4: Powder X-ray diffraction patterns of Na_3PO_3S. The patterns containing the β-phase were obtained relatively quickly in order to minimize exposure to ambient humidity and therefore appear noisier. The calculated powder diffraction pattern for the α-phase was obtained from data in reference 21.

obtained, the sample was left on the countertop. The next morning, a slight change in sample color and granularity were observed; therefore, another PXRD pattern was obtained, revealing that the sample was now mostly α-Na_3PO_3S after only 16 hours in ambient conditions. Subsequent experiments led to samples that converted from the β- to the α-phase at various times scales (16 hrs-8 days) (see Figs. 2-4, 2-5). Attempts to reproduce this quench were often met with difficulty. Usually the PXRD of the product was observed to contain a small amount of the α-phase in addition to the β-phase.

The fact that atmospheric water played a role in this transformation came to light because the phase transformation was observed to occur at especially high rates on days when it rained. This was later confirmed by producing a sample of the β-phase and dividing it into two aliquots, one that was stored in a desiccator and one that was exposed to ambient conditions. The dessicated sample was observed to persist as the β-phase for much longer than the sample exposed to ambient relative humidities. It should be noted that the sample, which was stored in the desiccator, was periodically exposed to ambient conditions for short amounts of time while its PXRD pattern was being obtained. Therefore, we cannot determine with absolute certainty whether the desiccated sample would have undergone the transition in the complete absence of moisture.

A series of humidity-controlled chambers were next prepared using saturated salt solutions in order to determine the rate of the phase transition as a function of relative humidity [29]. At a relative humidity of 6.6% the β-phase remained unaffected. The material never fully converted to the α-phase when stored under 33.1% RH. In the case of 54.5 and 69.9% RH, the hydrated phase of the material, $Na_3PO_3S \cdot 12H_2O$ [30], formed so rapidly, as not to afford any observation of the β- to α-phase transition, if indeed the

conversion took place by this path. The current data suggest that there may be a minimum relative humidity necessary for the transition (33.1<x< 54.5% RH). Thus far,

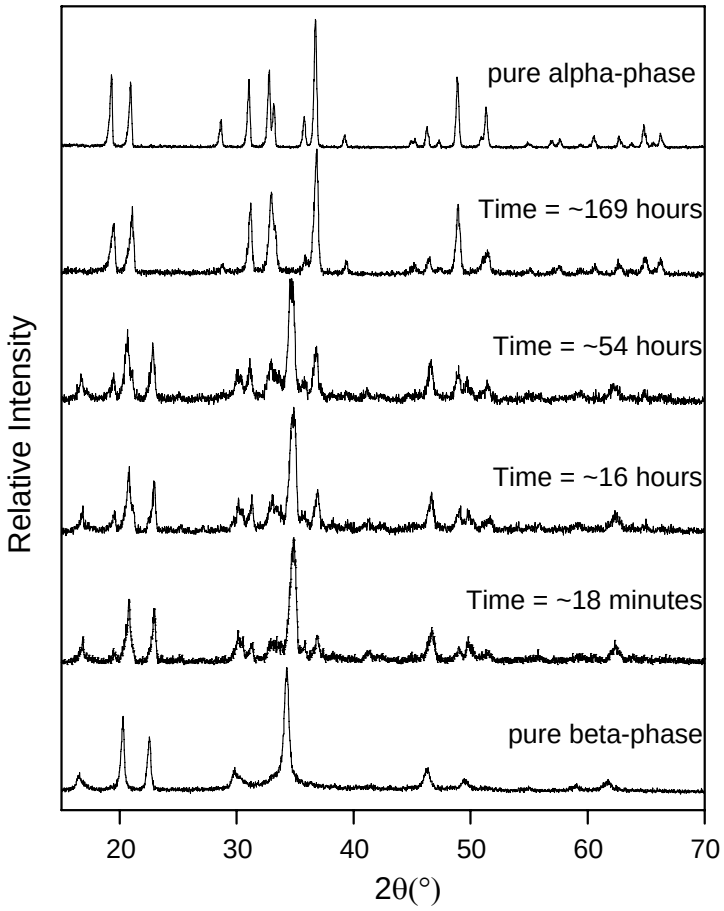

Fig. 2-5: PXRD patterns monitoring one of the slower room-temperature β- to α-phase transitions. In this experiment there is no time = 0 pattern. The pattern of the pure β-phase was produced from another experiment (on a dry day) and is provided for comparison. The pattern of the pure α-phase prepared in solution is also provided for comparison purposes. These experiments were conducted under ambient (uncontrolled) humidity.

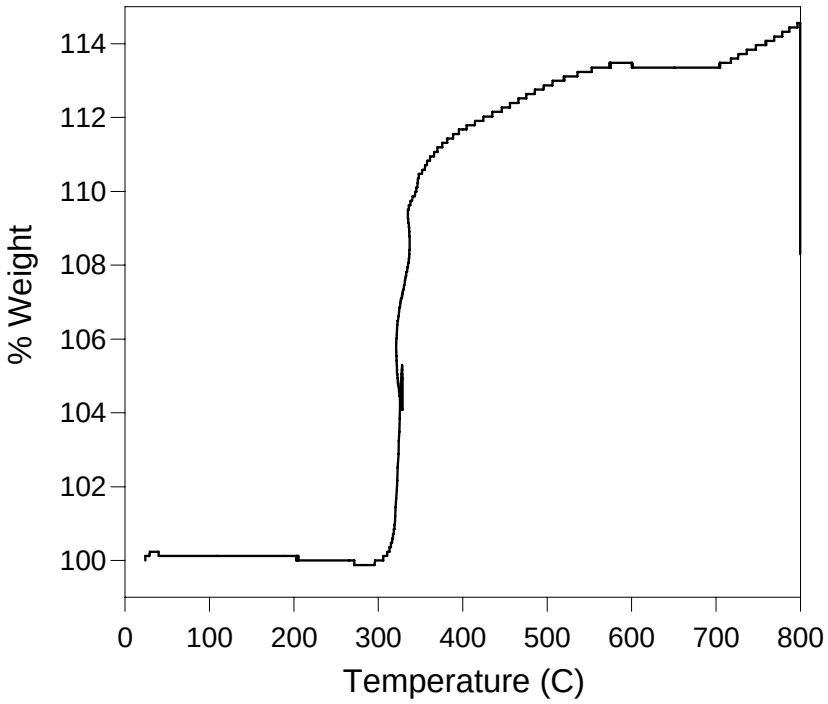

Fig. 2-6: Thermogravimetric analysis diagram of α-Na_3PO_3S obtained in air

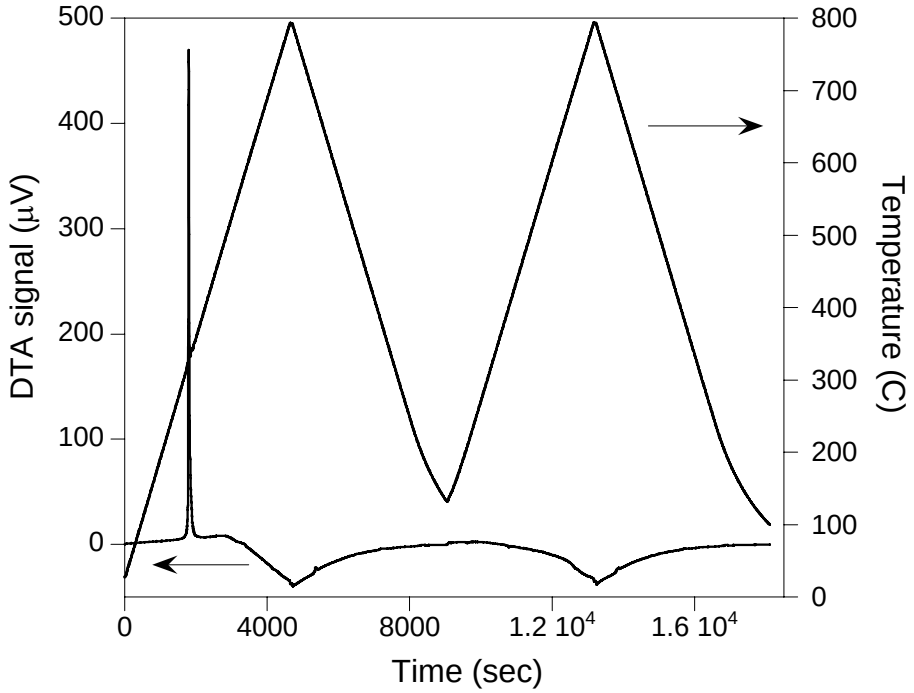

Fig. 2-7: Differential thermal analysis diagram of α-Na_3PO_3S obtained in air

Since the α-phase is relatively stable under normal laboratory conditions (~40% RH), further characterization of this material was possible. DTA and thermogravimetric analysis of α-Na_3PO_3S in air indicate that the material is stable up to ~315° C, when an exothermic oxidative decomposition to $Na_4P_2O_7$, Na_2SO_4, and some volatile form of sulfur occurs (see Figs. 2-6, 2-7, 2-8). The decomposition is accompanied by an observed weight gain of 13.23%. The calculated weight gain is 13.31%. This result disagrees with the findings of Lambert and Yasuda who observed decomposition at 120-125° C [28].

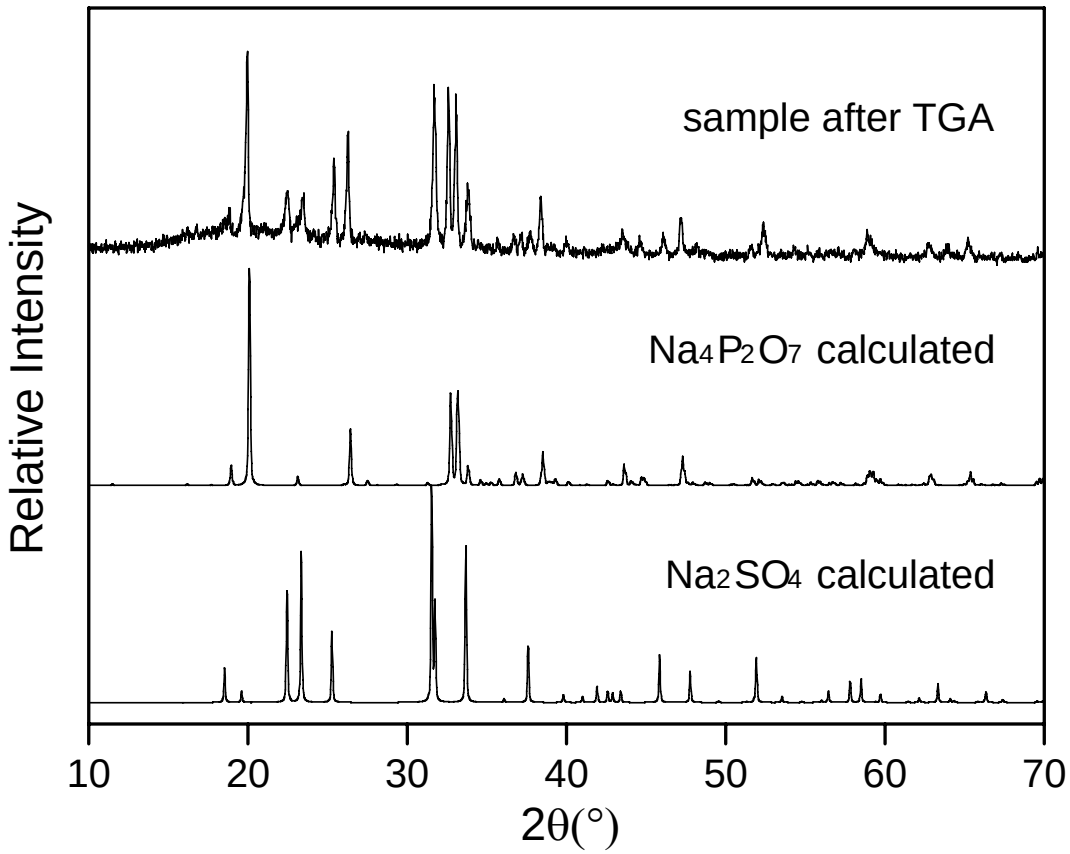

Fig. 2-8: PXRD pattern obtained after thermal analysis of α-Na_3PO_3S in air. Calculated patterns are derived from the Inorganic Crystal Structure Database File # 10370 and 66554 for $Na_4P_2O_7$ and Na_2SO_4 respectively.

attempts to determine the rate of the phase transition as a function of relative humidity have been qualitative. *In situ* diffraction studies under controlled humidity conditions will be presented in Chapter 3 [31].

α-Na_3PO_3S crystallizes in a noncentrosymmetric space group, R3c (see Fig. 2-1). The lack of an inversion center leads to a second order, nonlinear optical (NLO) property known as second harmonic generation (SHG) [32]. SHG of a powdered sample of α-Na_3PO_3S was measured using a modified Kurtz NLO system [33], with a Nd:YAG laser, as described elsewhere [34]. The incident light of 1064nm was converted to 532nm

with an efficiency of ~200x that of α-quartz. Since α-Na_3PO_3S was SHG active, a phase matching experiment was performed in which the material was found to be non-phase matchable (Type 1). In a non-phase matchable material, the SHG response goes to zero with increasing particle size (see Fig. 2-9). The $<d_{eff}>$ is calculated to be 7.8 pm/V [34].

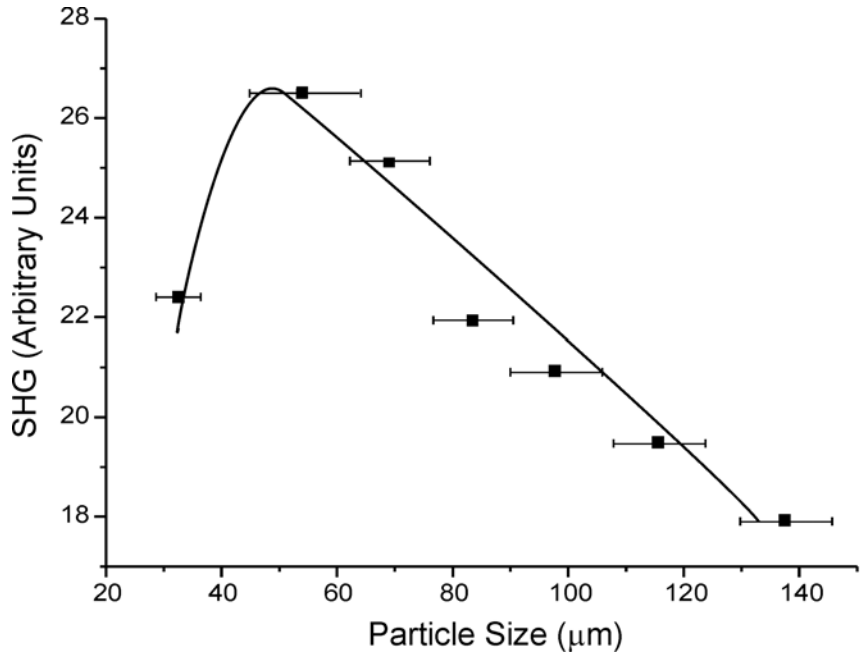

Fig. 2-9: Results of α-Na_3PO_3S phase matching experiment. The line is superimposed to guide the eye and is not a fit to the data.

4. Conclusions

Recently, oxythiophosphate materials have proven to be selective and recyclable in the remediation of toxic heavy-metal ions [4]. Also, properties of oxythiophosphates, such as ionic conductivity, have been demonstrated to be tunable by varying the anionic composition [19,21,35]. Na_3PO_3S presents us with another glimpse of the interesting physicochemical properties possible in oxythiophosphates. We have shown sodium monothiophosphate to be a remarkable phase-change material, as well as an SHG active

compound. This wide variety of properties supports the prediction that further work in this field is warranted and should lead to the discovery of new and interesting materials.

5. Acknowledgements

Thank you to Prof P. Shiv Halasyamani and Dr. Kang-Min Ok (University of Houston) for the SHG measurements. Thank you to Dr. Peter Wildfong for fruitful discussions about phase transformations. Thank you to Dr. Matthias Zeller and Dr. Cora Lind for translations of the German references.

References

[1] C. Kubierschky, J. Prakt. Chem. 31 (1885) 93-111.

[2] M. Pompetzki, M. Jansen, Monatsh. Chem. 133 (2002) 975-986.

[3] E. Zintl, A. Bertram, Z. Anorg. Allg. Chem. 245 (1940) 16-19.

[4] A. E. Gash, P. K. Dorhout, S. H. Strauss, Inorg. Chem. 39 (2000) 5538-5546.

[5] I. A. Stenina, A. D. Aliev, P. K. Dorhout, A. B. Yaroslavtsev, Inorg. Chem. 43 (2004) 7141-7145.

[6] K. K. Palkina, S. I. Maksimova, N. T. Chibiskova, T. A. Tripol'skaya, G. U. Wolf, T. B. Kuvshinova, Izv. Akad. Nauk SSSR, Neorg. Mater. 27 (1991) 1028-1031.

[7] A. Clearfield, A. I. Bortun, S. A. Khainakov, L. N. Bortun, V. V. Strelko, V. N. Khryaschevskii, Waste Manage. 18 (1998) 203-210.

[8] A. Clearfield, J. A. Stynes, J. Inorg. Nucl. Chem. 26 (1964) 117-129.

[9] R. Brec, Solid State Ionics 22 (1986) 3-30.

[10] M. Curini, O. Rosati, U. Costantino, Curr. Org. Chem. 8, (2004) 591-606.

[11] M. Ai, K. Ohdan, J. Mol. Catal. A: Chem. 159 (2000) 19-24.

[12] E. Manova, C. Severac, A. Andreev, R. Clément, J. Catal. 169 (1997) 503-509.

[13] M. Piana, B. L. Cushing, J. B. Goodenough, N. Penazzi, Ann. Chim-Rome 93 (2003) 985-995.

[14] S. Yang, Y. Song, K. Ngala, P. Zavalij, M. S. Whittingham, J. Power Sources 119-121 (2003) 239-246.

[15] Y. V. Kuzminskii, B. M. Voronin, N. N. Redin, J. Power Sources 55 (1995) 133-141.

[16] M. N. Satyanarayan, A. Deepthy, H. L. Bhat, Crit. Rev. Solid State 24 (1999) 103-191.

[17] A. I. Valeev, N. D. Kundikova, V. M. Churikov, G. T. Pterovskii, K. O. Shchavelev, O. S. Shchavelev, N. A. Yakobson, J. Opt. Technol. 68 (2001) 495-499.

[18] P. G. Lacroix, R. Clément, K. Nakatani, J. Zyss, I. Ledoux, Science 263 (1994) 658-659.

[19] M. Pompetzki, R. Dinnebier, M. Jansen, Solid State Sci. 5 (2003) 1439-1444.

[20] M. Pompetzki, L. van Wüllen, M. Jansen, Z. Anorg. Allg. Chem. 630 (2004) 384-388.

[21] M. Pompetzki, M. Jansen, Z. Anorg. Allg. Chem. 628 (2002) 641-646.

[22] S. R. Byrn, R. P. Pfeiffer, J. G. Stowell, Solid-State Chemistry of Drugs, SSCI, Inc., Indiana, (1999) pp 241-244.

[23] D. Burnett, F. Theilmann, J. Booth, Int. J. Pharm. 287 (2004) 123-133.

[24] E. Vadas, P. Toma, G. Zografi, Pharm. Res. 8 (1991) 148-155.

[25] Y. Masuda, K. Hashimoto, Y. Ito, Thermochim. Acta 163 (1990) 271–278.

[26] D. Grohol, A. Clearfield, J. Am. Chem. Soc. 119 (1997) 4662-4668.

[27] W. Brockner, B. Jendrzok, F. Menzel, V. R. Jensen, M. Ystenes, J. Mol. Struct. 319 (1994) 85-100.

[28] S. K. Yasuda, J. L. Lambert, Inorg. Syn. 5 (1957) 102-104.

[29] H. Nyqvist, Int. J. Pharm. Tech. & Prod. Mfr. 4 (1983) 47-48.

[30] B. M. Goldstein, Acta Crystallogr. B38 (1982) 1116-1120.

[31] N. J. Takas, J. A. Aitken, J. Solid State Chem.180 (2007) 2034-2043.

[32] J. F. Nye, Physical Properties of Crystals, Oxford University Press: New York, (1957).

[33] S. K. Kurtz, T. T. Perry, J. App. Phys. 39 (1968) 3798-3813.

[34] K. M. Ok, N. S. Bhuvanesh, P. S. Halasyamani, Inorg Chem. 40 (2001) 1978-1980.

[35] M. Pompetzki, M. Jansen, Z. Anorg. Allg. Chem. 629 (2003) 1929-1933.

Chapter 3

An *In Situ* Time-of-Flight Neutron Powder Diffraction Study of the Humidity-Induced Phase Transition in Sodium Monothiophosphate

Abstract:

Anhydrous β-Na_3PO_3S, obtained by rapid cooling, has been observed to convert to the more thermodynamically stable, anhydrous α-Na_3PO_3S upon exposure to a humid atmosphere. Though water plays a critical role in this polymorphic transformation, it is absent in both the initial and final materials. *In situ* time-of-flight neutron powder diffraction was used to track the progress of this transition as a function of time. Diffraction data were acquired using the Intense Pulsed Neutron Source (IPNS) at Argonne National Laboratory. An empirical whole pattern fitting method was used to determine the polymorphic phase composition over time. The resulting data were evaluated using several solid-state kinetic models. The kinetics of this transition has been determined to be best described by either 1- or 2-dimensional diffusion. The significance of these models with respect to the physical phenomenon is discussed.

1. Introduction:

The earliest discovered oxythiophosphate material was sodium monothiophosphate dodecahydrate, $Na_3PO_3S•12H_2O$, having been synthesized over 160 years ago [1,2]. The anhydrous salt of sodium monothiophosphate was first prepared in 1940 by Zintl and Bertram [3]. The structure of this phase was recently solved by Jansen et al. through the use of X-ray and neutron powder diffraction methods [4]. Despite this long history, there are still many interesting properties to be discovered with respect to this material [5].

Our work is currently focused on the use of sodium monothiophosphate as a starting material for the preparation of new, more complex metal oxythiophosphate materials. However, before venturing into these more diverse systems, it became imperative that we study sodium monothiophosphate, the precursor salt. In the process, an unusual transition between anhydrous crystalline phases, facilitated by atmospheric water, was observed [5].

Spontaneous isothermal phase transitions must involve conversion to a more thermodynamically stable phase to supply a thermodynamic driving force for the conversion. The humidity-induced phase transition reported here is no exception, as it is observed to occur from a sample of β-Na_3PO_3S [5,6], obtained by fast cooling from high temperatures, to α-Na_3PO_3S, the room temperature stable phase.

Phase transitions induced by exposure to a humid atmosphere are not unusual [7-14]; however, these transitions typically involve conversion between an anhydrous and a hydrated phase [7,11-14]. Conversions between anhydrous phases have been observed

among small molecule organic solids. More research on these solids has been carried out in support of the pharmaceutical industry as a result of the importance of the relationships between polymorphism, physical stability and bioavailability [7,15-17]. However, these transitions are most often from an amorphous to a crystalline state [9,18,19]. Among inorganic materials, observations of anhydrous crystalline to anhydrous crystalline phase transitions catalyzed by atmospheric water are rare. In fact, the only such report known to these authors is that of humidity-induced polymorphic transitions between the high- and low-temperature phases of lithium, sodium and potassium formate [20]. In this report, it was observed that the high-temperature phases of these formates, trapped by rapid cooling, transformed to the low-temperature phases relatively quickly upon exposure to a humid atmosphere, despite the fact that the quenched high-temperature phases were found to persist under vacuum. Unfortunately, no detailed study of the transformation, measurements of the process, or discussion of a potential mechanism was put forth.

Knowing that these transitions are rare in the inorganic literature, *in situ* neutron diffraction experiments were carried out at the Intense Pulsed Neutron Source at Argonne National Lab under controlled humidity conditions to better characterize this phenomenon. This report will describe the treatment of the acquired neutron diffraction data by an empirical whole pattern fitting method, the model fitting process to determine appropriate solid-state kinetic models, and an interpretation of the physical meaning of these models in regard to this particular solid-state phenomenon.

2. Experimental

2.1 Synthesis

2.1.1 Synthesis of α-Na_3PO_3S

α-Na_3PO_3S was prepared by hydrolysis of $PSCl_3$ in an aqueous solution of NaOH, followed by dehydration via suspension in anhydrous methanol, as described elsewhere [5,21]. The product obtained by this method is a fine white powder and further grinding is not necessary prior to transferring of this material to the vanadium canister for neutron diffraction measurements.

2.1.2 Synthesis of β-Na_3PO_3S

A sample of β-Na_3PO_3S was obtained by heating approximately 0.4 g α-Na_3PO_3S in a fused-silica tube, sealed under vacuum (~10^{-3}mbar), to 600° C at a rate of 10° C/min in a programmable furnace and held at that temperature for 30 minutes. The sample was then rapidly cooled by immersion of the sealed tube in an ice water bath to obtain a quenched sample of β-Na_3PO_3S. This process was repeated multiple times to obtain a satisfactory amount of material for neutron powder diffraction experiments. Several grams of the quenched sample of β-Na_3PO_3S were ground using a mortar and pestle in a helium filled glovebag before being transferred to the vanadium sample canister for neutron diffraction measurements (see section 2.2.3 General Neutron Diffraction Procedures).

2.2 Physical Measurements

2.2.1 Differential Thermal Analysis

Differential thermal analysis (DTA) was performed using a Shimadzu DTA-50, which was calibrated using a three-point calibration curve based on the melting points of indium, zinc and gold metals. The differential signal was balanced prior to the beginning of each experiment. Data were recorded using the Shimadzu TA60-WS collection program. Experiments were performed at a rate of 10° C/min. Samples were contained in carbon-coated fused-silica ampoules sealed under vacuum (~10^{-3} mbar). All DTA samples were referenced against an alumina sample, contained similarly and of comparable mass. Multiple heating and cooling cycles were performed in the DTA experiments to differentiate between reversible and irreversible thermal events.

2.2.2 Powder X-ray Diffraction Procedures

Powder X-ray diffraction (PXRD) patterns were obtained on a Rigaku D/max-B, powder X-ray diffractometer, model number D2013, using copper K_α radiation and operating at 35 kV and 22.5 mA. Samples were prepared by adhering the sample to double-sided tape over a glass specimen slide. All diffraction patterns were collected from 10 to 70° in 2θ using a step size of 0.024° at a scan rate of 2°/min.

2.2.3 General Neutron Diffraction Procedures

Neutron diffraction experiments on the polymorphs of Na_3PO_3S were conducted using the General Purpose Powder Diffractometer (GPPD) at the Intense Pulsed Neutron Source (IPNS) located in Argonne National Laboratory. The neutrons which were used

for diffraction varied in wavelength from 0.2 to 5.7Å. All samples were prepared in a helium-filled glovebag and loaded into vanadium canisters for data collection.

2.2.3.1 High Temperature Neutron Diffraction Procedures

A sample of several grams of α-Na_3PO_3S was used, as prepared, and loaded into a 7/16 inch vanadium canister under a helium atmosphere. The canister was covered with parafilm to minimize exposure to air during transfer to the instrument. The sample was placed in the Howe furnace [22], a vanadium foil resistive-element furnace, and evacuated. Once a desirable vacuum had been achieved ($<10^{-5}$mbar), a neutron powder diffraction pattern of α-Na_3PO_3S was obtained at room-temperature over the course of 259,334 pulses. This neutron diffractogram will hereafter be referred to as the "α-phase reference pattern".

The sample was next heated from room temperature to 600° C at a rate of 8° C/min. The sample was allowed to equilibrate at this temperature until diffraction of the α-phase was no longer observed, and a diffraction pattern corresponding to the γ-phase was readily apparent. A neutron diffraction pattern of the γ-phase was obtained by summing 20 diffractograms, which were each acquired for ~54,000 pulses or ~30 minutes each, giving a total of 1,080,160 pulses. The sample was next cooled to 505° C at a rate of 8° C/min, and equilibrated at this temperature until diffraction of the γ-phase was no longer observed, and diffraction of the β-phase became readily apparent. A neutron diffraction pattern of the β-phase was obtained by summing 15 diffractograms, which were each acquired for ~54,000 pulses or ~30 minutes each, giving a total of

810,108 pulses. The program ISAW [23] was used to sum the various diffractograms acquired throughout the course of the experiment.

2.2.3.2 Controlled Humidity Neutron Diffraction Procedures

The experimental setup to measure the humidity-catalyzed phase transition between β- and α-Na_3PO_3S was developed specifically for this experiment [24] (see Fig. 3-1). Two dry nitrogen gas cylinders were each manipulated through the use of computer controlled mass flow controllers. One of these dry N_2 lines was bubbled through one linear centimeter of D_2O to obtain a humidified gas flow, while the second N_2 line remained dry. The two gases were then combined, and their relative flow rates adjusted to calibrate a variable-humidity gas flow.

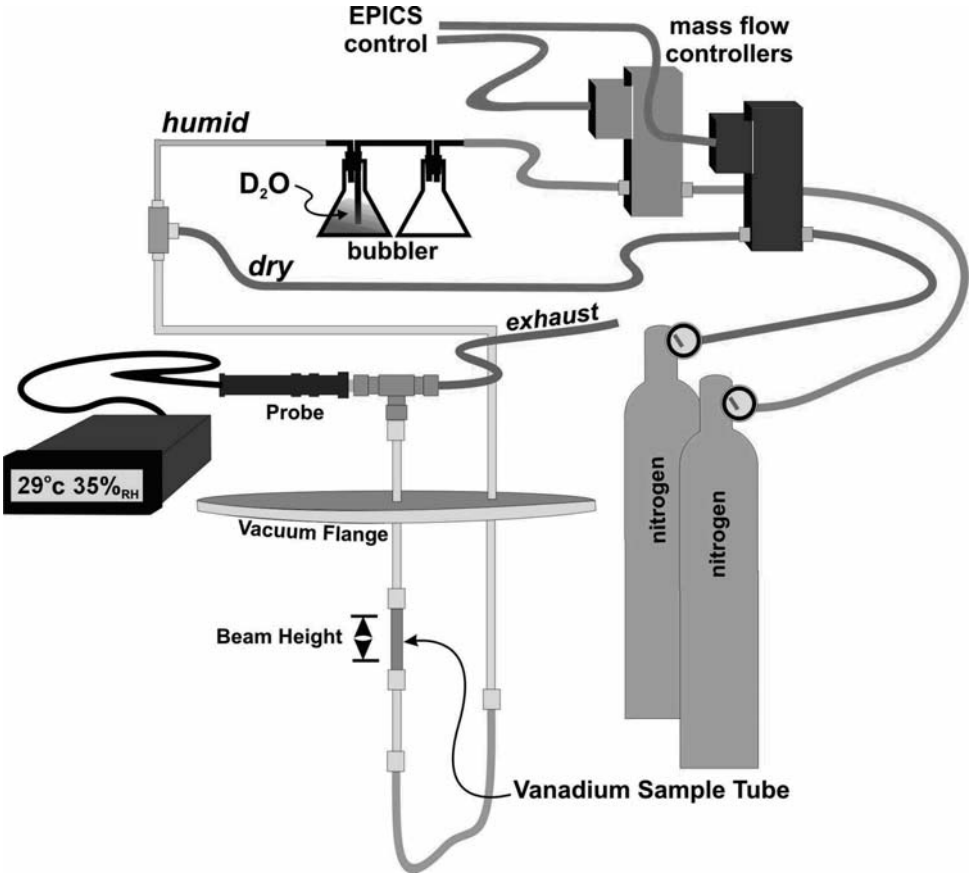

Fig. 3-1: Diagram of the controlled humidity apparatus used for *in situ* neutron powder diffraction experiments.

The sample of β-Na_3PO_3S, obtained by quenching, was contained in a vanadium tube with glass wool plugs at both the top and bottom. The sample was first placed in the stream with only dry gas flowing to acquire a single reference pattern of the β-phase prior to any transformation. This diffractogram will hereafter be known as the "β-phase reference pattern", which was collected for 54,000 pulses on the same sample that was later induced to convert to the α-phase by exposure to a humid gas flow. Once the β-phase reference pattern was collected, the humid gas flow was initiated with predetermined flow rates to provide a relative humidity (RH) of 35%. 51 Neutron

diffractograms of the transition were collected for ~54,000 pulses or ~30 minutes each (see Fig. 3-2). One single diffractogram during the transition was collected for a larger number of pulses, 79,894. All data used for whole pattern fitting were taken from detector bank 5 centered at 53°. All controlled humidity neutron diffraction data reported herein were collected at an ambient temperature of 29° C.

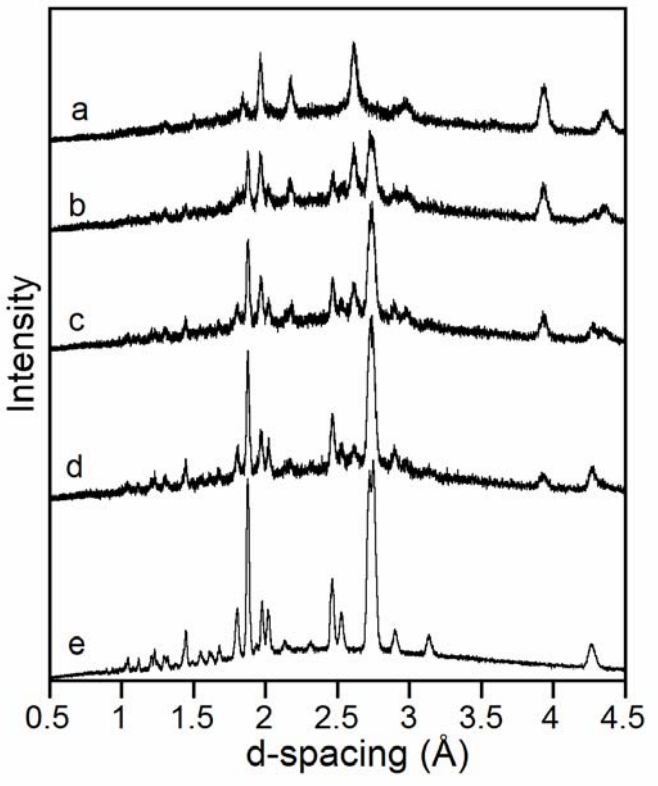

Fig. 3-2: Neutron powder diffractograms of the sample throughout the transition from pure β-Na_3PO_3S (a) to α-Na_3PO_3S (e). The midpoints, b, c and d represent the sample at approximately 30, 50 and 70% conversion to the α-phase respectively.

Initial observations of the outgas humidity, were far lower than the anticipated value of 35%RH. However, the outgas humidity was observed to change over time, eventually climbing up to 45%RH (see Fig. 3-3). At the end of data collection, the sample was removed from the gas stream and the outgas humidity was directly measured to be 33%RH, a value which is very near the set humidity of 35%RH and within the acceptable limits of the uncertainty of the hygrometer probe.

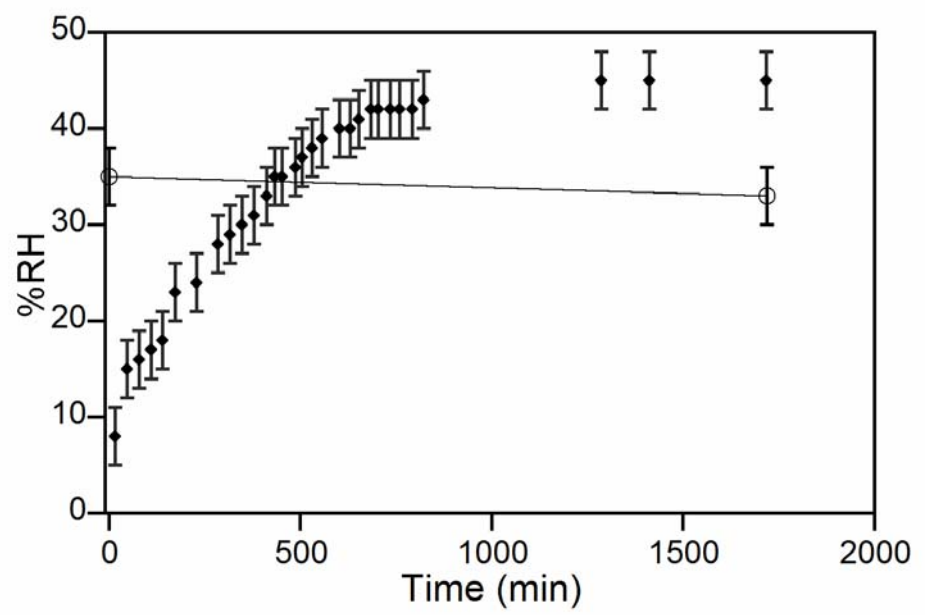

Fig. 3-3: Outgas humidity measured as a function of time. The open circle data points represent the humidity of the outgas measured without the sample in the gas stream both before and after experimentation.

3. Results

3.1 Data Treatment:

The phase composition of the sample through time was determined by an empirical whole pattern fitting method. The whole pattern fitting method was used by

assuming that the absence of a third phase during the transition meant that the transition represents a strictly two-phase system, an assumption that the refinements seem to support. This model seems applicable since, at no time during the transformation, was any diffraction pattern observed other than those corresponding to the α- and β-phases of sodium monothiophosphate. All of the measured diffraction patterns were thus assumed to be readily modeled as some mole fraction of the β-phase (X), and the complimentary mole fraction of the α-phase (1-X). The use of two-phase Rietveld refinement would have been preferred over an empirical whole pattern fitting method; however, Rietveld refinement requires knowledge of all structures involved, and the structure of the β-phase has, so far, eluded us and others [6].

3.2 Model Development

The assumption of the two phase system can be generally modeled in the manner described by Eq. 3-1, assuming a constant flux of diffracted particles, either photons or neutrons. In this equation, $I_m(d)$ is the intensity predicted by the model as a function of d-spacing, $I_\beta(d)$ and $I_\alpha(d)$ are the intensities of the reference β- and α-phase reference patterns respectively as a function of d-spacing, and X is the average mole fraction of the β-phase present in the sample during the time interval being measured.

$$I_m(d) = X\, I_\beta(d) + (1 - X)\, I_\alpha(d) \qquad \text{Eq. 3-1}$$

The diffraction data in question, however, were acquired using a pulsed neutron source, which is susceptible to changes in total neutron flux over time. As such, several scaling factors were introduced to accommodate changes in total flux. These scaling factors force the adaptation of Eq. 3-1 to the form in Eq. 3-2. In this equation, F_{ref} is a

scaling factor which allows for differences in measured flux between reference patterns and F_{tot} is a scaling factor which scales the entire model to allow for variations between the reference patterns and the individual diffractograms measured during the transition.

$$I_m(d) = F_{tot}\left\{\left[X\, I_\beta(d)\right] + F_{ref}\left[(1-X)\, I_\alpha(d)\right]\right\} \qquad \text{Eq. 3-2}$$

The best fit model was determined by the minimization of the crystallographic R factor as defined in Eq. 3-3 [25].

$$R = \frac{\int\left[I_{meas}(Q) - I_{calc}(Q)\right]^2 dQ}{\int\left[I_{meas}(Q)\right]^2 dQ} \qquad \text{Eq. 3-3}$$

Where Q [25] is defined as:

$$Q = \frac{4\pi * \sin(\theta)}{\lambda} = \frac{2\pi}{d} \qquad \text{Eq. 3-4}$$

Diffraction data corresponding to the α-phase reference pattern, the β-phase reference pattern, and an experimental pattern, whose composition was to be determined, were copied into a single Excel spreadsheet [26]. Excel Solver, using a generalized reduced gradient method [27], was employed to determine the values of X, F_{ref}, and F_{tot}, which would provide the lowest value of the crystallographic R factor (see Fig. 3-4). A zero-point correction was also manually applied to the α-phase reference pattern to minimize the crystallographic R factor. A numerical columnar integration method was employed, since more sophisticated numerical integration methods assume the data to be a smooth, continuous function, which, in this case, it is not.

The refinement of the three variables proceeded as follows. The value of F_{ref} was determined only once, based on a sample measured at late experimental time, when dX/dt is minimal. The value of this refined parameter was determined for several other data points, but was not found to change significantly. Therefore, this parameter was not refined for other data points, but was applied as a fixed scaling factor. The values of X and F_{tot} were refined for each point in time independently.

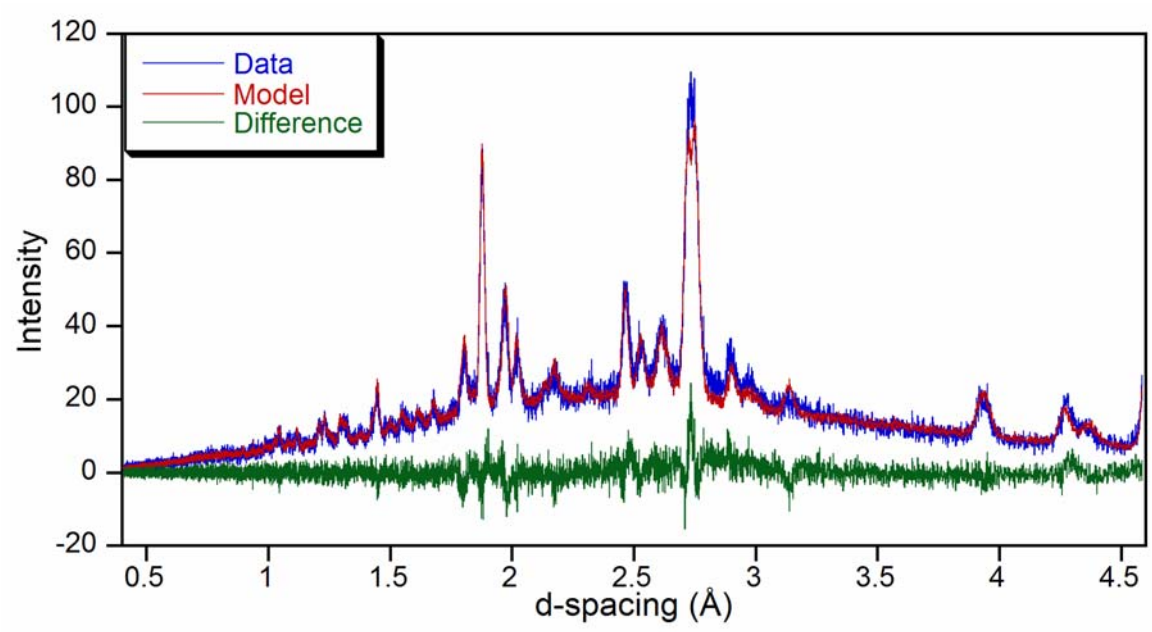

Fig. 3-4: One of the neutron diffractograms from the whole pattern fitting process. The displayed diffractogram corresponds to 1,003 minutes exposure to deuterated humid atmosphere and 58.75% conversion to the α-phase. The crystallographic R factor of this model is 1.67%.

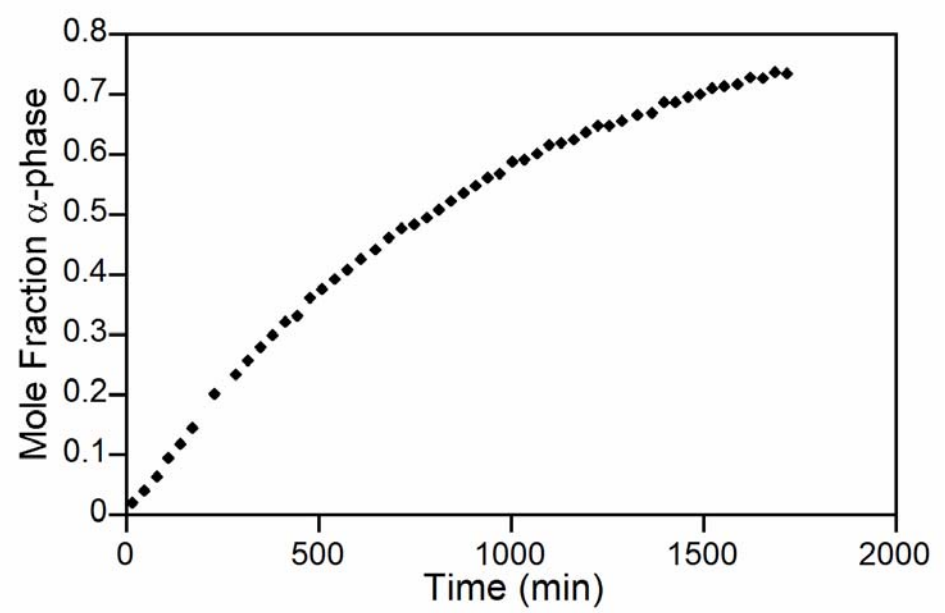

Fig. 3-5: Kinetic data describing the polymorphic phase transition through time.

β- to α-phase kinetics were modeled by plotting the mole percent converted (α-phase) versus the mean time of that pattern's data collection period (see Fig. 3-5). It should be noted that while this choice of time placement is not rigorously accurate, given the potential variations in neutron flux over time, it is an adequate approximation. Eleven solid-state kinetic models [7] were linearized and the kinetic data were applied to each.

It is strictly impossible to determine the mechanism by which a solid-state reaction proceeds simply by determining which model forms the best fit line when it is applied; however, it is possible to rule out a model due to clearly poor intercepts, slopes, or R^2 values. Several models were therefore discarded, because of a failure to accurately describe the transformation. The Prout-Tompkins, one-dimensional advance of phase boundary, and the four power laws [7] that were used, were discarded due to the

unrealistic y-intercepts predicted and the generally poor fit of the data by analytical and graphical inspection (see Table 3-1). All models should theoretically intercept the y-axis very near to zero, except the one-dimensional advance of phase boundary model, which should intercept the y-axis very near to one.

Table 3-1: Summary of the linearization of all kinetic models used.

Kinetic Model	Mathematical Form[a]	Slope	Intercept	R^2
Prout-Tompkins	$\ln(\alpha/(1-\alpha)) = kt + c$	2.041×10^{-3}	-1.956	0.8304
One-dimensional Advance of Phase Boundary	$1-\alpha = kt$	-4.029×10^{-4}	0.8678	0.9411
Two-dimensional Advance of Phase Boundary	$1-(1-\alpha)^{1/2} = kt$	2.776×10^{-4}	0.0531	0.9750
Three-dimensional Advance of Phase Boundary	$1-(1-\alpha)^{1/3} = kt$	2.071×10^{-4}	0.0309	0.9833
One-dimensional Diffusion	$\alpha^2 = kt$	3.511×10^{-4}	-0.0293	0.9947
Two-dimensional Diffusion	$(1-\alpha)\ln(1-\alpha)+\alpha = kt$	2.490×10^{-4}	-0.0349	0.9947
Three-dimensional Diffusion	$1-\frac{2}{3}\alpha-(1-\alpha)^{2/3} = kt$	8.239×10^{-5}	-0.0163	0.9851
Power Law n = 1/4 [b]	$\alpha^n = kt$	2.259×10^{-4}	0.6117	0.7691
Power Law n = 1/3 [b]	$\alpha^n = kt$	2.720×10^{-4}	0.5208	0.7970
Power Law n = 1/2 [b]	$\alpha^n = kt$	3.362×10^{-4}	0.3775	0.8457
Power Law n = 1 [b]	$\alpha^n = kt$	4.029×10^{-4}	0.1322	0.9411

[a] In equations presented, α represents the amount of product formed at time t.

[b] It should be noted that while potentially descriptive, power laws hold no physical meaning.

The remaining five models were evaluated in the following manner. The idealized linear model was used to calculate a theoretical time for each of the measured percent compositions. The actual time of the measurement was then subtracted from this theoretical value to give a Δt between the model and the experimental data to obtain a graph of Δt vs. t. If a certain model was truly representative of the system, the graph of Δt vs. t should be found to vary linearly with time, if the slope and intercept of the theoretical line are inaccurate. However, in the case that the slope and intercept of the theoretical line are accurate, the Δt vs. t line should have a slope of 0 and no data point should vary from 0 by more than ±15 minutes (see Fig. 3-6 (top)). The model/data time drift is allowed this window because most data were collected over a time period of ~30 minutes, and the data were plotted at the center point of this collection time frame. If the equation of the model cannot be made to meet these criteria for at least some portion of the data, then the model is not likely to be an accurate description of this transition (see Fig. 3-6 (bottom)).

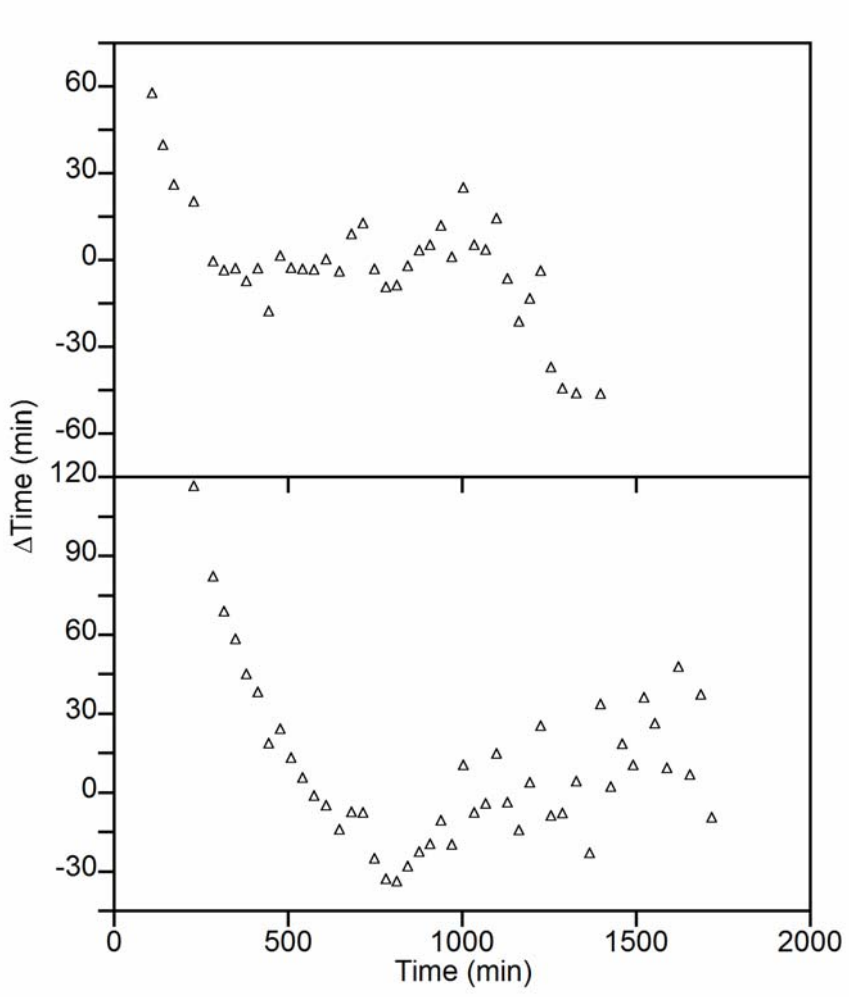

Fig. 3-6: Refined graph of time residuals (Δ time vs. time) for one-dimensional diffusion (top), note the linear range from 285-1226 minutes. Unrefinable graph of time residuals (Δ time vs. time) for three-dimensional diffusion (bottom), note that there does not appear to be any linear portion of the residual.

The Δt vs. t graphs of the two- and three-dimensional advance of phase boundary models were found to vary in a pseudo-parabolic fashion, and were, therefore, not considered to be suitable models to describe the transition. The three-dimensional diffusion model [28] was found to vary in a third-order fashion and, therefore, did not contain any significant linear portion which could be further evaluated. The Δt vs. t

residual plots of the one- and two-dimensional diffusion models were each found to contain a portion of data that varied linearly in time. The one- and two-dimensional diffusion models were each then applied exclusively using their respective linear ranges and further evaluated (see Table 3-2).

Table 3-2: Summary of linearization of promising kinetic models.

Kinetic Model	**Residual Shape**	**Linear Range (min)**	**Number of points > ±15 min[a]**	**R^2 of Linear Data Range**
Two-dimensional Advance of Phase Boundary	Parabolic	N/A	N/A	N/A
Three-dimensional Advance of Phase Boundary	Parabolic	N/A	N/A	N/A
One-dimensional Diffusion	Partial Linear	285-1226	3	0.9989
Two-dimensional Diffusion	Partial Linear	381-1523	6	0.9984
Three-dimensional Diffusion	Third Order	N/A	N/A	N/A

[a] This column denotes the number of data points within the linear range which do not fall within the 15 minute tolerance window for calculated v. observed values.

4. Discussion

To more completely convey the nature and relationship of the phases involved in the phase transition described, it is appropriate to first generally discuss the thermal behavior of Na_3PO_3S. DTA of α-Na_3PO_3S, performed under vacuum, reveals three thermal events in the temperature range of 25-650° C [5]. A single endothermic event occurs upon heating at 561° C, and two exothermic events occur upon cooling at 491° C and 452° C respectively. All thermal events are reproducible on multiple cycles, and PXRD analysis of the residue after the DTA experiment shows it to be α-Na_3PO_3S [5]. (Slight differences in transition temperatures between this report and those in reference 5 are a result of differing heating/cooling rates used, leading to small differences in thermal lag.)

In situ neutron diffraction experiments at high temperature, using the Howe furnace, indicated that as α-Na_3PO_3S is heated, it is converted to a new γ-phase at 561° C [5,29]. The existence of this phase was unclear until now, as it was not able to be trapped upon quenching. Upon cooling, the γ-phase is converted to the β-phase at 491° C. The β-phase next is converted back to the room-temperature stable α-phase upon cooling to 452° C. The structure of the β-phase has not been determined to date; however, the neutron powder diffraction pattern of the γ-phase which was measured *in situ* at high temperatures can be modeled and now will be be discussed.

Neutron powder diffraction of γ-Na_3PO_3S gave the pattern appearing in Fig. 3-7. The pattern is characterized by broad diffraction lines and high symmetry. The pattern

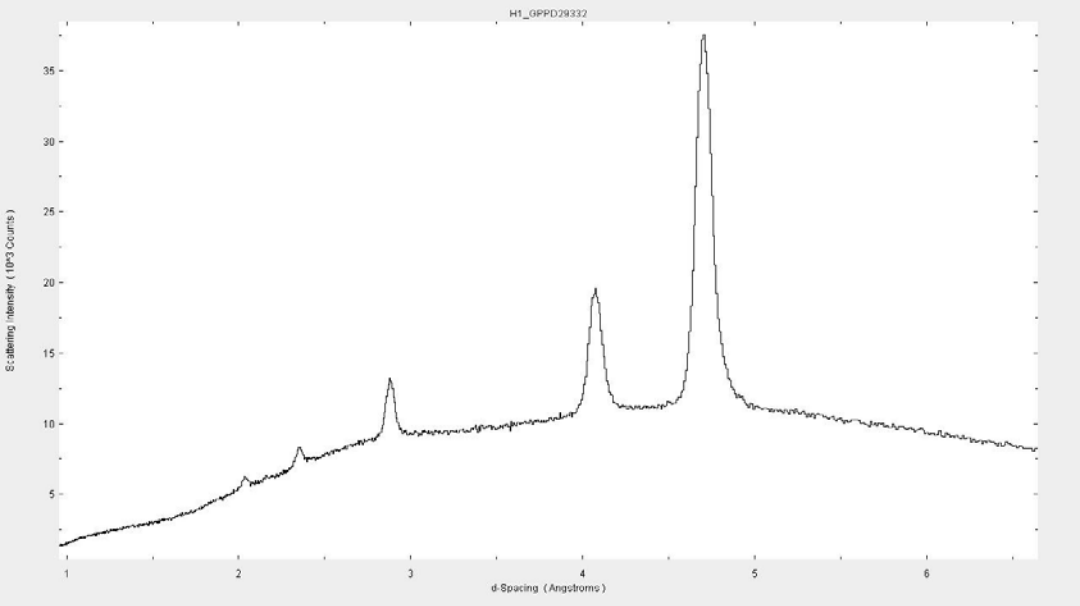

Fig. 3-7: The high temperature neutron powder diffraction pattern of γ-Na_3PO_3S acquired at 600° C.

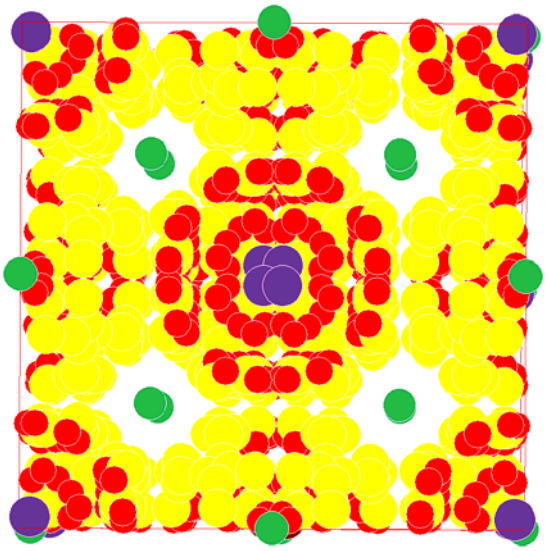

Fig. 3-8: Conceptual image of the plastic crystal state of γ-Na_3PO_3S. Oxygen is red; phosphorus is purple; sulfur is yellow; sodium is green.

was indexed manually to a face-centered cubic cell and the *a* parameter was refined with the use of the program CELREF to a value of a = 8.114(21) Å.[30]

γ-Na_3PO_3S is a plastic crystal. This means that portions of the structure have gained rotational freedom at high temperatures, but the energy present is still not sufficient for melting the crystal. In this case, the monothiophosphate anion is dynamically disordered as it revolves about its center of mass, and appears to be averaged over all rotational positions. Conceptually, this would appear similar to the static rotational disorder in Fig. 3-8.

While the β-phase is thermally stable between 452 and 491° C, it has also been reported that this phase may be trapped by rapid cooling [5,6]. A DTA of the trapped β-phase was also acquired (see Fig. 3-9). The DTA diagram of the sample of β-Na_3PO_3S is similar to that of the α-phase, except for an irreversible exothermic event which occurs upon heating at ~300° C, and which is followed by all of the same thermal events which were observed for a sample of the α-phase. Similar to the thermal behavior of the α-phase, PXRD analysis of the DTA residue after thermal analysis shows the material to be α-Na_3PO_3S. This leads us to the conclusion that the quenched β-phase thermally converts to the α-phase at ~300° C. The temperature at which the trapped β-phase thermally converts to the thermodynamically stable α-phase is important because it highlights the temperature suppression of 275° C for this transition at room-temperature caused by exposure to relative humidity.

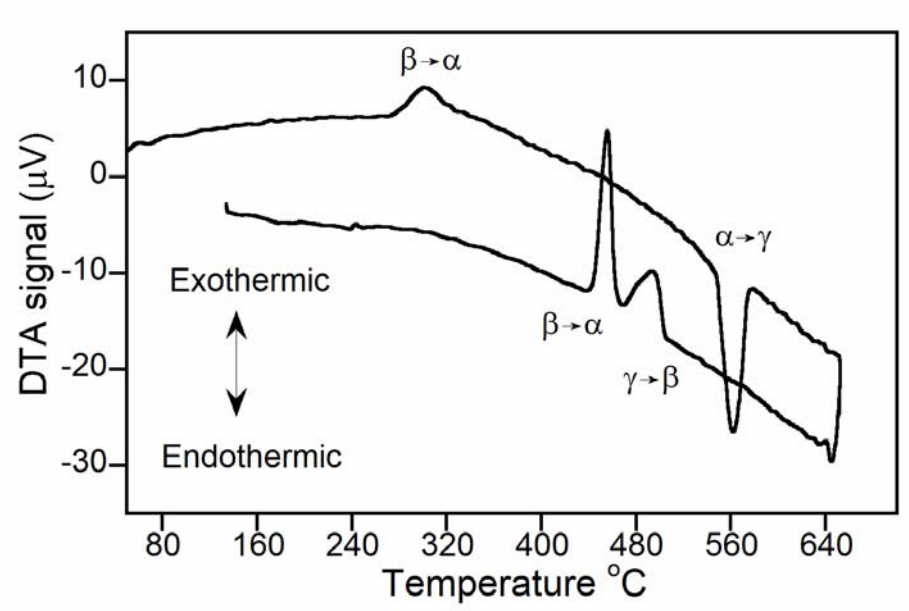

Fig. 3-9: DTA diagram of β-Na_3PO_3S obtained under vacuum. An irreversible exothermic event occurs on heating at ~300° C and corresponds to the thermal relaxation of β-Na_3PO_3S to α-Na_3PO_3S. The remaining thermal events are reproducible on multiple cycles.

The humid atmosphere used in the *in situ* neutron diffraction experiment was composed of D_2O due to the high coherent neutron scattering cross-section of deuterium which would help to facilitate the observation of any hydrated phase which could form during the course of the experiment. However, no such hydrated phase was observed. It is possible that the use of D_2O may give rise to an isotope effect in the determination of the kinetics of the reaction, but the existence or extent of this effect has not been determined.

The lack of an observable third phase during the course of the transition helps to validate the use of the two-phase linear combination model for the determination of sample composition. The use of this model can also be justified by the data that compose Fig. 3-10. All of the R factors determined throughout the course of the experiment are low (< 2.33%). The plot of R factor vs. time does seem to indicate some type of bias though, as the R factors at early times are systematically larger than those occurring later in the experiment. This effect is explained by the crystallinity of the predominant polymorph though time.

The quench process used to obtain β-Na_3PO_3S generates a phase having inherently poor crystallinity, resulting in a low signal to noise ratio. α-Na_3PO_3S has an inherently higher degree of crystallinity (see Fig. 3-2). The linear combination method used to model the system is not able to differentiate noise from signal in either the transitioning sample or the reference pattern(s), making it more prone to poorer fits when the signal to noise ratio is lower. Thus, the portion of the transition that is predominantly the β-phase is more susceptible to poorer fits. This interpretation is justified by the point marked by an open circle in Fig. 3-10. The only difference between this data point and its surrounding neighbors is increased data collection time. The R factor corresponding to this increased collection, and consequently improved signal to noise ratio, is on par with those data points that occur later in the experiment, when the sample has predominantly converted to the α-phase.

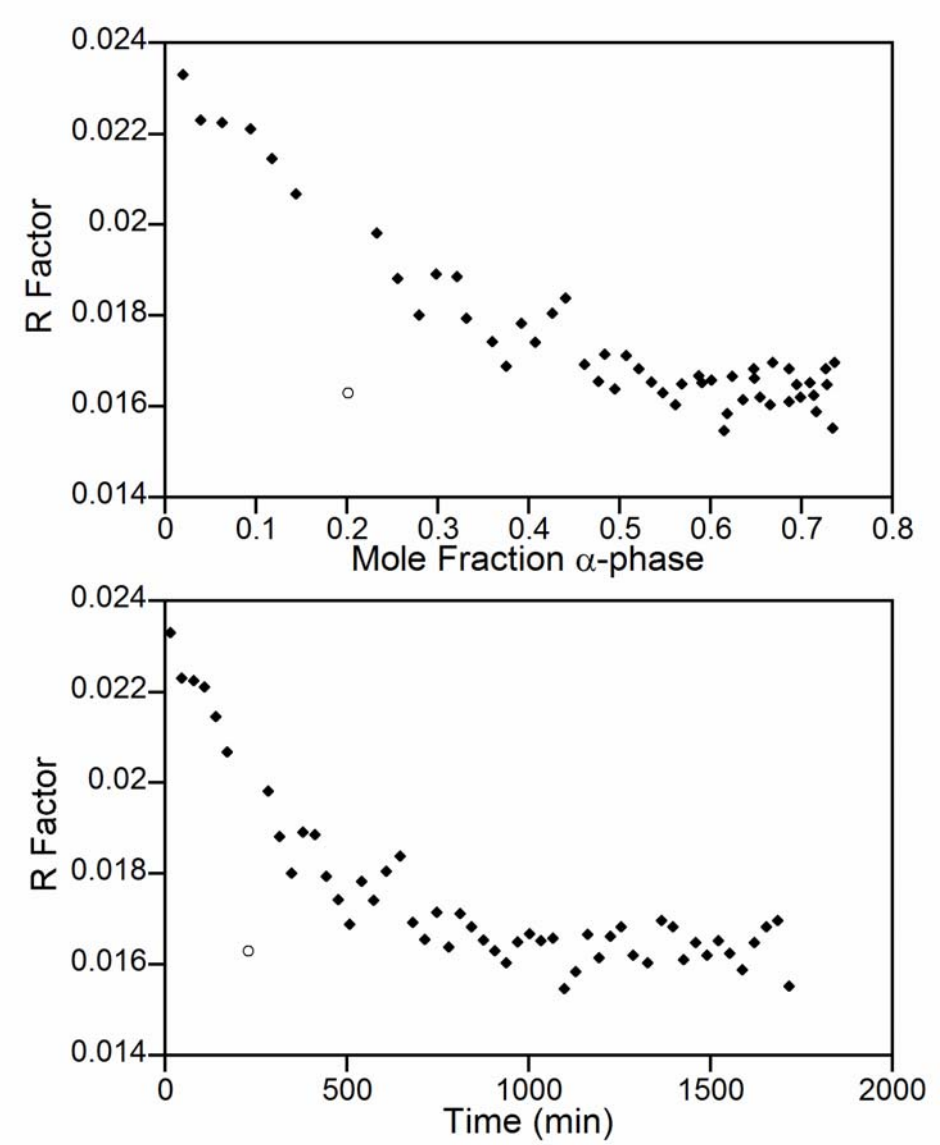

Fig. 3-10: Refined R factors as a function of the mole fraction of the α-phase (top). Refined R factors as a function of time (bottom).

The levels of the outgas humidity measured while the sample was in the gas flow (see Fig. 3-3) provide insight into the interaction of the solid with a humid gas. At early times during the experiment, the outgas humidity was consistently measured to be lower than the set value, indicating water missing from the outgas flow. Conversely, later in the experiment, the outgas humidity was measured to be greater than the set value, indicating a surplus of water in the outgas flow. This time-dependant behavior implies that the sample absorbs water out of a humid atmosphere, utilizes it to facilitate the phase transition, and releases it back into the atmosphere upon completion of the transformation. This type of behavior seems to support a diffusional model for the kinetics of the transition. The water must be absorbed from the gas flow, reducing the measured outgas humidity, diffuse though any already converted shell to the unreacted core of the particle, where it catalyzes a phase transition and then either diffuses deeper to the still unreacted core, or diffuses back out of the particle into the gas stream, where it contributes to a higher-than-anticipated outgas humidity. Furthermore, the higher-than-anticipated outgas humidity measured during the release of water back into the gas flow supports the assertion that this transition, although catalyzed by water, yields an anhydrous product.

The two best fitting kinetic models, both of which are diffusion based models, are plotted in their linearized forms in Fig. 3-11. Both models fail to accurately describe the data at either early or late experimental times. The slow kinetic rates early in the experiment are most likely a result of a lag time, a period of time during which crystallization occurs more slowly than expected while the system attempts to reach a steady-state. One cause of the lag time can be traced to the physical apparatus used

during the neutron diffraction experiments. The humid gas flow had directionality relative to the sample and, as noted by the outgas humidity measurements, strongly interacts with the sample. It seems reasonable to infer that the humidity of the flow gas is not constant throughout the sample, but, at early times, is higher on the upstream side of the sample and lower on the downstream side of the sample. This geometrical arrangement implies that the sample is not uniformly reacting with the humid gas flow at early times in the experiment, and some time is required to allow the sample to equilibrate with the humid gas flow before any kinetic rate equation can be meaningfully applied to the system. At later times in the experiment, the system begins to slow prematurely. This is a well known failing of many solid state kinetic models and originates from particle size dispersion and sample morphology [31].

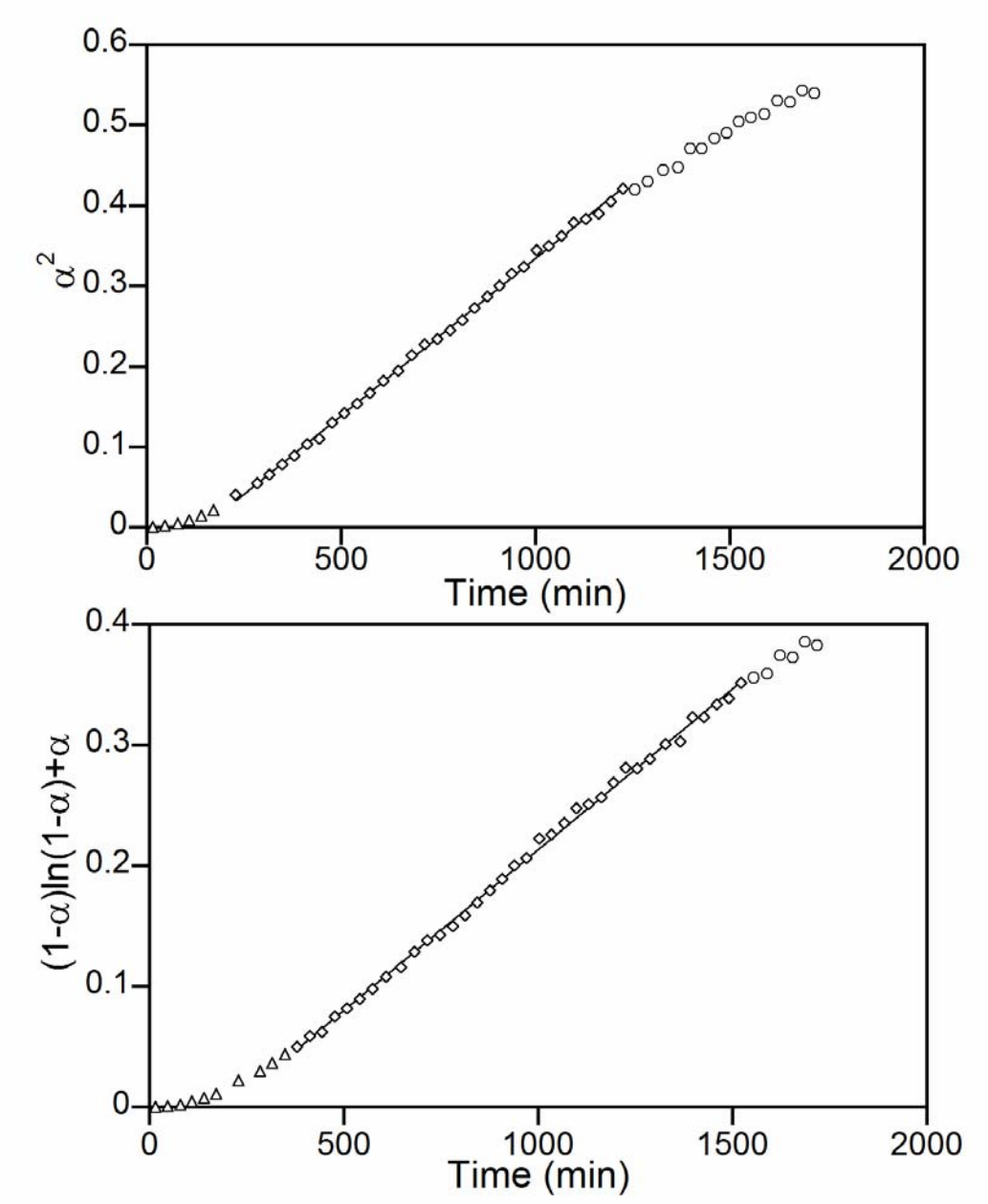

Fig. 3-11: Linearized form of the one-dimensional diffusion model plotted vs. time (top), and the linearized form of the two-dimensional diffusion model plotted vs. time (bottom). Triangles indicate lag time prior to equilibration of the flow gas humidity with the sample. Diamonds indicate the range over which the transition may be considered linear. Circles indicate slowing of the reaction at later times due to uncontrolled factors.

The best fitting kinetic models suggest that the humidity-induced phase transition is a fundamentally diffusion driven process, which requires the reactant, water, to be transiently present in the interior of the particle for the transformation to take place. Unfortunately, the analysis of the data makes no clear distinction between the appropriateness of either the one- or two-dimensional diffusion models, and so a brief discussion of their assumptions, successes and failings is appropriate.

The one-dimensional diffusion model [28] may be applied to systems in which an isotropic material in a plate morphology is undergoing a diffusion-limited process either with another solid, a liquid or a gas. This is a result of the tremendous surface area available on the plate faces, relative to the area of the plate edges. There is another circumstance in which this model might hold true, and that is for an anisotropic material, undergoing a diffusion limited process in which one set of crystal faces have significantly lower diffusion energy barriers relative to those faces which are orthogonal to them. If the difference is indeed large enough, a diffusion limited process would indeed appear to be one-dimensional. The sample morphology would continue to have an effect on the kinetics of the transformation, but its importance would diminish greatly.

The two-dimensional diffusion model [28] may be applied to isotropic materials with an acicular morphology undergoing a diffusion-limited process with a solid, liquid or gas. The two-dimensional approximation of this model is again due to the tremendous area of the wire side relative to that of the top and bottom. Similar to the argument made above, this model may also be applied to anisotropic systems, if the barrier to diffusion is much greater in one direction than the other two. The sample morphology again will

continue to play a role in the kinetics of the transformation, but with greatly diminished importance.

β-Na_3PO_3S has been previously indexed by Jansen et al. as hexagonal [6]. This assignment, if it is indeed correct, could support either possibility, as hexagonal materials have one dimension which is unique. If the unique direction were to have exceptionally low diffusion barriers relative to the other two, this would support the one-dimensional model; and if it were to have high diffusion barriers relative to the other two, this would support the two-dimensional model. The present experiment is not able to differentiate between the two models, since matters that potentially affect the kinetic process such as particle size [32,33], size distribution, and morphology [7] were not considered prior to experimentation and, in some cases, are impossible to control, as a result of the sample preparation methods employed.

5. Conclusions

A phase transition from β-Na_3PO_3S to α-Na_3PO_3S, two anhydrous inorganic crystalline species, has been observed. The temperature of this transition has been determined to be suppressed by 275° C by exposure to a humid atmosphere. Measurements of this humidity-induced phase transition have been made by *in situ* neutron powder diffraction. The sample phase composition through time was determined by an empirical whole pattern fitting method in the absence of structural knowledge of the β-phase. The kinetics of this transition has been determined to be either one- or two-dimensional diffusion. The diffusional character of the process is also supported by the observation that water was absorbed from the humid gas stream early in the

experiment and later released from the sample back into the flowing gas stream. At no point during the course of the experiment was any hydrated phase observed to be present in the sample. Although no hydrated phase was observed, the requirements of the diffusional models, coupled with the absorption/desorption of the gaseous water, indicate that water must be intimately involved in the interior of the transitioning particles during this process. The exact nature of this involvement is not yet fully understood; but, we look forward to further experimentation to reveal more details of this phenomenon which is so unusual among solid-state inorganic materials [29].

6. Acknowledgements:

The author gratefully acknowledges the patient assistance of Mr. Evan Maxey and Dr. Jim Richardson of the Intense Pulsed Neutron Source at Argonne National Laboratory, especially for the careful design of the controlled-humidity apparatus. We also thank Argonne National Lab and the Intense Pulsed Neutron Source for beam time (IPNS-4557). Thanks to Dr. Peter Wildfong for extended discussions regarding the study of solid-state kinetics. Thank you to the Department of Chemistry and Biochemistry at Duquesne University for the travel funds which made the trip to Argonne National Lab possible.

References

[1] A. Wurtz, Ann. Chim. Phys. 20 (1847) 472-482.

[2] C. J. Kubierschky, J. Prakt. Chem. 31 (1885) 93-111.

[3] E. Zintl, A. Bertram, Z. Anorg. Allg. Chem.245 (1940) 16-19.

[4] M. Jansen, M. Pompetzki, Z. Anorg. Allg. Chem. 628 (2002) 641-646.

[5] N. J. Takas, J. A. Aitken, Inorg. Chem. 45 (2006) 2779-2781.

[6] M. Pompetzki, L. van Wüllen, M. Jansen, Z. Anorg. Allg. Chem. 630 (2004) 384-388.

[7] Y. Sugawara, A. Nakamura, Y. Iimura, K. Kobayashi, H. Urabe, J. Phys. Chem. B. 106 (2002) 10363-10368.

[8] S. R. Byrn, R. P. Pfeiffer, J. G. Stowell, Solid-State Chemistry of Drugs, SSCI Inc., Indiana, 1999, pp. 443-460.

[9] D. Burnett, F. Theilmann, J. Booth, Int. J. Pharm. 287 (2004) 123-133.

[10] E. Vadas, P. Toma, G. Zografi, Pharm. Res. 8 (1991) 148-155.

[11] L. Beneš, K. Melánová, V. Zima, M. Trchová, E. Uhlířová, P. Matějka, Eur. J. Inorg. Chem. (2000) 895-900.

[12] M. Bartolomei, P. Bertocchi, E. Antoniella, A. Rodomonte, J. Pharmaceut. Biomed. 40 (2006) 1105-1113.

[13] J. B. Holt, I. B. Culter, M. E. Wadsworth, J. Am. Ceram. Soc. 45 (1962) 133-136.

[14] M. L. Foo, T. Klimczuk, R. J. Cava, Mater. Res. Bull. 40 (2005) 665-670.

[15] A. K. Sheridan, J. Anwar, Chem. Mater. 8 (1996) 1042-1051.

[16] A. Khawam, D. R. Flanagan, J. Pharm. Sci. 95 (2006) 472-498.

[17] T. Yoshinari, R. T. Forbes, P. York, Y. Kawashima, Int. J. Pharm. 247 (2002) 69-77.

[18] X. Xu, J. T. Han, D. H. Kim, K. Cho, J. Phys. Chem. B. 110 (2006) 2764-2770.

[19] C. J. Ellison, J. M. Torkelson, Nat. Mater. 2 (2003) 695-700.

[20] Y. Masuda, K. Hashimoto, Y. Ito, Thermochimica Acta. 163 (1990) 271-278.

[21] S. K. Yasuda, J. L. Lambert, Inorg. Syn. 5 (1957) 102-104.

[22] http://www.pns.anl.gov/ngs/ancillary/Sample%20Environments /Howe_Furnace.html (2007)

[23] T. Worlton, ISAW: Integrated Spectral Analysis Workbench, v. 1.8.0, http://www.pns.anl.gov/ISAW/ Intense Pulsed Neutron Source (2006).

[24] E. Maxey, J. Richardson, *unpublished work*.

[25] T. Egami, S. J. L. Billinge, Underneath the Bragg Peaks: Structural Analysis of Complex Materials, Pergamon Press, New York, 2003, p. 26,37.

[26] Microsoft® Office Excel 2003, Copyright 1985-2003, Microsoft Corporation.

[27] L. S. Ladson, A. D. Waren, A. Jain, M. Ratner, ACM T. Math Software, 4 (1978) 34-50.

[28] J. H. Sharp, G. W. Brindley, B. N. N. Achar, J. Am. Ceram. Soc. 49 (1966) 379-382.

[29] N. J. Takas, J. A. Aitken, *work in progress*.

[30] J. Laugier and A. Filhol, &&Programme CELREF, ILL," Grenoble, France, 1978.

[31] R. E. Carter, J. Chem. Phys. 34 (1961) 2010-2015.

[32] P. T. Cardew, R. J. Davey, A. J. Ruddick, I. Chem. E. Symposium Series No. 69. 123-133.

[33] F. Huang, J. F. Banfield, J. Am. Chem. Soc. 127 (2005) 4523-4529.

Chapter 4

A Simple Aqueous Metathesis Reaction Yields New Lanthanide Monothiophosphates

Abstract:

This chapter describes the synthesis and characterization of two, new rare earth monothiophosphate materials, $LaPO_3S \cdot xH_2O$ and $NdPO_3S \cdot yH_2O$, and their properties in comparison to the corresponding orthophosphates prepared by a similar aqueous metathesis reaction. Each of these new materials was found to exist in an amorphous phase similar to a corresponding orthophosphate mineral. The new rhabdophane-type oxythiophosphates were found to display reversible dehydration and rehydration under mild conditions. The materials were found to be thermally unstable. Disproportionation was found to occur at less than 450° C under vacuum. Sulfur is lost during heating in air between 450 and 650° C, according to TGA experiments, yielding the orthophosphate. The monothiophosphate hydrates display broad photoluminescence in the visible under excitation by a 325nm laser. The compounds were also analyzed using differential thermal analysis, FT-IR and UV/Vis/NIR spectroscopy.

1. Introduction

Oxythiophosphates are an underrepresented class of materials [1-8] which, although similar in composition to orthophosphates and tetrathiophosphates, still embody a unique family of compounds, with a potentially distinct set of properties [2-4,7,8]. Understanding the relationship between composition and properties in these systems is of fundamental interest because rare earth materials are important to the fields of luminescence and nuclear energy, among others.[9-12] The early lanthanide phosphates ($LnPO_4$) form two naturally occurring minerals. Monazite (Ln = La to Gd) [13] has a monoclinic structure, incorporates no water, and is thermodynamically favored. Rhabdophane (Ln = La to Dy) is less stable and has a porous hexagonal structure which can be reversibly dehydrated [14]. While both of these minerals have been extensively studied [13-16], the analogous monothiophosphate compounds reported here represent new materials.

Rare earth phosphates are being widely studied for their luminescent properties, which may be useful in optical amplification devices [11], plasma display panels [12], and many other light emitting applications [17]. Depending on the material being studied and the intended application, the luminescence of lanthanide phosphates has been studied from the NIR to VUV [11,18]. Substitution of the monothiophosphate anion for orthophosphate can provide another degree of freedom in the attempt to develop higher quality phosphors for technological applications.

Many rare earth phosphates are found as naturally occurring minerals [13-16], implying that they are stable on the geologic time scale. This makes rare earth phosphates particularly attractive as a potential nuclear waste storage form [10, 9].

Lanthanide phosphates have exceptionally low aqueous solubilities; for instance, lanthanum phosphate has a solubility product constant of merely $3.7x10^{-23}$ [19]. This very sparing solubility means that radioactive rare earth nuclear waste stored as its phosphate will not contaminate the local area via water tables near the storage site. We expect lanthanide oxythiophosphates to display similarly useful low solubilities.

In this chapter, a simple aqueous metathesis reaction which has produced two new rhabdophane-type lanthanide monothiophosphate hydrates, $LaPO_3S{\cdot}xH_2O$ and $NdPO_3S{\cdot}yH_2O$ is described. One of our goals is to demonstrate the similarities and differences between our new rare earth oxythiophosphate materials and the known rare earth phosphates. This is the first step in determining the potential use of these materials. To this end, the materials have been characterized using thermal analysis techniques, diffuse reflectance UV/Vis/NIR, photoluminescence and infrared spectroscopy.

2. Experimental

2.1 Synthesis

2.1.1 α-Na_3PO_3S

Alpha-sodium monothiophosphate (α-Na_3PO_3S) was prepared by hydrolysis of $PSCl_3$ (Aldrich, 98%) in an aqueous solution of sodium hydroxide, and subsequently dehydrated by spinning in anhydrous methanol, as described elsewhere [5-7,20].

2.1.2 $LnPO_3S{\cdot}xH_2O$ and $LnPO_4{\cdot}yH_2O$ (where Ln = La, Nd):

Rhabdophane-type lanthanum and neodymium monothiophosphate hydrates and the corresponding phosphate hydrates were prepared by aqueous precipitation [21]. Four mmol of $LnCl_3$ ($LaCl_3$ Acros 99.99%; $NdCl_3$ Cerac 99.9%) was dissolved in 50 mL of double deionized (DDI) water (18 MΩ) to which was added a solution of either 4 mmol

α-Na_3PO_3S or 4 mmol $Na_3PO_4 \cdot 12H_2O$ (Fisher 98%) dissolved in 50 mL DDI water. The sodium monothiophosphate or phosphate solution was added drop-wise at a rate of ~1 mL/min to minimize the possibility of trapping unreacted material or byproduct within cavities of the particles. The solution was then filtered and energy dispersive spectroscopy (EDS) was used to determine whether further washing of the solid was necessary to remove any NaCl byproduct, which may be present. In most cases, further washing was not necessary; but, in cases where necessary, washing proceeded via sonication of the solid in 50 mL DDI water. The powders yielded by this process were generally white with a slight yellow cast in the case of the lanthanum-containing materials, and a lilac hue in the case of hydrated neodymium-containing materials. The color of the neodymium-containing products took on a deeper blue color upon dehydration.

2.2 Physical measurements

2.2.1 Scanning Electron Microscopy and Energy Dispersive Spectroscopy

Scanning electron microscopy (SEM) images were obtained using a Tescan VegaXMU scanning electron microscope equipped with an IXRF energy dispersive spectrometer. Samples were prepared on double-sided carbon tape adhered to an aluminum stub. The SEM was operated at 20 kV with a hot tungsten filament. X-ray maps were obtained over 27 minutes.

2.2.2 Powder X-ray Diffraction:

Powder X-ray diffraction (PXRD) patterns were obtained on a PANalytical X'Pert PRO MPD powder X-ray diffractometer with the X'cellerator detector, using copper K_α radiation and operating at 45 kV and 40 mA. Samples were prepared by

backfilling the sample into the aluminum holder. In the case where only exceptionally small samples were available, such as in the examination of thermal analysis residues, the use of a zero-background, Si wafer sample holder was employed. All diffraction patterns were collected from 2 to 70° in 2θ, using a step size of 0.0170°, at a scan rate of 1.1789°/min with the sample rotating.

2.2.3 Differential Thermal Analysis:

Differential thermal analysis (DTA) was performed using a Shimadzu DTA-50, which was calibrated using a three-point calibration curve based on the melting points of indium, zinc and gold metals. The differential signal was balanced prior to the beginning of each experiment. Data were recorded using the Shimadzu TA60-WS collection program. Experiments were performed at a rate of 10° C/min. Samples were contained in alumina pans under a static air atmosphere. All DTA samples were referenced against an alumina sample, contained similarly and of comparable mass. Multiple heating and cooling cycles were performed in the DTA experiments to differentiate between reversible and irreversible thermal events. DTA residues were routinely examined using PXRD and EDS.

2.2.4 Thermogravimetric Analysis:

Thermogravimetric analysis (TGA) was performed using a Shimadzu TGA-50. The instrument was consistently operated in the 20 mg sensitivity setting. TGA data were recorded using the Shimadzu TA60-WS collection program. Samples were ground and placed in Pt crucibles. All samples were heated at a rate of 2° C/min. Anhydrous samples were measured under a flow of N_2 gas (50 mL/min); hydrated samples were

heated in a static air atmosphere. TGA residues were routinely examined using PXRD and EDS.

2.3 Optical Spectroscopy:

2.3.1 Diffuse Reflectance:

Diffuse reflectance mid-IR spectra were obtained on a Nicolet Nexus 470 FT-IR *ESP* (Thermo Electron Corp.). Spectra were collected against a standard mirror background. Samples were prepared by loading the ground material into a sample cup. All spectra were obtained as the average of 64 scans from 400 to 4,000 cm^{-1}. Data manipulation was performed according to the Kubelka-Munk equation [22].

Diffuse reflectance UV/Vis/NIR spectra were obtained using a Cary 5000 UV/Vis/NIR spectrometer (Varian) equipped with a Praying Mantis diffuse reflectance accessory (Harrick Scientific Corporation). Barium sulfate was used as a 100% reflectance standard. Samples were prepared by loading the ground material into a sample cup. All spectra were obtained from 2,500 to 200 nm at a scan rate of 600 nm/min. Data manipulation was performed according to the Kubelka-Munk equation [22].

2.3.2 Photoluminescence:

Photoluminescence (PL) spectra were obtained at room temperature using a 325 nm He-Cd laser. The PL signal was detected using a 0.64 m monochromator and a GaAs photomultiplier tube in photon counting mode. The laser power density at the sample was 0.5 W/cm^2. The powder samples were contained between two sapphire plates with the edges sealed by rubber cement. The intensities of the PL spectra were corrected for the detection system response using a calibrated white-light source.

3. Results and Discussion:

3.1 Synthesis

Although simple, the synthetic method employed is worthy of some note, as other methods, such as alkali polysulfide fluxes, have proven too harsh to conserve the monothiophosphate anion in the lanthanide system. When attempting to prepare a lanthanum monothiophosphate material in a sodium polysulfide flux, Dorhout et al. found that a disproportionation of the monothiophosphate anion was observed, with the product being sodium lanthanum phosphate thiosulfate [23]. However, we have found that a simple aqueous metathesis, which produces sodium chloride as a byproduct, is able to conserve the monothiophosphate anion to form two new lanthanum and neodymium monothiophosphates.

3.2 Crystallinity and Phase

Due to the rapid precipitation method employed and the exceedingly low solubility product constant of the lanthanide monothiophosphates, the products obtained are largely amorphous by PXRD. However, a combination of electron diffraction and dark field TEM images revealed that a small component of the sample exists in nanocrystalline domains (10-20 nm), while the bulk of the sample is indeed amorphous. The PXRD patterns of the as-prepared phosphates can be tentatively matched to reference patterns of rhabdophane-type lanthanide phosphates. Other researchers have produced more crystalline rhabdophane-type orthophosphates by aqueous precipitation methods from acidic solutions [21,24]. However, our synthesis was developed to intentionally

avoid acidic environments, due to the sensitivity of the monothiophosphate anion under oxidizing conditions [25].

Although amorphous, the diffraction patterns of the as-prepared monothiophosphate materials bear strong similarities to the diffraction patterns of the as-prepared phosphates (see Fig. 4-1, 4-2). The ability of a monothiophosphate phase to structurally mimic an orthophosphate phase is not unheard of in the literature, and has previously been reported for $H_2Zr(PO_3S)_2$ and $H_2Hf(PO_3S)_2$, which are structural mimics of the equivalent orthophosphates [26]. The IR spectra of the as-prepared materials also support the proposition that these new lanthanum and neodymium monothiophosphates are similar in structure to the rhabdophane-type orthophosphates.

3.3 Infrared

Infrared absorption spectra have held an important role in the debate regarding the structure of rhabdophane-type $LnPO_4$, helping to determine the most appropriate space group for the structure [14]. The utility of the infrared spectra here is primarily to establish evidence for the persistence of the monothiophosphate moiety by observation of

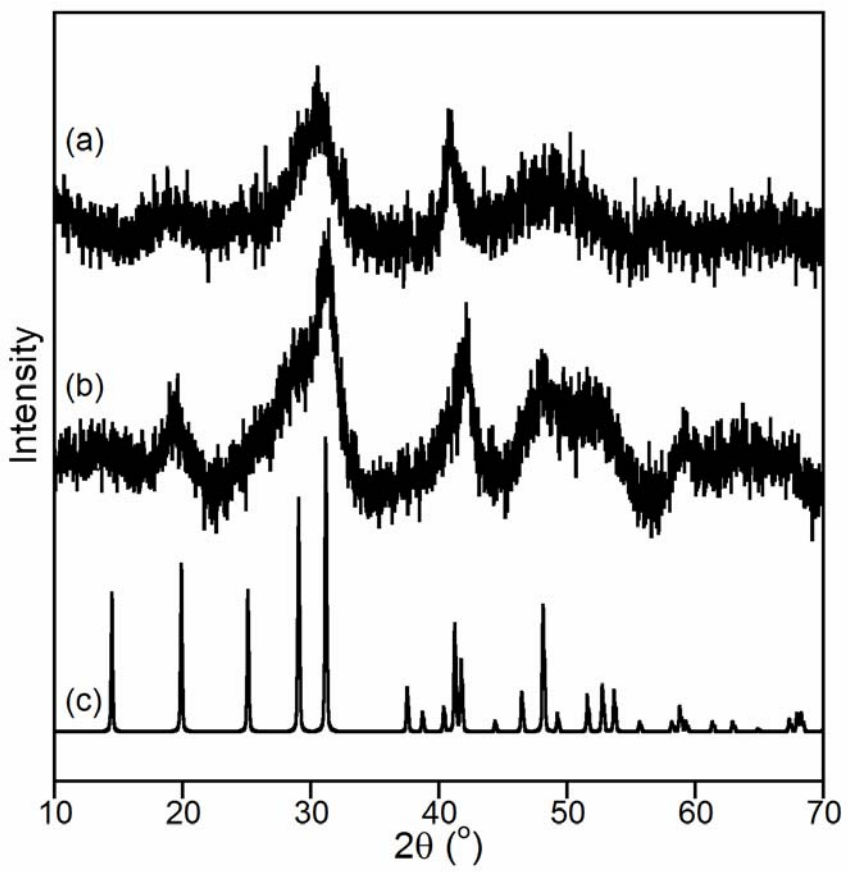

Fig. 4-1: Powder X-ray diffraction patterns of (a) the as-prepared $LaPO_3S$ hydrate, (b) the as-prepared $LaPO_4$ hydrate, (c) rhabdophane-type $LaPO_4$ (PDF# 00-046-1439).

materials (see Table 4-1, Fig. 4-3) [27]. The observation of the P-S stretch was observed at 496 and 497 cm^{-1} for La and Nd monothiophosphates respectively, which compare well to the value of 511 cm^{-1} observed in α-Na_3PO_3S.

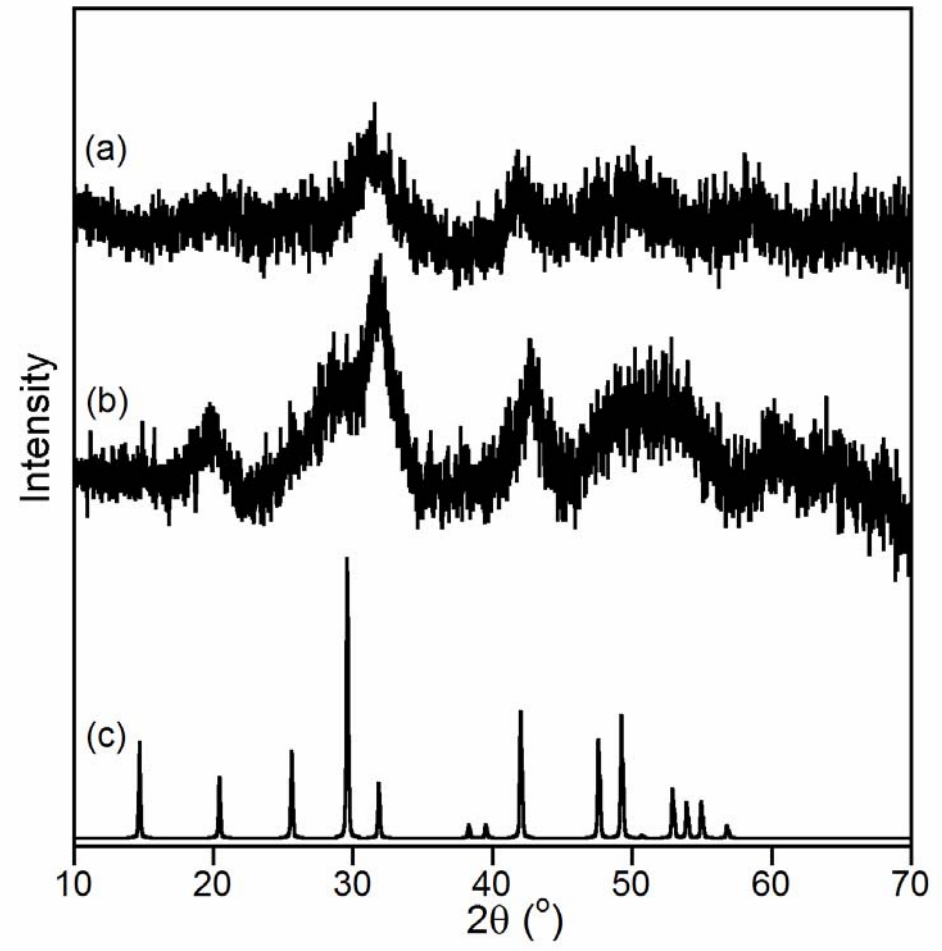

Fig. 4-2: Powder X-ray diffraction patterns of (a) the as-prepared $NdPO_3S$ hydrate, (b) the as-prepared $NdPO_4$ hydrate, (c) rhabdophane-type $NdPO_4$ (PDF# 00-004-0644).

Table 4-1: Summary of IR data compared with literature values.

As-prepared $LaPO_3S$ hydrate	As-prepared $LaPO_4$ hydrate	As-prepared $NdPO_3S$ hydrate	As-prepared $NdPO_4$ hydrate	Assignment [a]
3450,vs	3480,s	3420,vs	3490,s	Water of hydration [32]
1619,s	1633,s	1619,s	1629,s	
	1457,m		1467,m	
	1418,m		1418,m	
1097,s	1164,m	1097,s	1164,m	
1011m,br	1029,m,br	1006,m,sh	1036,m,br	T_2-A-E (rhab.) [10]
975m,br	970,m,br		972,m,br	A_1-A-E (rhab.) [10]
670,s	642,m,br	678,m	651,m,br	T_2-2B-A_2 (rhab.) [10]
566,m,br	574,m,br	568,m,br	581,m,br (unresolved)	T_2-A-E (rhab.) [10]
	553,m,br		556,m,br (unresolved)	T_2-2B-A_2 (rhab.) [10]
497,m,br		496,m,br		P-S (α-Na_3PO_3S) [32]

[a] Assignment and mode given are for the material in parentheses. Rhab. designates rhabdophane-type phosphate.

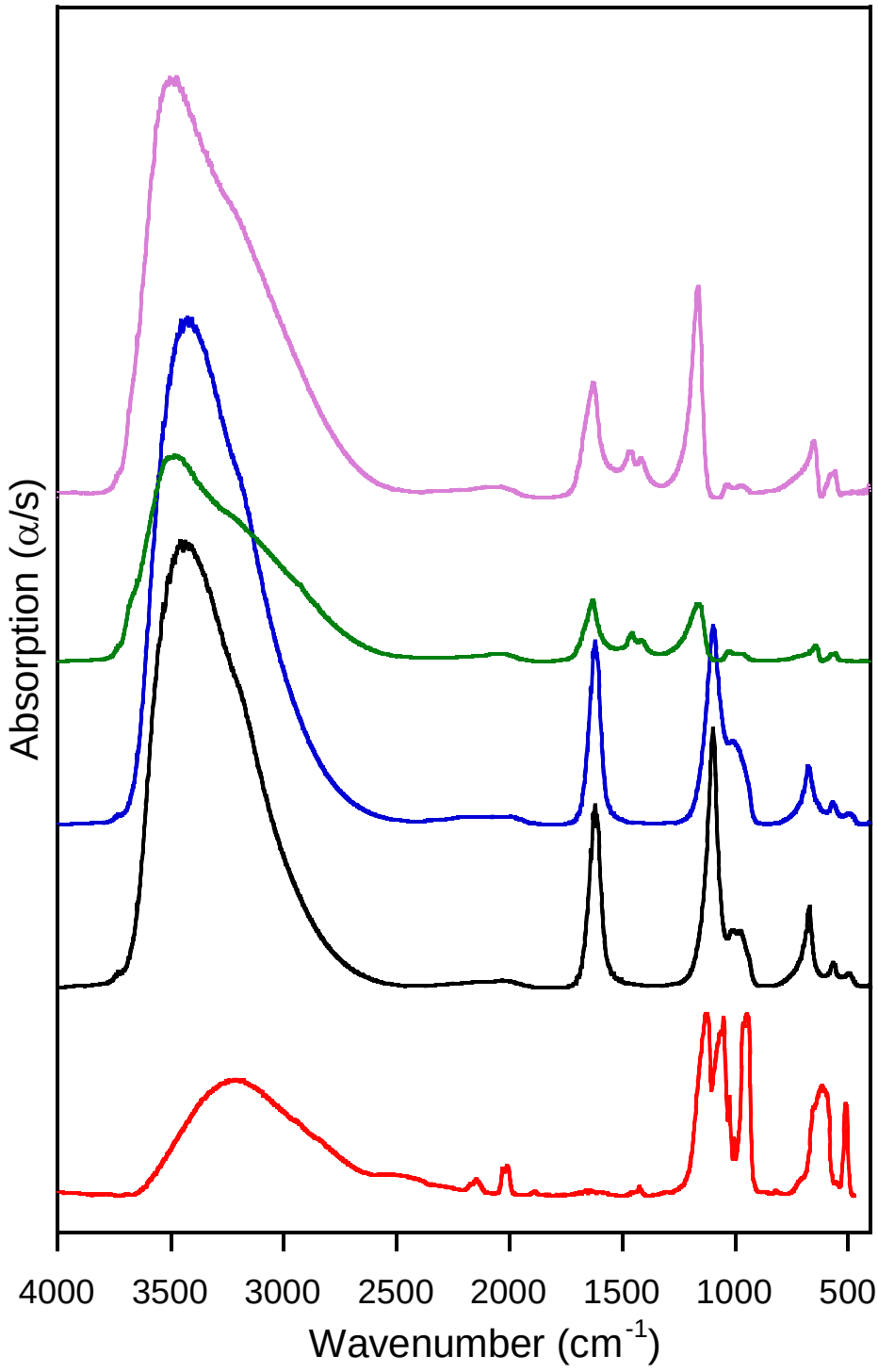

Fig. 4-3: IR absorption spectra of $NdPO_4$ as-prepared hydrate (purple), $LaPO_4$ as-prepared hydrate (green), $NdPO_3S$ as-prepared hydrate (blue), $LaPO_3S$ as-prepared hydrate (black), and α-Na_3PO_3S (red).

3.4 Band Gaps

Diffuse reflectance UV/Vis/NIR revealed the band gaps of the new materials to be 5.35eV for the as-prepared $LaPO_3S$ hydrate and 5.20eV for the as-prepared $NdPO_3S$ hydrate (see Fig. 4-4), which are off-white and faintly lilac powders respectively. These band gaps are reduced with respect to the orthophosphates, which have band gaps that are too large to be determined using our instrument. The optical spectrum of each of the neodymium rhabdophane-type materials is modified by the superposition of absorptions due to f-f transitions [28], as observed in other lanthanide-containing compounds [29-31].

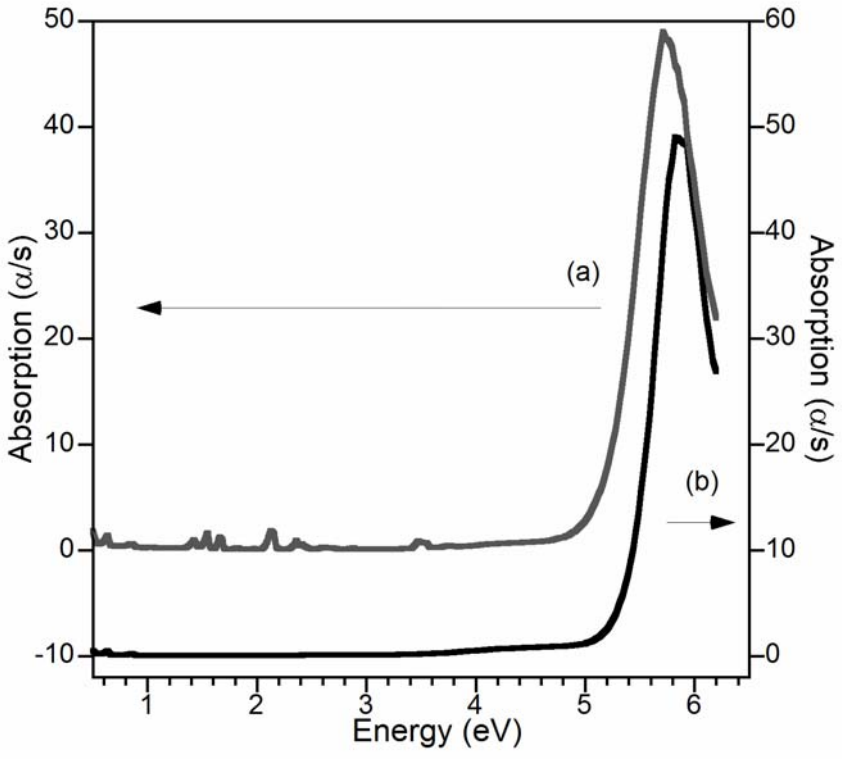

Fig. 4-4: Optical diffuse reflectance spectra of (a) the as-prepared $NdPO_3S$ hydrate and (b) the as-prepared $LaPO_3S$ hydrate. The Nd spectrum is modified by *f-f* transitions.

3.5 Photoluminescence

Photoluminescence spectra reveal that the photoluminescent intensity of the lanthanide monothiophosphate materials is comparable to that of the orthophosphates (see Fig. 4-5). The sulfur substitution seems to have given rise to an additional broad peak, centered at 3.205 eV in the PL spectrum of $LaPO_3S$ hydrate which may also appear in the other prepared materials with greatly reduced intensity. The PL spectrum of each of the neodymium rhabdophane-type materials is again modified by the superposition of *f-f* transitions [28-31]. One may readily observe that the net intensity of the as-prepared $LaPO_3S$ hydrate is noticeably less than the corresponding orthophosphate material, while

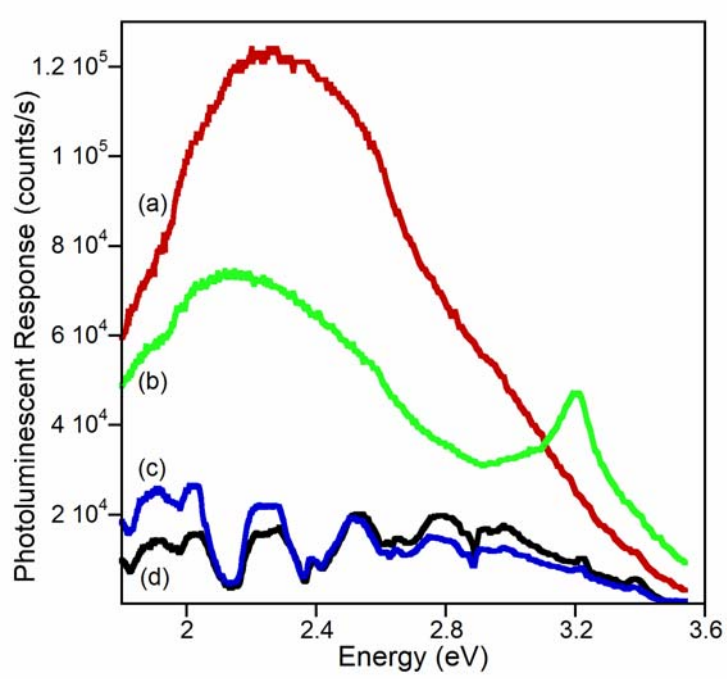

Fig. 4-5: Photoluminescence spectra of (a) $LaPO_4$ as-prepared hydrate, (b) $LaPO_3S$ as-prepared hydrate, (c) $NdPO_3S$ as-prepared hydrate, and (d) $NdPO_4$ as-prepared hydrate. Both Nd spectra are modified by absorptions arising from *f-f* transitions.

the PL response of the Nd-containing materials are largely similar. This difference in the PL response of the La-containing materials may be due to the varied level of hydration of the two materials (see section 3.6). [32-34] The total level of hydration of $LaPO_3S$ hydrate is increased by a factor of 1.34 relative to $LaPO_4$ hydrate. The total integrated photoluminescent intensity of $LaPO_3S$ hydrate is decreased by a factor of 1.46 relative to $LaPO_4$ hydrate. Further investigation is needed to determine the specific origins of the observed photoluminescent behavior.

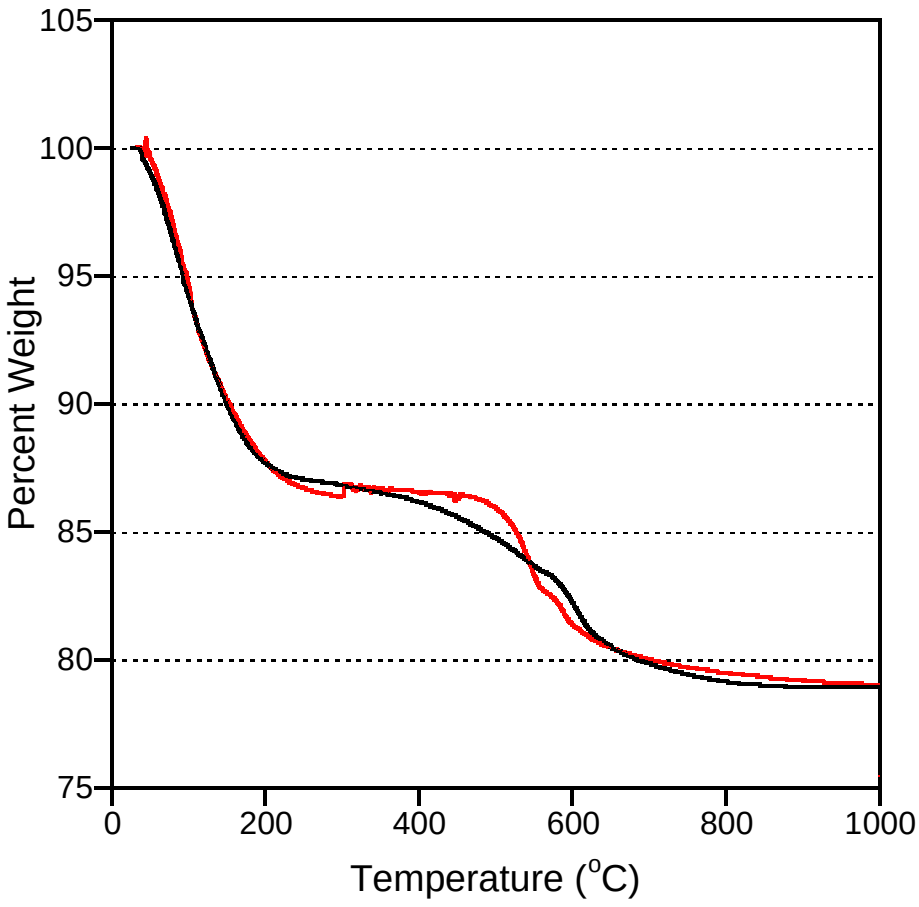

Fig. 4-6: Thermogravimetric analysis (TGA) of $LaPO_3S \cdot 2.57H_2O$ (black) and $NdPO_3S \cdot 2.27H_2O$ (red)

3.6 Hydration and Thermal Stability in Air

The rhabdophane-type lanthanide phosphates are known to contain a variable amount of water, cited in the literature as containing 0.5-3.0 molar equivalents [35-39]. The $LnPO_3S$ hydrate and $LnPO_4$ hydrate materials produced in this work are no exception, as TGA of the as-prepared products in a static air atmosphere reveals an early weight loss corresponding to loss of water from room temperature to ~200° C (see Fig. 4-6, 4-7 Table 4-2). Additionally, each of the as-prepared monothiophosphate materials displays a second and third weight loss, from 450 to 550° C, and from 550 to 650° C. The sum of these losses corresponds to the loss of sulfur with a concomitant addition of oxygen. These evaluations are based on EDS and PXRD patterns of the TGA residues. EDS analyses of the TGA residues reveal an absence of sulfur from the materials, and PXRD patterns of the post TGA residues show the materials to be phase-pure monazite-type $LnPO_4$ (see Fig. 4-8); this confirms that a phase transition does occur as a thermal event,[39] but is nonspecific as to the temperature of the event and whether or not it preceeds disproportionation.

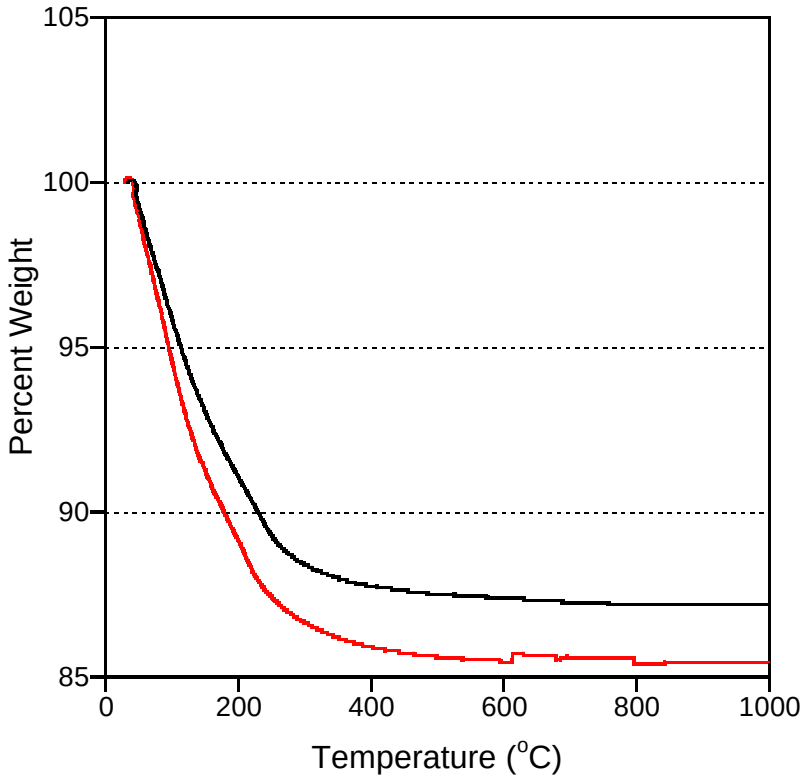

Fig. 4-7: TGA of $LaPO_4 \cdot 1.91H_2O$ (black) and $NdPO_4 \cdot 2.26H_2O$ (red).

Table 4-2: Summary of TGA weight loss data.

Material	Dehydration (1^{st} weight loss) (%)	Moles of water lost	Loss of sulfur with gain of oxygen (2^{nd} and 3^{rd} weight losses) (%)	Calculated value for 2^{nd} and 3^{rd} weight losses (%) [a]
$LaPO_3S \cdot xH_2O$	15.65	-2.57 H_2O	5.42	5.42
$NdPO_3S \cdot yH_2O$	13.49	-2.27 H_2O	7.47	5.42
$LaPO_4 \cdot xH_2O$	12.80	-1.91 H_2O	-	-
$NdPO_4 \cdot yH_2O$	14.25	-2.26 H_2O	-	-
dehydrated $LaPO_3S$	-	-	7.89	6.43
dehydrated[b] $NdPO_3S$	2.397	-0.35 H_2O	7.65	6.29
rehydrated $LaPO_3S \cdot H_2O$	5.80	-0.86 H_2O	6.07	6.05
rehydrated $NdPO_3S \cdot H_2O$	4.176	-0.99 H_2O	8.22	5.88

[a] This column of data were generated by assuming a stoichiometric formula for the compounds.

[b] While efforts were made to prevent rehydration of the sample during preparation for TGA experiments, a small amount of water was absorbed prior to beginning of the TGA experiment.

To further test the assignment of the two weight loss events, a sample of each of the $LnPO_3S$ hydrate samples was dried in an oven at 150° C for several hours. Thermogravimetric analyses of these materials were obtained under N_2 flow to minimize the possibility of rehydration during the early stages of the experiment. Indeed only the second and third weight losses were then observed (see Fig 4-9, Table 4-2). PXRD patterns of the dehydrated materials were also acquired, (see Figs. 4-10, 4-11) and did not show any marked change from the pattern of the hydrated samples.

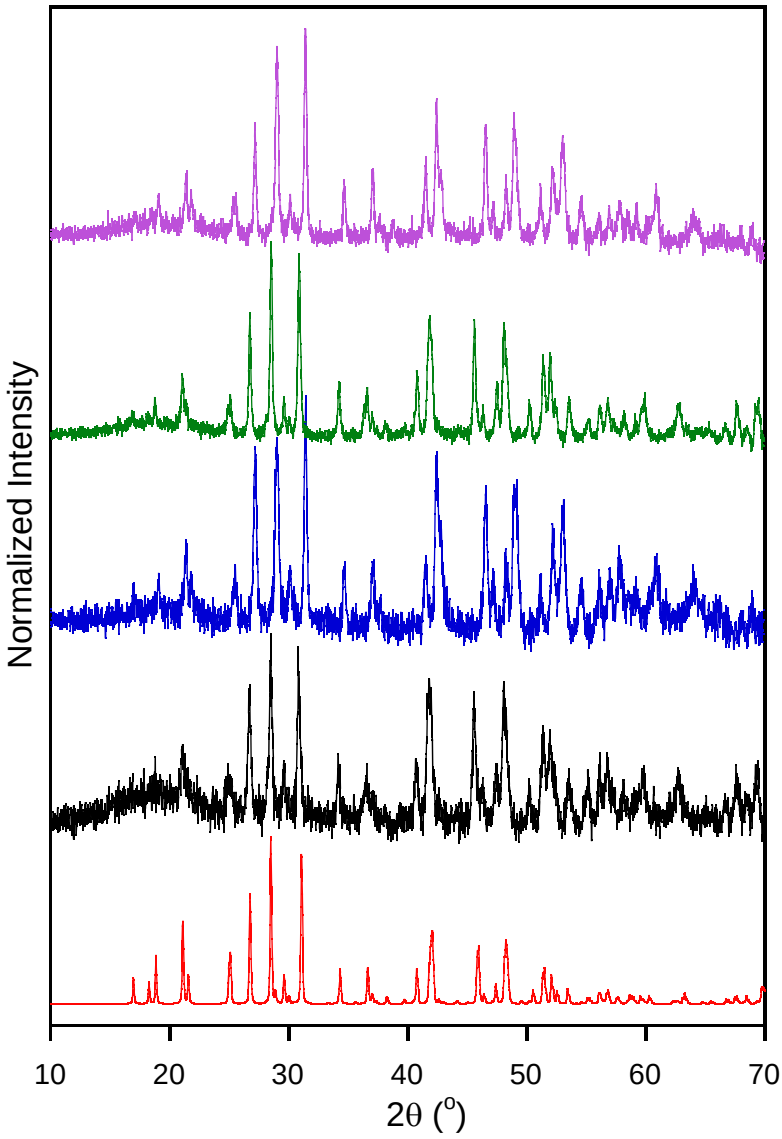

Fig. 4-8: PXRD patterns of 1000°C TGA residues: $NdPO_3S \cdot 2.27H_2O$ (purple), $LaPO_3S \cdot 2.57H_2O$ (green), $NdPO_4 \cdot 2.26H_2O$(blue), $LaPO_4 \cdot 1.91H_2O$(black), and monazite-type $LaPO_4$ (red) (PDF# 01-073-0188). Please note that these are the materials after TGA analysis. After TGA analysis, all materials were found to be monazite-type $LaPO_4$ or $NdPO_4$.

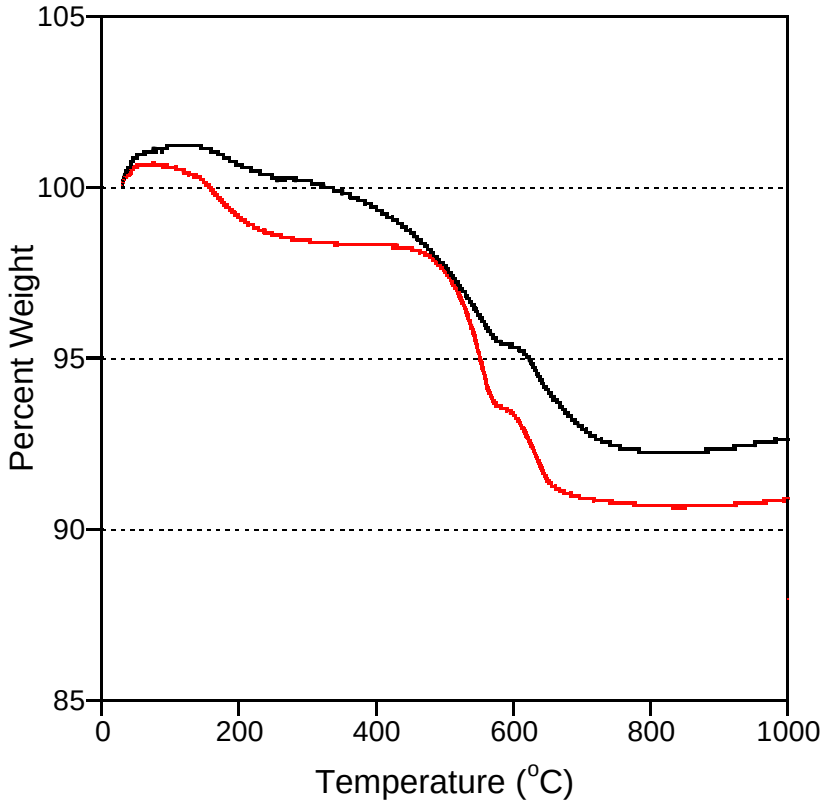

Fig. 4-9: TGA of $LaPO_3S$ dehydrate (black) and $NdPO_3S$ dehydrate (red). Early weight gains are due to partial rehydration due to exposure to atmospheric water.

at 150° C for several hours. The samples were then allowed to rehydrate by exposure to ambient laboratory conditions for several days (relative humidity ~20%). Thermogravimetric analyses of the materials were again performed, and the materials were now found to display similar weight loss events as the original samples; however, the hydration of each of the materials was found to have been reduced to approximately one molar equivalent of water (see Fig. 4-12, Table 4-2).

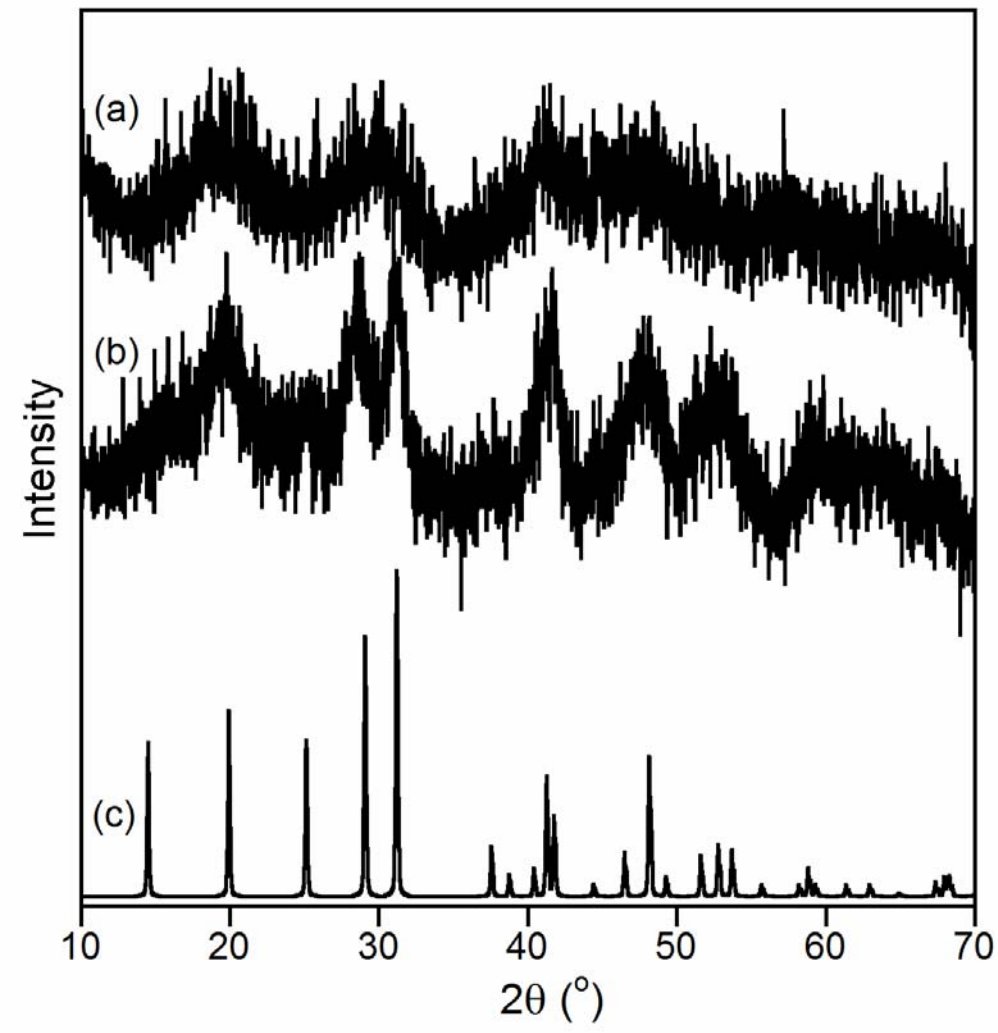

Fig. 4-10: PXRD patterns of (a) $LaPO_3S$ dehydrate, (b) $LaPO_4$ dehydrate, and (c) reference rhabdophane-type $LaPO_4$ (PDF# 00-046-1439).

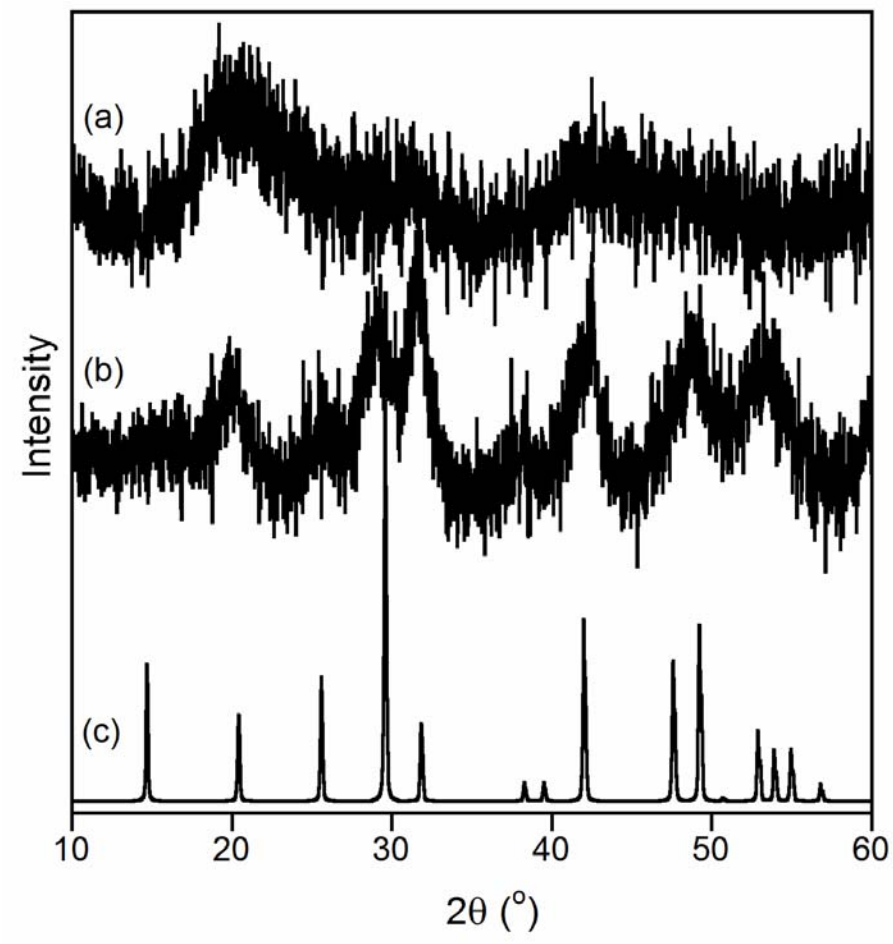

Fig. 4-11: PXRD patterns of (a) $NdPO_3S$ dehydrate, (b) $NdPO_4$ dehydrate, and (c) reference rhabdophane-type $NdPO_4$ (red) (PDF# 00-004-0644).

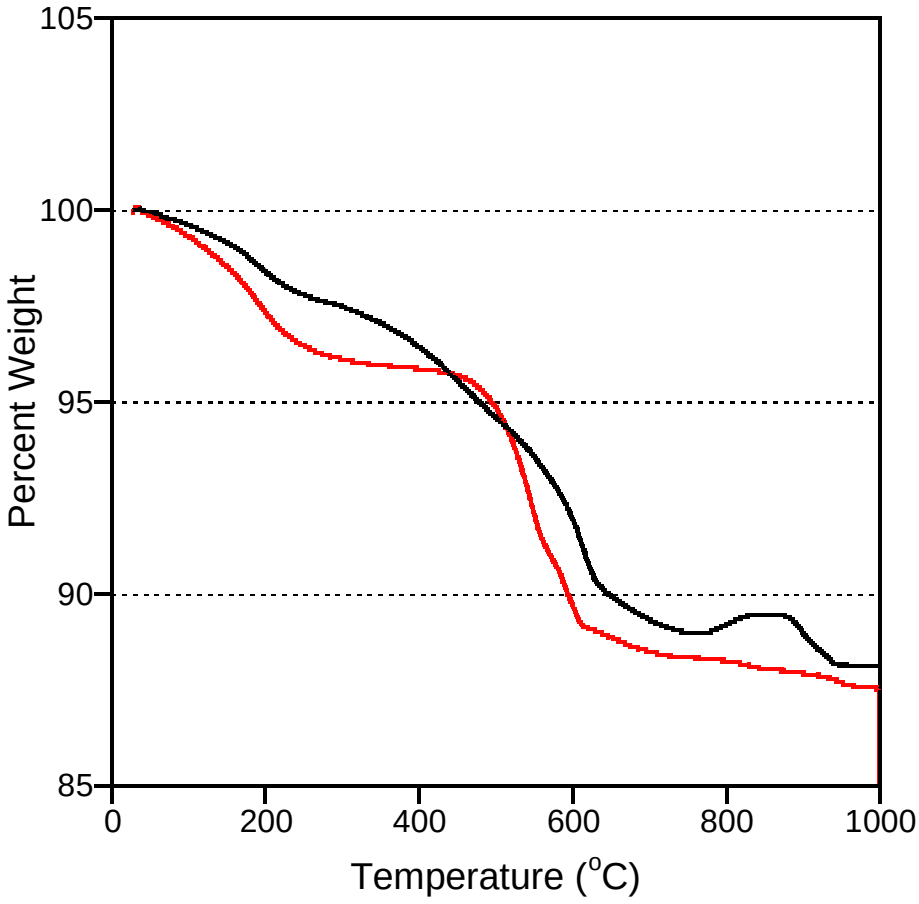

Fig. 4-12: TGA of $LaPO_3S$ dehydrate rehydrated in air (black) and $NdPO_3S$ dehydrate rehydrated in air (red).

DTA examination of the disproportionation and oxidation processes in air revealed that the disproportionation and phase transition to monazite-type $LaPO_4$ occur from approximately 300 to 800° C. (see Fig. 4-13a). The transformation from rhabdophane to the thermodynamically favored monazite is exothermic in the phosphate system [24,39]; however, the monothiophosphate compounds also undergo disproportionation, which convolutes the assignment of thermal events. Dehydration has been established as the first endothermic event, which ends before 200° C, and oxidation has been established as the third and/or fourth events based on correlations with the TGA data (see Fig. 4-13).

3.7 Thermal Stability of Dehydrated Samples in Vaccuo

The rhabdophane phase, in the orthophosphate system, is only a metastable phase; the monoclinic monazite structure is the more thermodynamically stable phase. Rhabdophane-type lanthanide phosphates convert thermally to the stable monazite structure between 500 and 900° C as an irreversible exothermic process [24,39]. Therefore, an attempt was made to thermally convert the rhabdophane-type monothiophosphate phases to the corresponding monazite-type phases by heating aliquots of the dehydrated rhabdophane $LnPO_3S$ to 1000° C in a furnace under static vacuum [39]. This process resulted in disproportionation; the PXRD patterns of the products were found to exactly match those of monazite-type $LnPO_4$. To investigate this process more carefully, a series of $LaPO_3S$ samples were dehydrated by heating in air to 150° C, sealed under vacuum and heated to maximum temperatures of 150, 300, 450, 600, 750, and 900° C. While X-ray maps of the 300° C sample indicated that the sample

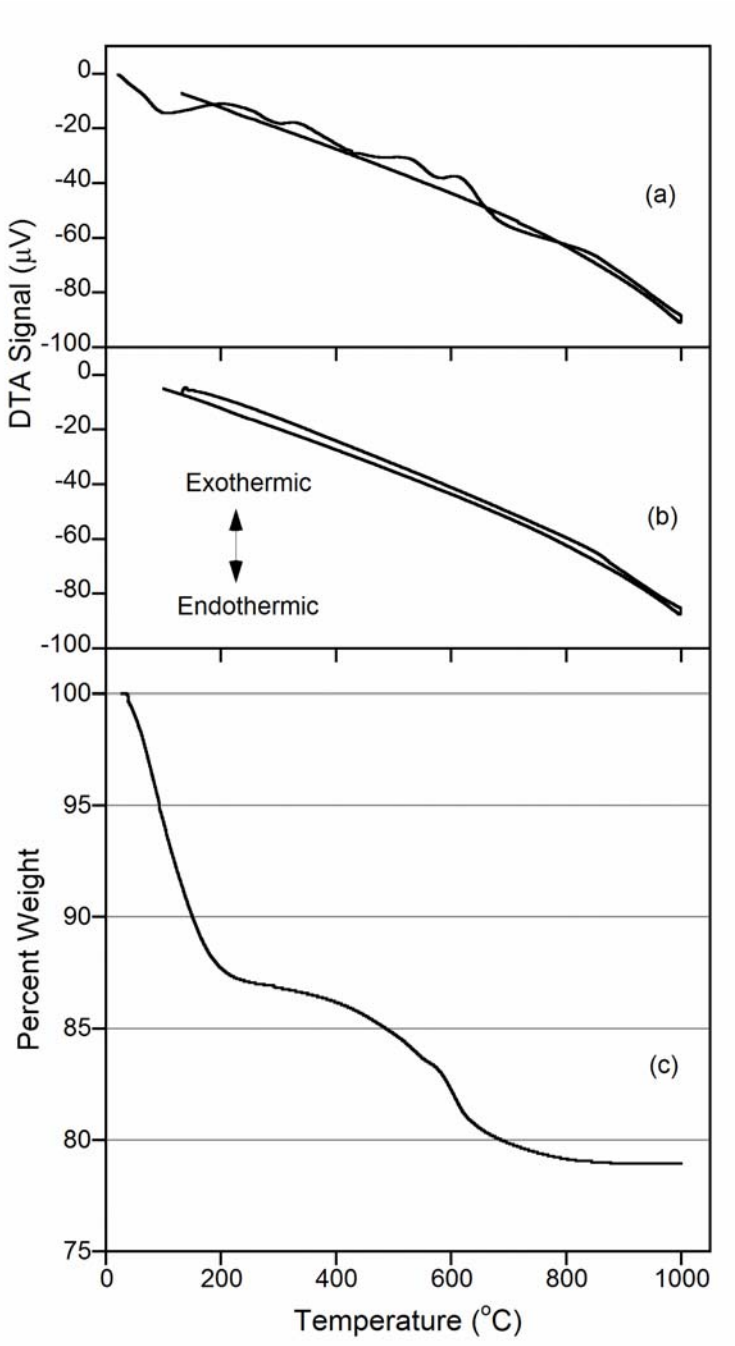

Fig. 4-13: (a) First DTA cycle of the oxidation of as-prepared $LaPO_3S$ hydrate carried out under a static air atmosphere. Dehydration occurs as an endothermic event up to ~150°C. Disproportionation and conversion to monazite-type $LaPO_4$ occur as a series of irreversible thermal events from 300 to 850°C. (b) Second DTA cycle showing no reversible thermal events. (c) The TGA weight loss profile of the as-prepared $LaPO_3S$ hydrate carried out under a static air atmosphere showing three distinct weight loss events.

was single phase, X-ray maps of the 450° C sample showed that the material had disproportionated. X-ray maps of the 900° C sample clearly showed phase segregation, as the sulfur was present in islands which also contained lanthanum and phosphorus (see Fig. 4-14). PXRD patterns of the residues revealed sharpened diffraction peaks for samples heated to 750 and 900° C (see Fig. 4-15). The PXRD pattern of these samples matched that of monazite-type lanthanum phosphate, however, the patterns did not indicate any secondary crystalline component. Therefore, the identity of the sulfur containing species remains unknown, however, it seems reasonable to suppose that it may be $LaPS_4$ based on the EDS results.

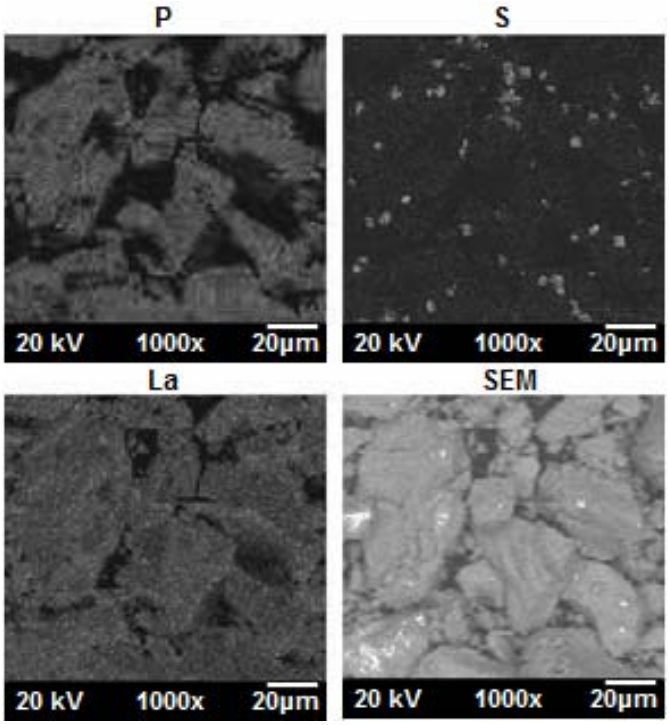

Fig. 4-14: Elemental maps and SEM image of dehydrated $LaPO_3S$ heated to 900°C under vacuum

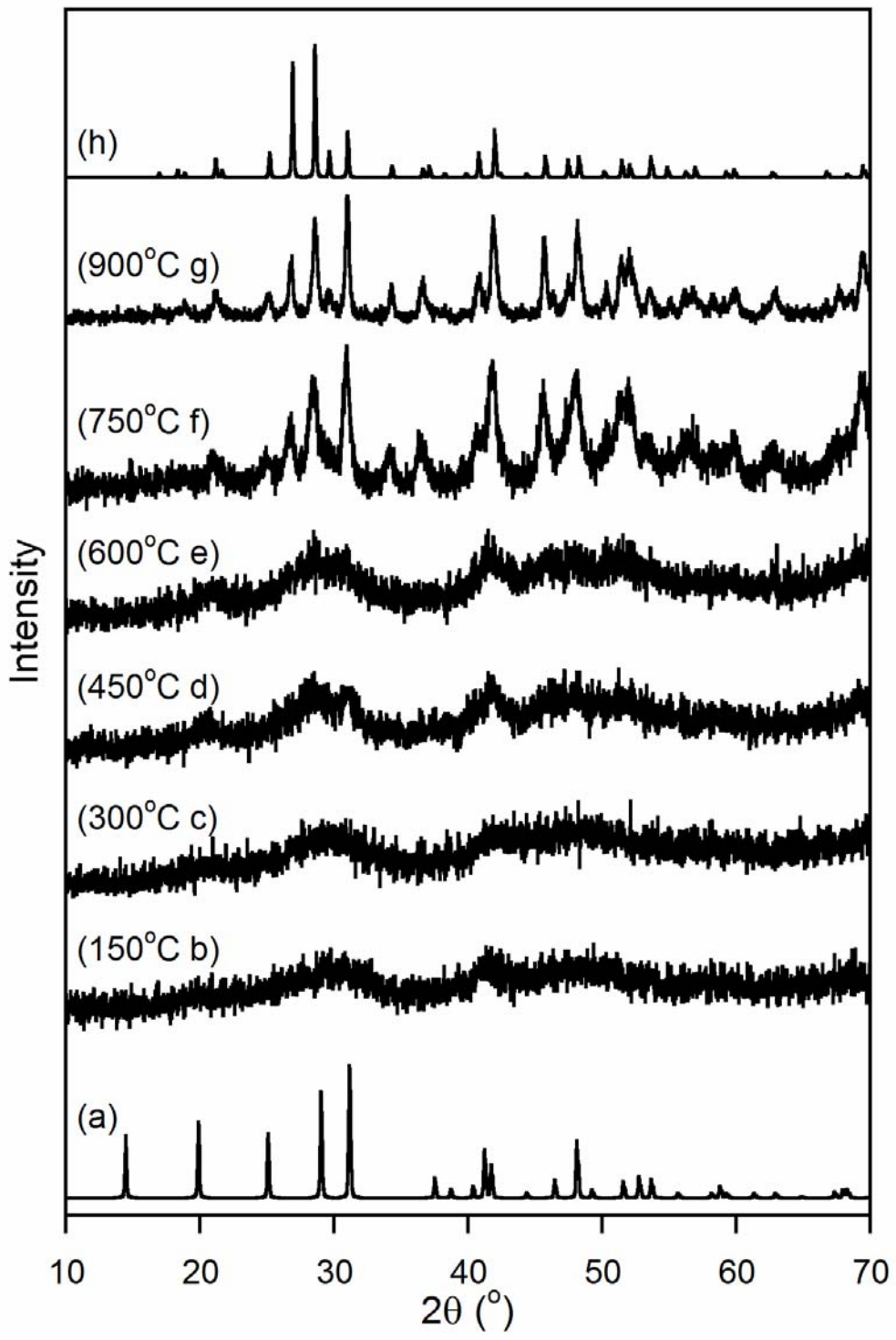

Fig. 4-15: Ex-situ PXRD diffraction patterns of dehydrated $LaPO_3S$ heated under vacuum to various temperatures a) rhabdophane-type $LaPO_4$ (PDF# 00-046-1439), b) 150°C, c) 300°C, d) 450°C, e) 600°C, f) 750°C, g) 900°C, h) monazite type $LaPO_4$ (PDF# 00-012-0283).

Several attempts were made to observe this disproportionation process under static vacuum by DTA; however, the DTA ampoules burst every time at around 600° C. It is interesting to note the temperature at which the DTA ampoules failed, as this corresponds to the temperature range during which the samples lose sulfur and gain oxygen during TGA experiments in air. The thermal stability of the material therefore, does not seem to be greatly affected by the presence of air. The lack of an effect by air on the thermal stability of the materials may mean that disproportionation in air may be similar to that observed under vacuum. The proposition that the second endothermic DTA event (300-400° C) may correspond to disproportionation could not be tested unambiguously, as the material has already begun to lose mass in this region, as indicated by TGA experiments.

4. Conclusions

A gentle and simple aqueous metathesis has been used to prepare two new lanthanide oxythiophosphate hydrates which are mimics of the naturally occurring orthophosphate mineral rhabdophane. Hydration and IR data support that the new monothiophosphate materials are structurally related to the mineral rhabdophane. At low temperatures, dehydration and rehydration may be cycled. The amount of water present in the structure may be a function of the crystallinity of the material, as evidenced by the limited capacity for uptake of water upon rehydration.

Both materials were found to retain the monothiophosphate anion up to a minimum temperature of 300° C under vacuum; however, at higher temperatures, disproportionation led to islands of an unknown sulfur-containing phase and a phase transition to monazite-type $LnPO_4$. The temperature of the phase transition which

finally yields monazite-type $LnPO_4$ cannot be pinpointed and may occur in concert with the oxidation process. The marked similarity of the chemistry of the trivalent lanthanides encourages us to predict that other lanthanide monothiophosphates may be formed by similar metathesis reactions. Additionally, the simplicity of this method makes it a desirable synthetic option for the discovery of other new oxythiophosphate materials which may be prone to decomposition or disproportionation under any but the gentlest of conditions.

5. Acknowledgements

Thank you to Ms. Lauren Slomka for much of the early exploration of this reaction system. Thank you to the Noble Dick Fund for a summer research fellowship for Ms. Slomka. Thank you to Dr. Nancy Giles and Mr. Xiaocheng Yang for photoluminescence measurements. Thank you to the National Science Foundation (Grant No. DMR-0508140) for supporting Dr. Giles and Mr. Yang. Thank you to the Bayer School of Natural and Environmental Sciences for funding. The powder X-ray diffractometer was purchased with funds from the National Science Foundation (Grant No. DUE-0511444).

References

[1] K. K. Palkina, S. I. Maksimova, N. T. Chibiskova, T. A. Tripol'skaya, G. U. Wolf, T. B. Kuvshinova, Izv. Akad. Nauk SSSR, Neorg. Mater. 27 (1991) 1028-1031.

[2] M. Pompetzki, M. Jansen, Z. Anorg. Allg. Chem. 629 (2003) 1929-1933.

[3] M. Pompetzki, L. van Wuelen, M. Jansen, Z. Anorg. Allg. Chem. 630 (2004) 384-388.

[4] M. Pompetzki, R. E. Dinnebier, M. Jansen, Solid State Sci. 5 (2003) 1439-1444.

[5] N. J. Takas, J. A. Aitken, Inorg. Chem. 45 (2006) 2779-2781.

[6] N. J. Takas, J. A. Aitken, J. Solid State Chem. 180 (2007) 2034-2043.

[7] A. E. Gash, P. K. Dorhout, S. H. Strauss, Inorg. Chem. 39 (2000) 5538-5546.

[8] I. A. Stenina, A. D. Aliev, P. K. Dorhout, A. B. Yaroslavtsev, Inorg. Chem. 43 (2004) 7141-7145.

[9] R. C. Ewing, L.-M. Wang, Rev. Miner. Geol. 48 (2002) 673-699.

[10] B. Glorieux, R. Berjoan, M. Matecki, A. Kammouni, D. Perarnau, Appl. Surf. Sci. 253 (2007) 3349-3359.

[11] J.-K. Jung, J.-S. Oh, S.-I. Seok, T.-H. Lee, J. Lumin. 114 (2005) 307-313.

[12] R. P. Rao, D.J. Devine, J. Lumin. 87-89 (2000) 1260-1263.

[13] E. N. Silva, A. P. Ayala, I. Guedes, C. W. A. Paschoal, R. L. Moreira, C.-K. Loong, L. A. Boatner, Opt. Mater. 29 (2006) 224-230.

[14] H. Assaaoudi, A. Ennaciri, A. Rulmont, Vib. Spectrosc. 25 (2001) 81-90.

[15] K. Wang, J. Zhang, J. Wang, C. Fang, W. Yu, X. Zhao, H. Xu, J. Appl. Crystallogr. 38 (2005) 675-677.

[16] Y. Hikiichi, C. F. Yu, M. Miyamoto, S. Okada, J. Alloy Compd. 192 (1993) 102-104.

[17] B. Moine, G. Bizarri, Opt. Mater. 28 (2006) 58-63.

[18] Y. Wang, C. Wu, J. Wei, J. Lumin. 126 (2007) 503-507.

[19] M. Kawase, T. Suzuki, K. Miura, Chem. Eng. Sci. 62 (2007) 4875-4879.

[20] S. K. Yasuda, J. L. Lambert, Inorg. Syn. 5 (1957) 102-104.

[21] S. Lucas, E. Champion, D. Bregiroux, D. Bernache-Assollant, F. Audubert, J. Solid State Chem. 177 (2004) 1302-1311.

[22] P. Kubelka, F. Munk, Z.Tech. Phys. 12 (1931) 593-601.

[23] M. G. Zhizhin, H. A. Pounds, F. M. Spiridonov, L. N. Komissarova, P. K. Dorhout, J. Alloy. Compd. 418 (2006) 90-94.

[24] R. Kijkowska, Thermochim. Acta. 404 (2003) 81-88.

[25] E. Thilo, E. Schone, Z. Anorg. Chem. 259 (1949) 225-232.

[26] A. Clearfield, J. A. Stynes, J. Inorg. Nucl. Chem. 26 (1964) 117-129.

[27] G. Socrates, Infrared Characteristic Group Frequencies: Tables and Charts, John Wiley and Sons, New York, 1994.

[28] F. A. Cotton, G. Wilkinson, C. A. Murillo, M. Bochmann, Advanced Inorganic Chemistry, John Wiley and Sons, New York, 1999, pp 1108-1129.

[29] G. B. Jin, E. S. Choi, R. P. Guertin, J. S. Brooks, T. H. Bray, C. H. Booth, T. E. Albrecht-Schmitt, J. Solid State Chem. 7 (2007) 2129-2135.

[30] G. W. Burdick, C. K. Jayasankar, F. S. Richardson, Phys. Rev. B. 50 (1994) 16309-16325.

[31] Y. Hasegawa, Y. Wada, S. Yanagida, J. Photochem. Photobiol., C. 5 (2004) 183-202.

[32] G. M. Davies, R. J. Aarons, G. R. Motson, J. C. Jeffery, H. Adams, S. Faulkner, M. D. Ward, Dalton Trans. (2004) 1136-1144.

[33] G. M. Davies, S. J. A. Pope, H. Adams, S. Faulkner, M. D. Ward, Inorg. Chem. 44 (2005) 4656-4665.

[34] A. Beeby, I. M. Clarkson, R. S. Dickins, S. Faulkner, D. Parker, L. Royle, A. S. de Sousa, J. A. G. Williams, M. Woods, J. Chem. Soc. Perkin Trans. 2. (1999) 493-503.

[35] J. F. W. Bowles, D. G. Morgan, Miner. Mag. 48 (1984) 146-148.

[36] C. R. Patra, G. Alexandra, S. Satra, D. S. Jacob, A. Gedanken, A. Landau, Y. Gofer, New J. Chem. 29 (2005) 733-739.

[37] S. Gallini, J. R. Jurado, M. T. Colomer, Chem. Mater. 17 (2005) 4154-4161.

[38] V. Buissette, M. Moreau, T. Gacoin, J.-P. Boilot, J.-Y. Chane-Ching, T. Le Mercier, Chem. Mater. 16 (2004) 3767-3773.

[39] R. G. Jonasson, E. R. Vance, Thermchim. Acta 108 (1986) 65-72.

Chapter 5

Attempts to Prepare Iron Monothiophosphate Unveil an Unusual Reaction in an Uncommon System

Abstract: This chapter will present reactions intended to prepare iron(III) monothiophosphate. Reactions were attempted using a wide range of synthetic strategies, including solution metathesis, solvothermal synthesis, and solid state metathesis at elevated temperatures. Additionally, a room-temperature solid-state metathesis reaction was also found to occur between $FeCl_3$ and α-Na_3PO_3S at room temperature. This reaction is accelerated dramatically by exposure of the reaction mixture to a humid air supply. The unusual characteristics of this reaction, the seemingly fine differences which affect its outcome, and the results of the other syntheses will be presented.

1. Introduction

Oxythiophosphates are an underexplored class of materials [1-8] which, although similar to orthophosphates and tetrathiophosphates in many ways, might still display a distinct set of properties.[2-4,7,8] Although the first oxythiophosphate material was reported as early as 1847,[9] they have remained relatively unknown. Determination of the crystal structure of α-sodium monothiophosphate,[10] recent discovery of a meta-stable high temperature phase, β-Na_3PO_3S,[3] and the effective use of Na_3PO_3S as a

reagent [7] in the formation of new materials have renewed interest in exploring this family of compounds.

Interest in the iron(III) monothiophosphate system was driven by a desire to demonstrate the general applicability of metathesis reactions to form new monothiophosphate materials. Thus far, we have demonstrated that $LaCl_3$ and $NdCl_3$ can be reacted with Na_3PO_3S to produce lanthanide monothiophosphates with the byproduct, NaCl.[11] The ability to generalize this reaction scheme to systems other than the lanthanides would open many new possibilities for the rapid expansion of the oxythiophosphate family, which, until this work, contained only 29 members.

Additionally, interest in preparing iron(III) monothiophosphate was prompted by the iron phosphate and tetrathiophosphate systems, which have demonstrated potential as technologically useful materials. It was our hope that research into the iron monothiophosphate system might spawn interest in its further development in similar applications. Lithium iron(II) phosphate has shown potential as a cathode material for lithium ion batteries. [12-14] Iron(III) phosphate has been shown to be an effective catalyst for the oxidative dehydrogenation of isobutyric acid to methacrylic acid.[15,16] Iron(III) phosphate can also be used as a means to remove arsenic from non-potable water.[17] Iron thiophosphates have also shown potential in the field of cathodic materials for lithium ion batteries,[18] and have displayed interesting magnetic properties at low temperatures.[19] Since, useful properties have been discovered in the iron phosphate and thiophosphate systems, it seems worthwhile to explore the chemistry of the iron monothiophosphate system.

2. Experimental

2.1 Synthesis

FeF_3 (Strem 99%), $FeCl_3$ (Strem 98%), $FeBr_3$ (Strem 99%) and Na_3PO_4 (Alfa technical grade) were used as obtained. All water used was double-deionized (DDI) (18MΩ cm^{-1}), obtained from a Barnstead NANOpure Ultrapure Water System.

2.1.1 α-Na_3PO_3S

Alpha-sodium monothiophosphate (α-Na_3PO_3S) was prepared by hydrolysis of $PSCl_3$ (Aldrich, 98%) in an aqueous solution of sodium hydroxide, and subsequently dehydrated by spinning in anhydrous methanol, as described elsewhere [5-7,20].

2.1.2 Solvothermal Synthesis

α-Na_3PO_3S (3.33 mmol) was combined with 3.33 mmol $FeCl_3$ in a 23 mL Teflon-lined Parr autoclave to which was added 4 mL of either: 2 M HCl, DDI water, 2 M NH_4OH, 4 M NH_4OH, or 6 M NH_4OH. All reaction bombs were sealed and heated to 160° C for 12 hrs. The reaction vessels were opened upon radiatively cooling to room temperature.

2.1.3 Aqueous Synthesis

$FeCl_3$ (2.04 mmol) dissolved in 100 mL of 1M HCl was combined with 2.69 mmol Na_3PO_3S dissolved in 100 mL of 1M HCl, forming an orange solution. The solution was stirred and evaporated to dryness *in vacuo* without heating.

2.1.4 High Temperature Solid-State Metathesis

One mmol of $FeCl_3$ was ground together with 1 mmol of α-Na_3PO_3S in a mortar and pestle for 10 minutes. The reactants were then loaded into a fused-silica tube and

heated to various temperatures. One sample was heated to 300° C at 25° C/h, held at 300° C for 36 h, heated to 600° C at 10° C/h, held at 600° C for 36 h, and cooled at 10° C/h. All other samples were heated to the target temperatures of 150, 200 or 250° C at a rate of 20° C/h and held at that target temperature for 72 h. These samples were then cooled at a rate of 5° C/h.

2.1.5 Room-Temperature Solid State Metathesis

2.1.5.1 Mechanochemical Reaction by Hand

Mechanochemical reaction between FeX_3 and Na_3PO_3S was accomplished by grinding by hand in an agate mortar with pestle in an Ar-filled glovebox for 10 minutes. A typical reaction consisted of 1 mmol each of FeX_3 and Na_3PO_3S. Digital images of the mechanochemical reaction were obtained in the glovebox using a Panasonic digital camera model GP-KR222.

2.1.5.2 Mechanochemical Reaction by Ball Mill

Milling of reaction mixtures was performed using a Retsch MM200 ball mill with two 10 mL agate jars and three agate grinding balls per jar in an Ar-filled glovebox. A typical reaction consisted of 10 mmol each of FeX_3 and Na_3PO_3S. All mechanochemical reactions utilizing the ball mill were performed by setting the mill to an oscillation frequency of 30 Hz over 90-minute intervals.

2.2 Physical measurements

2.2.1 Powder X-ray Diffraction

Powder X-ray diffraction (PXRD) patterns of products obtained by solvothermal and solution syntheses were obtained on a Rigaku D/max-B, powder X-ray diffractometer in a Bragg-Brentano geometry, using graphite monochromated copper Kα radiation (1.5406 Å) and operating at 35kV and 22.5mA. Intensities were recorded with a scintillation detector. Samples were prepared by adhering the sample to double-sided tape over a glass specimen slide. These diffraction patterns were collected from 10 to 70° in 2θ using a step size of 0.024° at a scan rate of 1 or 2°/min.

Powder X-ray diffraction patterns of solid-state reaction products were obtained on a PANalytical X'Pert PRO MPD powder X-ray diffractometer with the X'cellerator detector, using copper Kα radiation and operating at 45 kV and 40 mA. Samples were routinely prepared in an Ar-filled glovebox, using an inert atmosphere sample holder covered with Kapton film. Afterwords, the protective Kapton film was removed to obtain a PXRD pattern of the material when exposed to a humid atmosphere. These diffraction patterns were collected from 2 to 70° in 2θ, using a step size of 0.0170°, at a scan rate of 1.1789°/min.

2.2.2 Differential Thermal Analysis

Differential thermal analysis (DTA) was performed using a Shimadzu DTA-50, which was calibrated using a three-point calibration curve based on the melting points of indium, zinc and gold metals. The differential signal was balanced prior to the beginning of each experiment. Data were recorded using the Shimadzu TA60-WS collection

program. Experiments were performed at a rate of 10° C/min. Samples were contained in alumina pans under a static air atmosphere. All DTA samples were referenced against an alumina sample, contained similarly and of comparable mass. Multiple heating and cooling cycles were performed in the DTA experiments to differentiate between reversible and irreversible thermal events. DTA residues were routinely examined using PXRD.

3. Results and Discussion

The synthesis of $FePO_3S$ was proposed based on variations of the metathesis strategy which had proved productive in the synthesis of $LnPO_3S$ hydrates.[11] Solvothermal, aqueous precipitation, high-temperature solid-state (HTSS), and room-temperature solid-state (RTSS) synthetic methods were each attempted.

3.1 Solvothermal Synthesis

Solvothermal synthesis was attempted using acidic, neutral and basic aqueous solutions. The acidic solvent reaction yielded no solid except for a small yellow sphere at the bottom of the reaction autoclave which was presumably elemental sulfur. This reaction smelled very strongly of H_2S. All of the neutral and basic solvent reactions contained both a black powder and clear crystals of varying quality and size. PXRD of the black component of these mixtures invariably revealed the presence of FeS_2, (see Fig. 5-1) indicating the decomposition of the monothiophosphate anion, the only source of sulfur in the reaction mixture. Single crystals of the clear material could not be isolated, and this material could not be identified by its PXRD pattern.

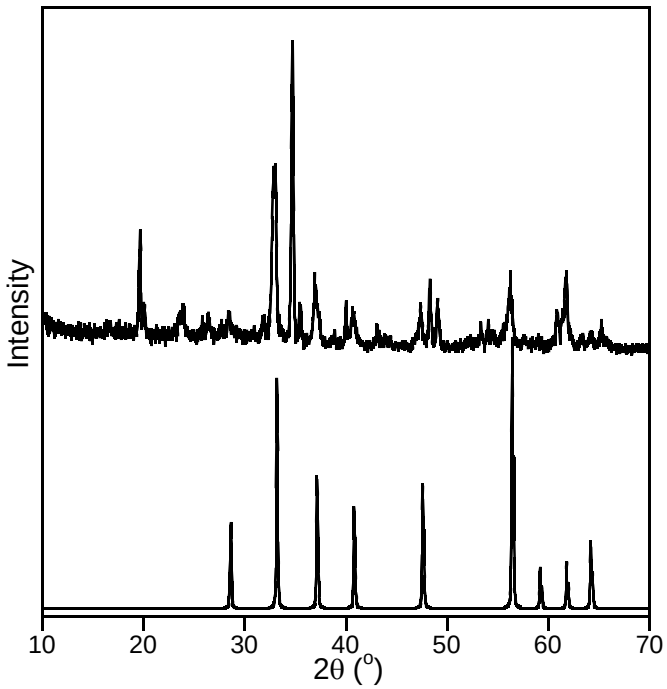

Fig. 5-1: (Top) Representative PXRD pattern of black product of basic solvothermal reaction in the attempt to form $FePO_3S$. (Bottom) calculated PXRD pattern of FeS_2 PDF # 00-001-1295.

3.2 Aqueous Synthesis

Aqueous precipitation methods analogous to those used to prepare $LnPO_3S{\cdot}xH_2O$ [11] and $H_2Zr(PO_3S)_2{\cdot}1.5H_2O$ [7] were also attempted. One difficulty arising from this preparation method was a lack of reproducibility in the observed PXRD patterns obtained of the product mixture. When dissolved $FeCl_3$ was reacted with dissolved Na_3PO_3S an orange solution was formed. After 24 hrs of stirring, a precipitate failed to form. The lack of a significant difference in solubility between the product to be isolated and the NaCl byproduct was a cause of difficulty. To obtain a product(s) which might be characterized, the solution was evaporated to dryness under vacuum. PXRD of the solid residue revealed the presence of NaCl and other diffraction peaks. Reproducing the

reaction led to residues which gave different diffraction patterns. Both attempts to produce $FePO_3S$ by metathesis in acidic solution produced the anticipated byproduct of NaCl, however, the second phase could not be obtained reproducibly, leading to the proposition that there may be multiple phases which are able to be formed in this system. The PXRD patterns of two attempts to utilize this method are summarized in Fig. 5-2.

Other researchers have previously demonstrated that the monothiophosphate anion is capable of reducing ferricyanide under the proper pH conditions (5-13).[21] Such conditions were intentionally avoided in this synthesis by performing the reactions in 1M HCl solution. Acidic conditions introduce the possibility of decomposition of the monothiophosphate anion as evidenced by the smell of H_2S over the reaction mixture; however, the potential of acidic decomposition is preferable over anionic dimerization.

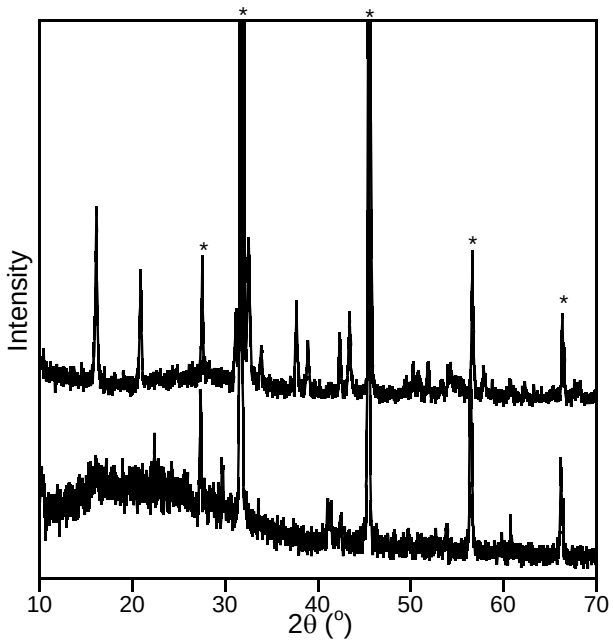

Fig. 5-2: Comparison of two separate attempts to form $FePO_3S$ by solution metathesis in acidic solution. * denotes peaks due to the byproduct of sodium chloride.

Many attempts were made to separate the byproduct of NaCl from the desired product phase. Several solvents were used, and in most cases, separation was incomplete, or the diffraction pattern of the desired phase after separation was amorphous. These results are summarized in Table 5-1.

Table 5-1: Summary of attempts to separate NaCl byproduct from $FePO_3S$.

Solvent	NaCl	$FePO_3S$	Result
Conc. NH_4OH	sol.	insol.	Product amorphous
Ethanol	sl. sol.	sol.	Not separated
Isopropanol	v. sl. sol	sol	Not separated
Isobutanol	insol.	v. sl. sol.	Unable to dry product
Dimethylformamide	insol.	insol.	Not separated

3.3 High-Temperature Solid-State Metathesis

High-temperature, solid-state metathesis has proven effective in the production of carbon nanotubes, optoelectronic materials, and especially refractory materials such as aluminum nitride, actinide borides and high temperature ceramics.[22-26] This strategy was also attempted in the synthesis of $FePO_3S$. Initially, 1 mmol of black $FeCl_3$ was ground together with 1 mmol of white α-Na_3PO_3S in a mortar and pestle for 10 minutes. This grinding process resulted in a color change which is illustrated in Fig. 5-3. The reactants were then loaded into a fused-silica tube and heated to 300° C for 36 h followed by 600° C for 36 h. This reaction resulted in a product which gave a PXRD pattern in air

corresponding to NaCl, FeS_2, and an unidentified phase (see Fig. 5-4). Since FeS_2 was formed, decomposition of the monothiophosphate anion can be inferred. Therefore, reduced reaction temperatures of 250, 200 and 150° C were utilized. Diffraction peaks arising from the presence of FeS_2 were found in both the 200 and 250° C samples. Only the sample heated to 150° C was found not to include FeS_2 (see Table 5-2).

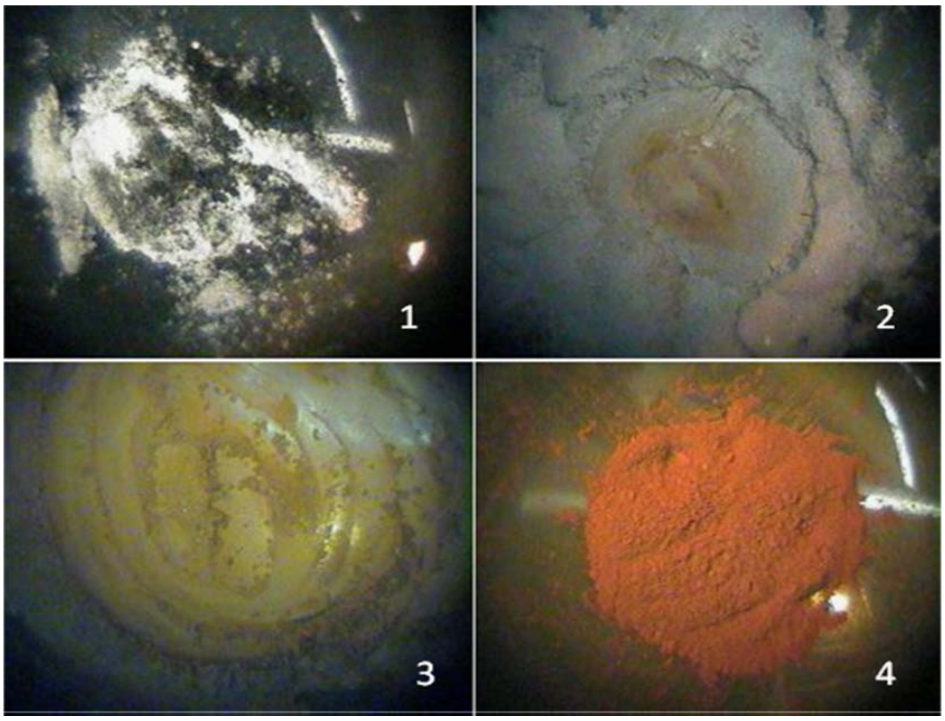

Fig. 5-3: Color change observed upon grinding $FeCl_3$ with α-Na_3PO_3S. The reaction proceeds from 1 to 4 over the course of ~10 minutes of grinding in a mortar with pestle.

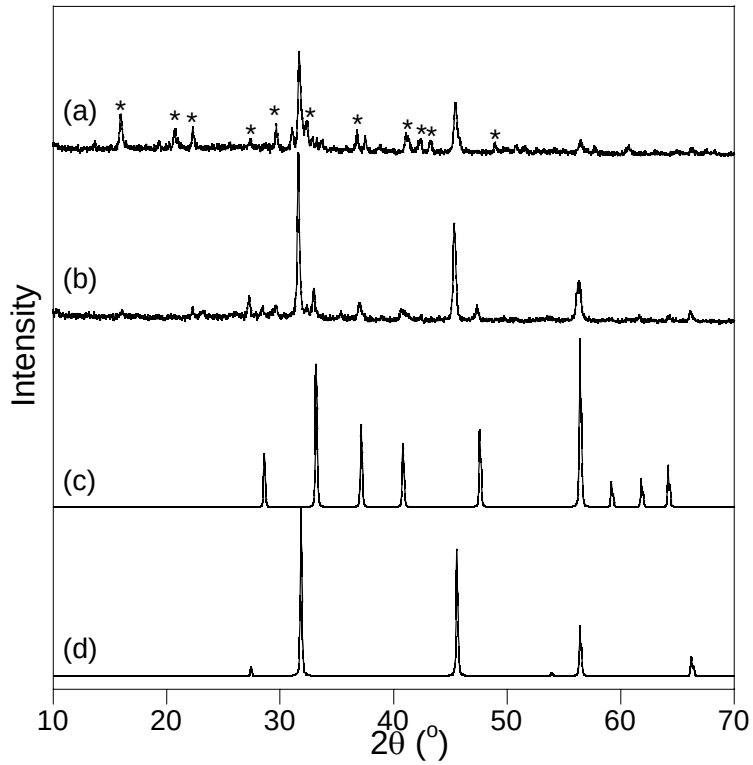

Fig. 5-4: PXRD of products of high temperature metathesis reactions in attempt to form $FePO_3S$ compared to NaCl and FeS_2. a) Observed product diffraction pattern obtained from 150° C sample, b) Observed product diffraction pattern obtained from 150° C sample, c) Calculated diffraction pattern of FeS_2 (PDF # 00-001-1295) and d) Calculated diffraction pattern of NaCl (PDF # 00-001-0993). * Denotes peaks corresponding to unidentified phase.

Table 5-2: Summary of HTSS results indicating thermal instability of the monothiophosphate anion in the Fe^{3+} system.

Temperature	Time	PXRD results[a]
300,600°C	36,36h	NaCl, FeS_2, minor phase unidentified
300°C	72h	NaCl, FeS_2, minor phase unidentified
250°C	72h	NaCl, FeS_2, minor phase unidentified
200°C	72h	NaCl, minor FeS_2, minor phase unidentified
150°C	72h	NaCl and New Phase

[a] All of the PXRD experiments summarized in this table were acquired in air.

The solid-state formation of iron pyrite from the high-temperature reaction mixture was examined using DTA, and a large number of exothermic (irreversible) thermal events were found to take place at low temperatures upon heating. Based on the observation that FeS_2 is formed in samples heated to 200° C, but not in samples heated to 150° C, the formation of FeS_2 is inferred to occur as the thermal event marked as point b in Fig. 5-5.

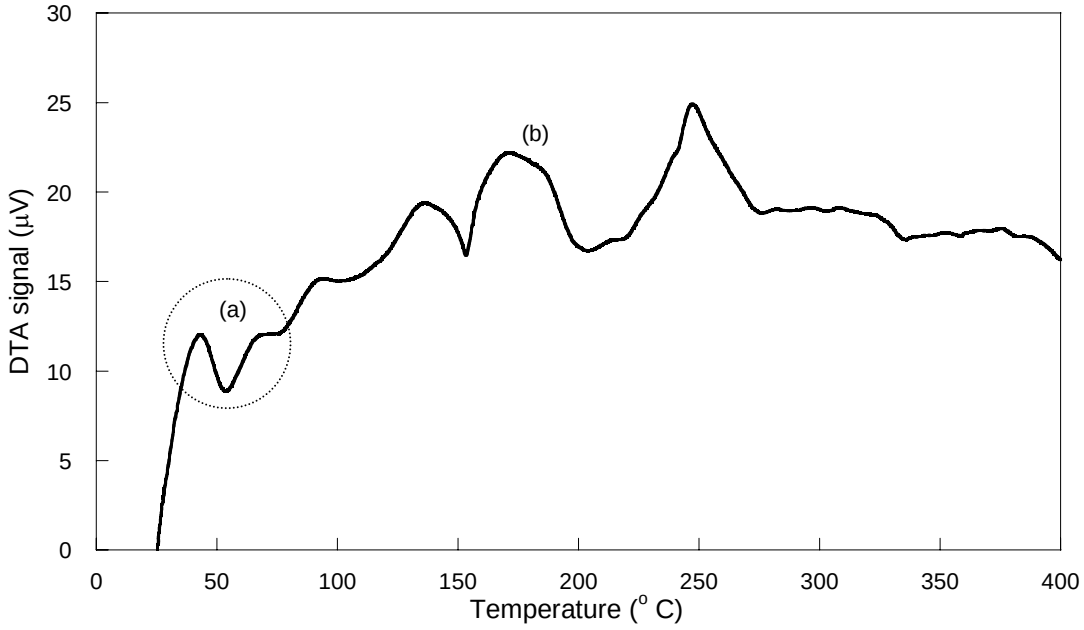

Fig. 5-5: DTA of the thermal reaction between $FeCl_3$ and α-Na_3PO_3S. a) Instrumental artifact, b) Probable formation of FeS_2 based on *ex-situ* PXRD observations.

Decomposition was not observed at low reaction temperatures (< 150° C). It is quite unusual for a solid state reaction to proceed at temperatures as low as 150° C without the use of an accelerating medium such as a flux. The low temperature at which the reaction proceeded coupled with the color change observed upon grinding the

reactants together led to an investigation of whether or not the reaction might proceed at temperatures as low as room temperature in the solid state.

3.4 Room Temperature Solid State Metathesis

As all chemistry students are taught in their first year, a color change is one of the most basic indications that a chemical reaction has taken place. When black $FeCl_3$ and white α-Na_3PO_3S are ground together by hand in a mortar and pestle, the mixture is observed to change color from gray to red/orange. To examine this apparent room-temperature solid-state reaction in a reproducible fashion, α-Na_3PO_3S was folded together [27] (gently stirred without application of pressure) with an equimolar ratio of $FeCl_3$ to form a uniform, unreacted, gray mixture which was loaded into the ball mill in a glovebox and ground for a minimum of 90-minute intervals. Aliquots were periodically examined by PXRD under inert atmosphere followed by ambient atmospheric conditions (relative humidity = 14- 60%). The results of these mechanochemical experiments appear in Figs. 5-6, 5-7.

Despite a marked color change over the course of as little as ten minutes of grinding, PXRD patterns taken under Ar after 9 hours of grinding still displayed only patterns which could be indexed to the starting materials, α-Na_3PO_3S and $FeCl_3$. Possible explanations for this lack of observable diffraction peaks include the production of an amorphous product, which would not produce any new peaks by PXRD, or the production of a volume of product at the surface of the reacting particles which is highly colored, but below the detection limits of PXRD. As diffraction peaks originating from

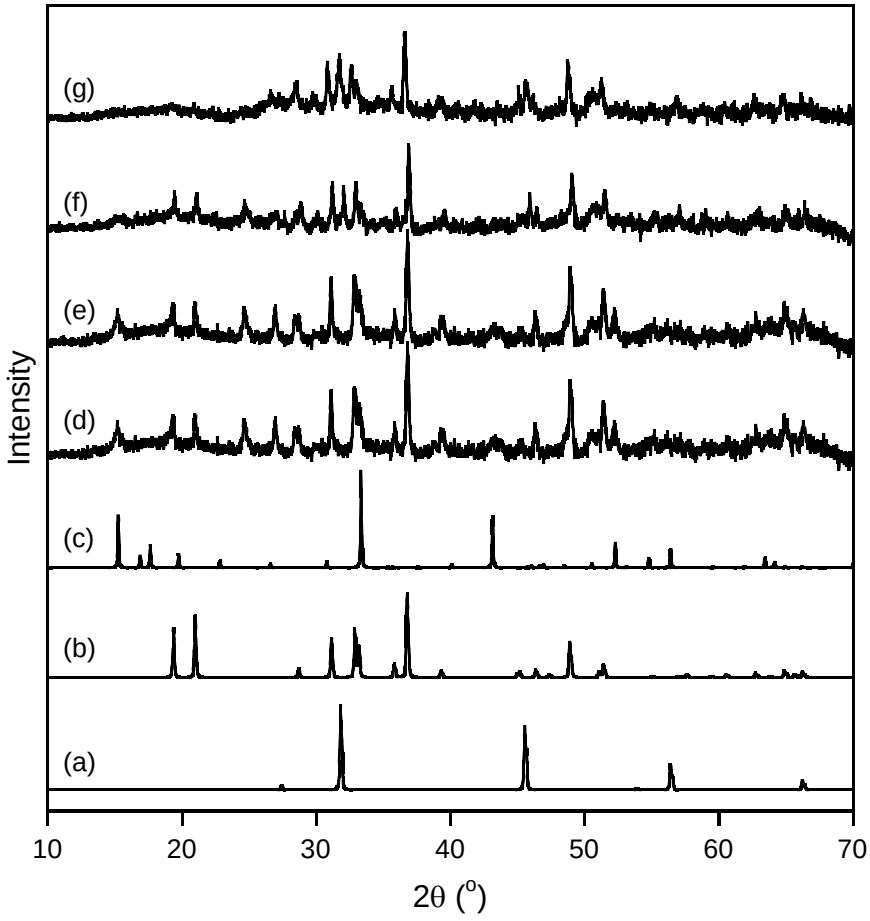

Fig. 5-6: PXRD patterns obtained under Ar of the grinding reaction with ball mill between α-Na_3PO_3S and $FeCl_3$ as compared to NaCl and the starting materials. a) NaCl, b) α-Na_3PO_3S, c) $FeCl_3$, d) 90 min grinding, e) 9hrs grinding, f) 18hrs grinding, g) 27hrs grinding

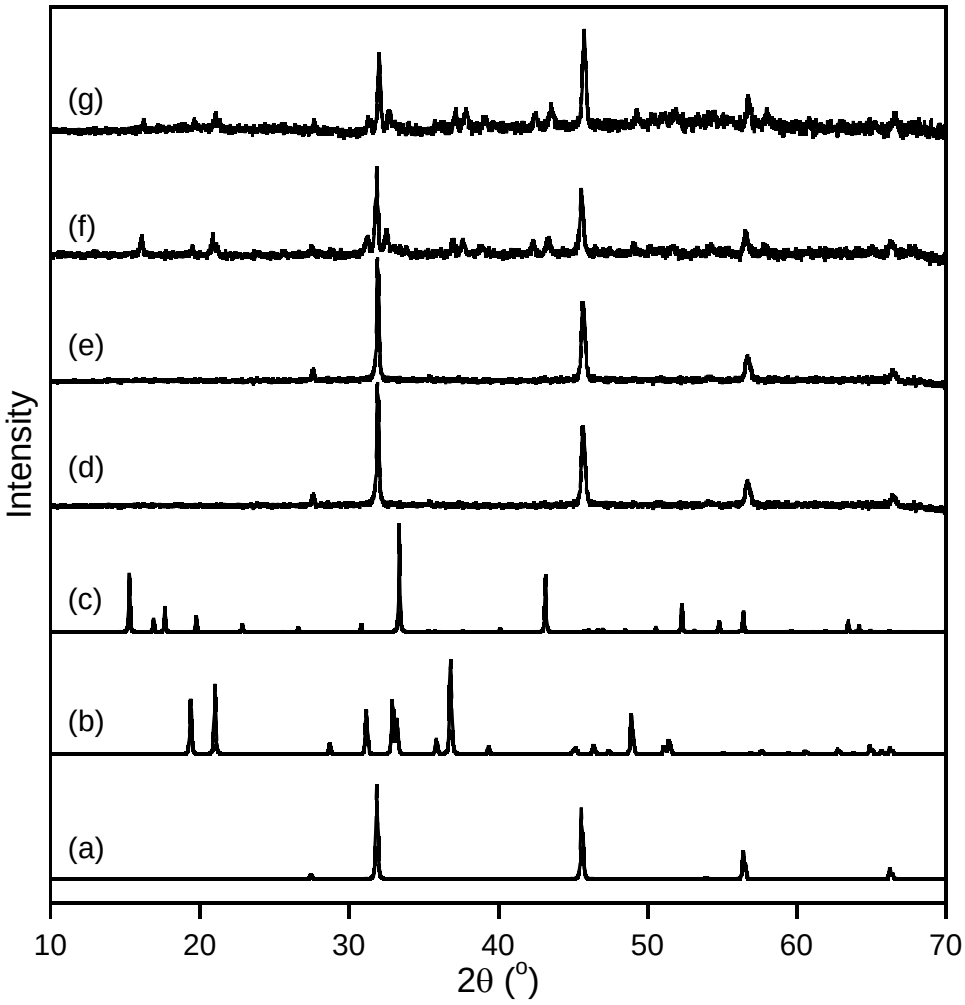

Fig. 5-7: PXRD patterns obtained in humid atmosphere of the grinding reaction with ball mill between α-Na_3PO_3S and $FeCl_3$ as compared to NaCl and the starting materials. Note the early appearance of peaks due to the byproduct of NaCl, and that secondary phase(s) are only observed after longer grinding periods. a) NaCl, b) α-Na_3PO_3S, c) $FeCl_3$, d) 90 min grinding, e) 9hrs grinding, f) 18hrs grinding, g) 27hrs grinding

product phase(s) began to become apparent upon longer and longer grinding times, the latter explanation seems more plausible.

The fact that this solid state reaction proceeds at room temperature is remarkable, as examples of such reactions are exceedingly rare. Such reactions at room temperature have thus far produced alkaline earth molybdates,[28] and zinc phosphate (hopeite phase).[29] In each of these cases, the byproduct of the reaction was also sodium chloride. What makes the room temperature solid-state metathesis reaction presented here even more unusual is the role played by atmospheric water.

As previously noted, the reaction between α-Na_3PO_3S and $FeCl_3$, while producing a color change upon short periods of grinding, still initially afforded only the diffraction patterns of the starting materials. If this mixture which, despite its change in color, is exposed to atmospheric humidity (observed relative humidies 14-60%), the reaction proceeds to completion in less than 30 minutes (see Fig. 5-7). This is inferred by the production of NaCl, and the disappearance of diffraction peaks indicative of starting materials, both of which are observed to take place upon exposure to atmospheric water. It should be noted that in cases where no significant production of crystalline product can be detected by PXRD prior to exposure of the sample to humid atmosphere, only diffraction due to NaCl is observed upon exposure of the sample to atmospheric water. In cases where significant diffraction of product phase(s) is observed prior to exposure of the sample, diffraction peaks of the product phase(s) is still observed upon exposure to atmospheric water.

The first remarkable quality of this room-temperature solid-state metathesis reaction is that it does indeed proceed, albeit slowly, under neat, dry conditions upon

simple mechanochemical treatment. Reactions between solids necessarily occur at the boundary between two reacting particles. The rate limiting step in most solid-state chemical reactions is therefore the diffusion of reactants through a boundary of newly formed product at the interface of the reactant particles. The rate of a solid-state reaction can be increased by the use of volatile materials, which make available fresh surfaces for the reaction to exploit. $FeCl_3$ is such a material, with a small, but measurable vapor pressure at 25° C.[30]

The high lattice energies of the alkali halide byproducts produced in such a reaction have been implicated as the driving force of the reaction.[28] However, it may be that the volatility of the reactant materials play as great, or greater a role in determining whether or not the reaction proceeds. To test this hypothesis, reactions were attempted between α-Na_3PO_3S and equimolar ratios of both $FeBr_3$, which is appreciably volatile, and FeF_3, which is non-volatile. In the case of $FeBr_3$, a color change was observed upon grinding the materials together in a mortar and pestle, and the reaction was found to produce crystalline byproducts immediately upon exposure to a humid atmosphere, just as was the case with $FeCl_3$. When a similar procedure was carried out with FeF_3, no visible reaction was apparent upon grinding in a mortar and pestle, and only the diffraction patterns of the starting materials were apparent even upon exposure to a humid atmosphere.

To validate this comparison, the lattice energies of the reagents and products should be compared, or at least their respective $\Delta_f G°$ values. Since the reactions were observed to take place between both $FeBr_3$ and $FeCl_3$ with α-Na_3PO_3S, these reactions can be assumed to be spontaneous. The known values of $\Delta_f G°$ for the materials involved are

summarized in Table 5-3. The free energy of a reaction can be represented as the $\Delta G_{rxn} = \Delta_f G°_{prod.} - \Delta_f G°_{react.}$. Since α-$Na_3PO_3S$ is a constant in all reactions, and if the iron(III) monothiophosphate product is assumed to be the same product regardless of the reactants, (This assumption has not been proven.) The values of $\Delta_f G°$ for these materials may be treated as a constant when comparing one reaction in this series to another. The only values which need to be considered appear in the far right column of Table 5-3. This column of data demonstrates that a more negative free energy of reaction can be calculated for the reaction between FeF_3 and α-Na_3PO_3S at room temperature than the corresponding reaction with $FeCl_3$, which is known to be spontaneous at room temperature by observation.

Table 5-3: $\Delta_f G°$ values pertinent to room-temperature reactions with $FeCl_3$ and FeF_3.

Iron Halide	$\Delta_f G°$ of FeX_3 [a] (kcal/mol)	$\Delta_f G°$ of byproduct [a] (x3) (kcal/mol)	$\Delta_f G°_{prod.} - \Delta_f G°_{react.}$ (kcal/mol "$FePO_3S$")
FeF_3	-232.393	-653.040	-420.647
$FeCl_3$	-79.824	-262.200	-182.376

[a] Thermo chemical data were obtained from reference 31.

The reaction involving a non-volatile reagent which should have produced a byproduct with a higher lattice energy (NaF), via a reaction with a more negative free energy, did not proceed, and the reaction involving a volatile reagent which produced a byproduct of lower lattice energy (NaBr) did proceed.

The second remarkable quality of this room-temperature solid-state metathesis reaction is that exposure to small amounts of gaseous water leads to a many-fold increase in its rate of reaction. This reaction may be accelerated to such speeds for one or more

reasons. The most apparent reason is that water acts as a plasticizing agent increasing the rate of diffusion even at room temperature. We have previously demonstrated that low levels of atmospheric water can sufficiently plasticize β-Na_3PO_3S to induce a phase transition to α-Na_3PO_3S.[6] Therefore, water may again be acting as a plasticizing agent in this reaction system, acting on either the α-Na_3PO_3S, the FeX_3 (where X = Cl, Br) or all members of the reaction system.

For the sake of completeness, the possibility that the reaction taking place might be driven by a red/ox reaction between Fe^{3+} and $[PO_3S]^{3-}$ should be considered. Ferricyanide has previously been shown to oxidize the monothiophosphate anion, in solution, to form the disulphanediphosphonate dimer [32,33] according to Eq. 5-1:

$$2\ Fe^{3+} + [PO_3S]^{3-} \longrightarrow 2Fe^{2+} + [O_3PSSPO_3]^{4-} \qquad \text{Eq. 5-1}$$

The possibility that this reaction takes place in the solid state cannot be excluded without the crystal structure or Mossbauer studies of the final product mixture; however, it can be ruled out as the driving force behind the reaction. To test whether this red/ox process might be responsible for the observed reaction, equimolar ratios of Na_3PO_4 and $FeCl_3$ were ground together in a ball mill for >90 h under Ar, and a color change was observed. Unfortunately, the phase produced cannot be unambiguously determined due to the low quality of the PXRD pattern obtained (see Fig. 5-8). However, this generalization of the reaction to include Na_3PO_4 excludes this red/ox process as the driving force behind the observed reaction, because a parallel red/ox reaction involving Fe^{3+} and $[PO_4]^{3-}$ is not chemically reasonable.

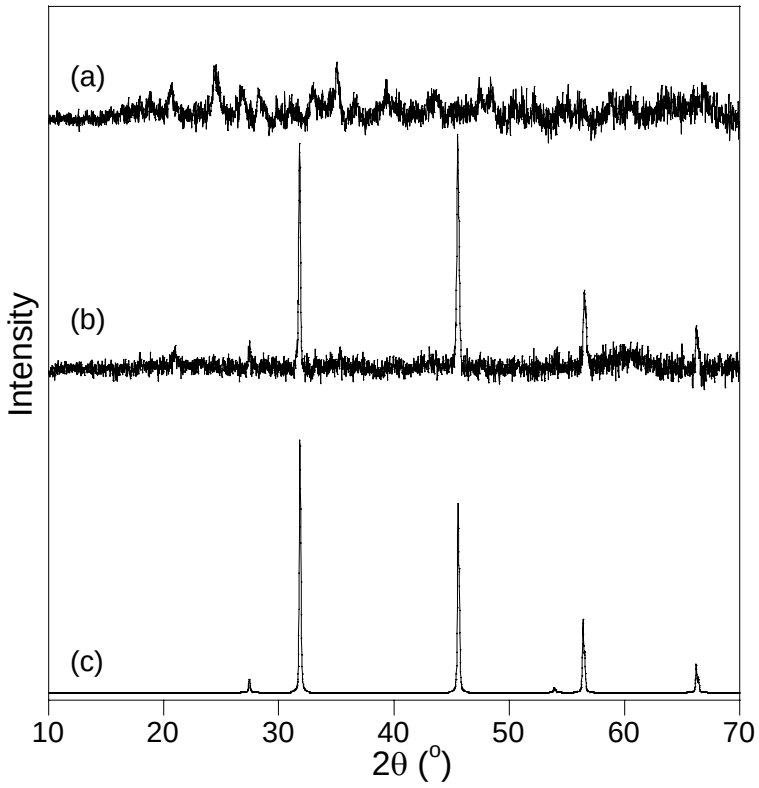

Fig. 5-8: PXRD patterns of the mechanochemical reaction with ball mill between Na_3PO_4 and $FeCl_3$ as compared to NaCl. a) PXRD pattern obtained under Ar, b) PXRD pattern obtained upon exposure to humid atmosphere, c) Calculated PXRD pattern of NaCl

chemically reasonable.

4. Conclusions

An unusual room temperature solid-state metathesis reaction has been observed to take place between α-Na_3PO_3S and either $FeCl_3$ or $FeBr_3$. It seems apparent that for this reaction to occur, the iron(III) halide must exhibit some degree of volatility, as a similar reaction was not found to occur using FeF_3. The speed of the reaction can be increased many fold upon exposure to a humid atmosphere, and we hypothesize that this acceleration is due to plasticization of one or both reactants. The possibility that a redox reaction forming the disulfanediphosphonate anion, by dimerization of the

monothiophosphate anion cannot yet be excluded, but must not be the driving force behind the reactivity, as a similar reaction is found to occur between $FeCl_3$ and Na_3PO_4.

5. Acknowledgements

Thank you to Mr. Austin Savatt for enthusiasm in this project. Thank you to Dr. Peter Wildfong for use of his ballmill. Thank you to the Bayer School of Natural and Environmental Sciences at Duquesne University and the Nobel Dick Fund for funding. The PANalytical powder X-ray diffractometer was purchased with funds from the National Science Foundation (Grant No. DUE-0511444).

References

[1] K. K. Palkina, S. I. Maksimova, N. T. Chibiskova, T. A. Tripol'skaya, G. U. Wolf, T. B. Kuvshinova, Izv. Akad. Nauk SSSR, Neorg. Mater. 27 (1991) 1028-1031.

[2] M. Pompetzki, M. Jansen, Z. Anorg. Allg. Chem. 629 (2003) 1929-1933.

[3] M. Pompetzki, L. van Wuelen, M. Jansen, Z. Anorg. Allg. Chem. 630 (2004) 384-388.

[4] M. Pompetzki, R. E. Dinnebier, M. Jansen, Solid State Sci. 5 (2003) 1439-1444.

[5] N. J. Takas, J. A. Aitken, Inorg. Chem. 45 (2006) 2779-2781.

[6] N. J. Takas, J. A. Aitken, J. Solid State Chem. 180 (2007) 2034-2043.

[7] A. E. Gash, P. K. Dorhout, S. H. Strauss, Inorg. Chem. 39 (2000) 5538-5546.

[8] I. A. Stenina, A. D. Aliev, P. K. Dorhout, A. B. Yaroslavtsev, Inorg. Chem. 43 (2004) 7141-7145.

[9] M. A. Wurtz, Ann. Chim. Phys. 3 (1847) 472-482.

[10]M. Pompetzki, M. Jansen, Z. Anorg. Allg. Chem. 628 (2002) 641-646.

[11] N. J. Takas, L. E. Slomka, X. Yang, N. Giles, J. A. Aitken, J. Solid State Chem. Accepted 30 July, 2008.

[12] A. Yamada, M. Hosoya, s.-C. chung, Y. Kudo, K. Hinokuma, K.-Y. Liu, Y. Nishi, J. Power Sources, 120 (2003) 232-238.

[13] K.-F. Hsu, S.-Y. Tsay, B.-J. Hwang, J. Mater. Chem. 14 (2004) 2690-2695.

[14] P. Tang, N. A. W. Holzwarth, Phys. Rev. B 68 (2003) 165107.

[15] E. Muneyama, A. Kunishige, K. Ohdan, M. Ai, J. Catal. 158 (1996) 378-384.

[16] M. Ai, K. Ohdan, J. Mol. Catal. A-Chem. 159 (2000) 19-24.

[17] V. Lenoble, C. Laclautre, V. Deluchat, B. Serpaud, J.-C. Bollinger, J. Hazard. Mater. 123 (2005) 262-268.

[18] K. Takada, Y. Michiue, T. Inada, A. Kajiyama, M. Kouguchi, S. Kondo, M. Watanabe, M. Tabuchi, Solid State Ionics 159 (2003) 257-263.

[19] Y. Takano, N. Arai, A. Arai, Y. Takahashi, K. Takase, K. Sekizawa, J. Magn. Magn. Mater. 274 (2004) e593-e595.

[20] S. K. Yasuda, J. L. Lambert, Inorg. Syn. 5 (1957) 102-104.

[21] H. Neumann, I. Z. Steinberg, E. Katchalski, J. Am. Chem. Soc. 87 (1965) 3841-3848.

[22] A. J. Lupinetti, J. L. Fife, E. Garcia, P. K. Dorhout, K. D. Abney, Inorg. Chem. 41 (2002) 2316-2318.

[23] J. L. O'Loughlin, C.-H. Kiang, C. H. Wallace, T. K. Reynolds, L. Rao, R. B. Kaner, J. Phys. Chem. B 105 (2001) 1921-1924.

[24] R. A. Janes, M. A. Low, R. B. Kaner, Inorg. Chem. 42 (2003) 2714-2719.

[25] E. G. Gillan, R. B. Kaner, Chem. Mater. 8 (1996) 333-343.

[26] R. W. Cumberland, R. G. Blair, C. H. Wallace, T. K. Reynolds, R. B. Kaner, J. Phys. Chem. B 105 (2001) 11922-11927.

[27] Ed. J. D. Darling, Better Homes and Gardens: New Cook Book, Meredith Publishing Group, Des Moines, IA, 1996.

[28] P. Parhi, V. Manivanan, Abstracts, 20th Rocky Mountain Regional Meeting of the American Chemical Society, Denver, CO, United States, August 29-September 1 (2007).

[29] P. Parhi, S. S. Singh, A. R. Ray, A. Ramanan, B. Mater. Sci. 29 (2006) 115-118

[30] D. S. Rustad, D. W. Gregory, Inorg. Chem. 27 (1988) 2837-2840.

[31] D. R. Stull, H. Prophet, JANAF Thermochemical Tables, Second Ed. US Dept. of Commerce (1971)

[32] V. Janickis, K. Maróy, Acta Chem. Scan. 48 (1994) 465-470.

[33] V. Janickis, K. Maróy, Acta Chem. Scan. 48 (1994) 461-464.

Chapter 6

Conclusions and Future Directions In Metal Monothiophosphates

1. Conclusions

1.1Expansion of the Family of Oxythiophosphates

At the beginning of this dissertation, a list of the known oxythiophosphate materials was presented. This list was exceptionally short and included only 29 compounds discovered over the course of more than 160 years. This work has added four new materials to the family of the oxythiophosphates, γ-Na_3PO_3S, in Chapter 3,[1] $LaPO_3S$ and $NdPO_3S$ hydrates in Chapter 4,[2] and "$FePO_3S$" in Chapter 5, although the exact chemical formula of this material remains unproven. These additions to the literature represent an increase in the known number of oxythiophosphate compounds by more than 13%; but, undoubtedly a large number of new oxythiophosphate materials still wait to be discovered.

1.2 Thermal Stability

For each material studied throughout this dissertation, the temperature at which the material decomposed or was oxidized in air was determined. Among the compounds studied, the temperature of oxidation/decomposition ranged from 200 to 450° C. The driving forces behind these processes vary from case to case.

Oxygen is, of course, a more electronegative element than sulfur, so a tendency toward oxidation of the monothiophosphate anion is not greatly surprising. The trend observed thus far is for these oxidations to form either an orthophosphate or a pyrophosphate product.

The oxidation in air of sodium monothiophosphate yielded sodium pyrophosphate and sodium phosphate.[3] The lanthanide monothiophosphate materials formed in Chapter 4 were found to oxidize to form monazite-type lanthanide phosphates.[2] In Chapter 5, iron monothiophosphate was found to thermally decompose. One of the thermal decomposition products formed has been identified as pyrite, FeS_2 by PXRD. This decomposition occurs as low as 200° C, indicating the iron monothiophosphate product to be thermally unstable.

1.3 Hard/Soft, Acid/Base Character

The hard/soft, acid/base principle is exhibited clearly by the chemistry of the oxythiophosphate anions. Among crystalline and non-crystalline materials, examples abound of a metal selectively coordinating to either the sulfur or oxygen moiety of the anion. In this dissertation, the detection of this principle is more subtle, but is exemplified by the thermal decomposition products observed.

In the cases where a hard acid is present, such as sodium, lanthanum or neodymium, with the monothiophosphate anion, oxidation is observed to form the corresponding pyrophosphate or phosphate. This oxidation produces a harder anion, increasing the compatibility of the cation and anion. In the case of a softer acid such as iron(III), thermal decomposition was observed to take place at even lower temperatures, and was not due to oxidation. Instead, sulfur was stripped from the monothiophosphate anion to

form FeS_2. Again the anion is altered in favor of increased hard/soft, acid/base compatibility.

1.4 The Role of Water

Throughout this dissertation, water was found to greatly affect the chemistry of the monothiophosphate anion. In Chapter 4, water played the seemingly indispensible role of a reaction medium, allowing preservation of the monothiophosphate anion in a system where other "soft" techniques had failed. The lanthanide monothiophosphate materials were also found to be tolerant toward reversible hydration and dehydration. Water was further found to act as a plasticizing agent in Chapter 3, reducing the temperature of a phase transition from β-Na_3PO_3S to α-Na_3PO_3S by 275° C. In Chapter 5, the presence of water vapor was found to accelerate the rate of reaction between solid $FeCl_3$ and solid α-Na_3PO_3S many times over. These extraordinary behaviors may come at a price however, and a solid state chemist or materials scientist must always be wary of the potential that water may lead to decomposition of the monothiophosphate anion.

2 Future Directions

2.1 Generalization of Room Temperature Solid State Metathesis

Reactions which occur at room temperature in the solid state are very rare. Such reactions may allow routes to materials which are not stable at elevated temperatures, such as iron monothiophosphate, or may allow routes to new meta-stable phases of compounds which are already known. The phase in which a material crystallizes, can have as much to do with the observed properties as its composition; therefore, fully exploring synthetic methods with the potential to expand both the number of known

materials and the number of phases available is paramount to the growth of solid-state chemistry and materials science.

This dissertation has proposed that the ability of a metathesis reaction to occur in the solid state at room temperature may depend on one of the reagents displaying a measurable volatility at room temperature. This hypothesis should be tested by attempting room-temperature solid-state metathesis reactions broadly using reagents such as $PbCl_2$, $CrCl_3$ NH_4Cl, or $ZrCl_4$. Preliminary work not described in this dissertation has shown the potential that $PbCl_2$ may also react with α-Na_3PO_3S via a room-temperature solid-state metathesis reaction. When conducting future research with solid-state metathesis reactions, precautions must be taken. Such experiments may proceed slowly upon grinding, as in the case of $FePO_3S$, or may react violently, as other researchers in the field of solid-state metathesis have observed.[4-6]

2.2 Expansion of the Family of the Oxythiophosphates

Preliminary work not discussed in this dissertation has also shown that an aqueous solution of $MnCl_2$ is capable of reacting with an aqueous solution of Na_3PO_3S to form an amorphous precipitation product. The apparently low solubility of the manganese monothiophosphate product makes separation from the byproduct of NaCl straightforward in this system. This compound, if further developed may display interesting magnetic properties, and could still become the first oxythiophosphate material to be magnetically studied.

Untold numbers of new oxythiophosphate materials remain to be discovered. These new materials may not always display the properties which are desired; however, new materials should always be sought with a specific goal in mind. To this end, one of

the most tantalizing prospects among new oxythiophosphate materials, is the development of zeotypic oxythiophosphates, which might be analogous to the known zeotypic aluminum phosphate (ALPO) phases.[7-9] ALPO phases are composed of an anionic framework, and contain open channels, several angstroms in diameter, which can hold water, and counterions.[10,11]

It has been shown that oxythiophosphates are capable of mimicking the structure of a related phosphate phase,[2,12,13] and are capable of selective ion exchange for heavy metal cations.[12] If an aluminum oxythiophosphate can be formed in an open structure analogous to the known ALPO phases, it would be a great boon to water purification in places with significant heavy metal contamination problems.[14,15] Accomplishing such a goal, would increase the advancement of materials science and solid-state chemistry, not to mention the still small family of the oxythiophosphates.

References

[1] N. J. Takas, J. A. Aitken, J. Solid State Chem.180 (2007) 2034-2043.

[2] N. J. Takas, L. E. Slomka, X. Yang, N. Giles, J. A. Aitken, J. Solid State Chem. Accepted 30 July, 2008.

[3] N. J. Takas, J. A. Aitken, Inorg. Chem. 45 (2006) 2779-2781.

[4] R. G. Blair, A. Anderson, R. B. Kaner, Chem. Mater. 17 (2005) 2155-2161.

[5] J. L. O'Loughlin, C.-H. Kiang, C. H. Wallace, T. K. Reynolds, L. Rao, R. B. Kaner, J. Phys. Chem. B 105 (2001) 1921-1924.

[6] E. G. Gillan, R. B. Kaner, Chem. Mater. 8 (1996) 333-343.

[7] S. Oliver, A. Kuperman, G. A. Ozin, Angew. Chem. Int. Ed. 37 (1998) 46-62.

[8] J. Yu, R. Xu, J. Li, Solid State Sci. 2 (2000) 181-192.

[9] J. Yu, K. Sugiyama, S. Zheng, S. Qiu, J. Chem, R. Xu, Y. Sakamoto, O. Terasaki, K. Hiraga, M. Light,[M. B. Hursthouse, J. M. Thomas, Chem. Mater. 10 (1998) 1208-1211.

[10] J. Yu, R. Xu, Acc. Chem. Res. 36 (2003) 481-490.

[11] M. Tiemann, M. Fröba, Chem. Mater. 13 (2001) 3211-3217.

[12] A. E. Gash, P. K. Dorhout, S. H. Strauss, Inorg. Chem. 39 (2000) 5538-5546.

[13] A.-F. Shihada, Z. Naturforsch. 48b, (1993) 1781-1783.

[14] T. Clarke, Nature Sci. Update. (June 25, 2003) http://www.nature.com/nsu/030623/030623-7.html

[15] F. R. Seigel, J. Geochem. Explor. 55 (1995) 265-273.